Modelling, Design and Experimental Study of Semi-Transparent Photovoltaic Windows for Commercial Building Applications

Konstantinos Kapsis

A Thesis
In the Department
of
Building, Civil and Environmental Engineering

Presented in Partial Fulfilment of the Requirements
For the Degree of
Doctor of Philosophy (Building Engineering) at
Concordia University
Montreal, Quebec, Canada

April 2016

CONCORDIA UNIVERSITY
SCHOOL OF GRADUATE STUDIES

This is to certify that the thesis prepared

By: Konstantinos Kapsis

Entitled: Modelling, Design and Experimental Study of Semi-Transparent Photovoltaic Windows for Commercial Building Applications

and submitted in partial fulfillment of the requirements for the degree of

Doctor of Philosophy (Building Engineering)

complies with the regulations of the University and meets the accepted standards with respect to originality and quality.

Signed by the final examining committee:

_____ Chair
Dr. G. Gouw

_____ External Examiner
Dr. D. Rousse

_____ External to Program
Dr. L.A.C. Lopes

_____ Examiner
Dr. H. Ge

_____ Examiner
Dr. R. Zmeureanu

_____ Thesis Supervisor
Dr. A. Athienitis

Approved by: _____
Dr. F. Haghighat , Graduate Program Director

April 29, 2016 _____
Dr. A. Asif, Dean
Faculty of Engineering and Computer Science

Abstract

Modelling, Design and Experimental Study of Semi-Transparent Photovoltaic Windows for Commercial Building Applications

Konstantinos Kapsis, PhD candidate
Concordia University, 2016

As the building sector is moving to net-zero energy building performance targets and beyond, the use of building integrated solar systems becomes essential. Semi-transparent photovoltaic (STPV) window technologies are expected to play a key role in on-site electricity generation of new and retrofitted high-performance commercial and institutional buildings. In most commercial and high-rise residential buildings where reducing the costs of cooling energy is important, STPV windows can be used as integrated strategy to reduce solar heat gains and generate solar electricity while still providing adequate daylight and view to the outdoors.

The research presented on this thesis is based on the conviction that window technologies should be considered as an integral part of a broad strategy of energy-conserving, energy-efficient building design. The main objective of this work is to provide a systematic study of STPV windows through experimental work and simulations that will allow these technologies to become ubiquitous on buildings in the near future. The end goal is to transform buildings from energy consumers to energy producers without compromising on occupancy comfort. Hence, all performance characteristics (e.g., electrical, thermal and daylighting) should be studied and quantified individually and in combination in order to capture the impact such technologies have on the building energy performance and occupancy comfort.

In this work, design concepts of windows integrating STPV technologies are developed, modelled and studied in typical perimeter zones. The thermal and electrical performance of four crystalline Si-based prototype STPV windows was studied experimentally. Specially designed prototypes were mounted in a calibrated hot-box calorimeter apparatus developed for this study. The apparatus is placed inside a two-storey high environmental chamber with a solar simulator (SSEC) and exposed to emulated sunlight produced by a continuous solar simulator. The SSEC facility allows tests to be performed under fully controlled and repeatable conditions (temperature and irradiance). Operating cell temperatures of up to 80.5°C were observed under 1000 W/m^2 irradiation, still air and ambient air temperature of 21°C. An experimental procedure for the determination of Solar Heat Gain Coefficient (SHGC) for STPV windows is also developed. It was found that the electricity generation from the STPV windows can result in up to 23% reduction of SHGC in comparison to a heat-absorbing (e.g., tinted or fritted glass) window with the same optical and thermal properties. In addition, the performance data

generated was used to verify thermal-electrical performance models for the prediction of cell operating temperatures and solar energy yield.

Low-order thermal models for various STPV window assemblies were developed. Using typical meteorological weather data as inputs, the thermal models could predict the operating cell temperatures of an assembly (e.g., double glazed low-e argon window with integrated photovoltaics) within ± 5°C, resulting in less than ±3% error in the annual solar energy yield. A general simulation methodology was developed integrating thermal, electrical and daylighting performance modelling. The methodology was applied to evaluate the potential benefits of various STPV facade designs in cooling-dominated commercial building applications under continental climate. The simulations revealed that the selection of the ideal STPV optical properties is sensitive on the daylight and lighting controls applied in the building, and photovoltaic cell technology utilized (crystalline Si-based spaced cells, a-Si "see-through" and fully transparent organic thin film technologies were examined). In regards to design of a building facade, it was shown that the three-section design concept integrating Si-based spaced PV cells on the upper section of the facade (daylight section) and "see-through" thin PV film on the middle section (view section) has the potential to maximize daylight utilization and view to the outdoors while minimizing the possibility for glare to occur and producing an optimal amount of solar electricity.

"Profound ideas are always obvious once they are understood".

Donald A. Normal, 1988 [1]

[1] *The design of everyday things: Revised and expanded edition*. Basic books, 2013.

Dedication

to my family and to fabulous four

Acknowledgments

First of all, I want to express my gratitude to my supervisor and mentor Prof. Andreas Athienitis for his guidance toward the formulation and realization of this comprehensive research project. I will be always thankful for your critical review of my work and the trust you showed me through the course of this long journey of knowledge. Πάντα ευγνώμων.

The work on chapter 3 was accomplished with the valuable input of Prof. Stephen Harrison at Queen's University. Also special thanks to Dr. Jiwu Rao for sharing his technical expertise through the course of this experimental work, to Joseph Hrib for building the solar calorimeter and allowing me to work on his machinery shop and to Jamie Yeargans for helping on the operation and troubleshooting of the solar simulator and environmental chamber laboratory. This experimental work would not be feasible without coordination provided by Jacques Payer.

Chapter 5 and 6 were completed with the critical input of my research fellow Vasken Dermardiros. I would still be struggling with the Matlab coding without your help.

I would like to also thank Prof. Siva Sivoththaman at Waterloo University, Prof. Mario Leclerc, at Université Laval and their research teams for the fruitful collaboration on the development of semi-transparent photovoltaic window technologies under project 12 of the NSERC (Natural Sciences and Engineering Research Council of Canada) Photovoltaic Innovation Network.

My appreciation goes to Canadian Solar Inc. for the assembly of the STPV prototype modules and Unicel Architectural Inc. for the integration of the STPV modules into double glazing insulated window units.

Many thanks to all my colleagues under IEA (International Energy Agency) SHC (Solar Heating and Colling) Task 40 "Net Zero Energy Solar Buildings" for the great discussions and arguments we shared. Special thanks to operating agent Josef Ayoub at NRCan (Natural Resources Canada) for his leadership and boldness.

In Africa, they have a saying "if you want to go fast, go alone. If you want to go far, go together". Thank you, my fellow researchers and friends at the Concordia Solar laboratory for making this trip enjoyable.

Finally, I would like to thank everybody who takes the time to reads this thesis. I would be delighted to discuss its content with you.

This work was funded by the Photovoltaic Innovation Network - a strategic NSERC research network. Additional support through a grant-in-aid from the ASHRAE (American Society of Heating, Refrigeration, and Air-Conditioning Engineers) is also acknowledged.

Abriviations

AM	air mass
a-Si	amorphous Silicon
BPS	building performance simulation
cDA	continuous daylight autonomy
CFD	computational fluid dynamics
COP	coefficient of performance
DGP	daylight glare probability
DSC	dye-Sensitized solar cells
EVA	ethylene-vinyl acetate
HVAC	heating, ventilating and air conditioning
IGU	insulated glazing unit
IR	infrared
LED	light-emitting diode
LPD	lighting power density
mono-Si	monocrystalline Silicon
MPPT	maximum power point tracking
μc-Si	micro-crystalline Silicon
nc-Si	nano-crystalline Silicon
NIR	near-infrared
OPV	organic photovoltaic
poly-Si	polycrystalline Silicon
PV	photovoltaic
PVB	polyvinyl butyral
PVDF	polyvinylidene fluoride
PVF	polyvinyl fluoride
RTD	resistance temperature detector
sDA	spatial daylight autonomy
SHGC	solar heat gain coefficient
SSEC	solar simulator and environmental chamber
STC	standard testing conditions
STPV	semi-transparent photovoltaic
STPV/T	semi-transparent photovoltaic/thermal
TCO	transparent conductive oxide
UV	ultra-violet
WWR	window-to-wall ratio

Nomenclature

Symbols

a	empirically-determined coefficient governing the upper temperature limit under low wind speeds and high solar irradiance
A	surface area (m^2)
b	empirically-determined coefficient governing the rate at which the back-surface temperature drops with the rise of the wind speed
c	correction factor
C_p	specific heat [J/(kg·K)]
E	energy (J)
f	packing factor
h	convective film coefficient [W/(m^2·K)]
I	current (A)
I_o	diode saturation current (A)
I_{sh}	shunt current (Ω)
k	slope of the line [(m^2·K)/W]
$\dot{m}$	mass flow rate (Kg/s)
N	fraction of absorbed solar energy reemitted
n_I	usual ideality factor (V)
N_s	number of cells in series
P	power (W)
Q	energy rate (W)
q_e	electron charge ($1.60218 \cdot 10^{-19}$ C)
R	resistance (Ω)
R_{sh}	shunt resistance (Ω)
S	incident solar irradiance (W/m^2)
SHGC	solar heat gain coefficient
T	temperature (K)
t	time (s)
U	thermal conductance [W/(m^2·K]
V	voltage (V)
WS	wind speed measured at standard 10-m height (m/s)

Greek Symbols

ε	emissivity
λ	wavelength (μm)
θ	solar angle of incidence (°)
σ	Stefan-Boltzmann constant [$5.6703 \cdot 10^{-8}$ W/(m^2·K^4)]
α	absorbance
α_I	ideality factor (V)
η	conversion efficiency

Greek Symbols (contd)

μ	temperature coefficient (%/°K)
ρ	reflectance
σ	variance
τ	transmittance

Subscripts

abs	absorber plate
b	back-surface
cav	window sealed cavity
cell	covered with PV cells
cond	through conduction
D	diode
el	electrical
enc	not covered with PV cells
f	front-surface
gap	cavity between window and interior shading device
guard	gruard box
i,j,k	index
in	indoor
L	light
lkg	leakage
mask	mask wall
meas	under test conditions
mp	under MPPT
net	net energy flow
o	exterior
oc	open circuit
out	outdoor
pla	plate
ref	under reference conditions
s	in series
sc	short circuit
sh	shade
sol	solar heat gains
st	under standard test conditions
th	thermal
vis	visible

Table of Contents

Chapter 1
Introduction

1.1 Introduction

There is currently a major transformation taking place in the building sector. Energy conservation and energy efficiency measures are becoming an integral part of the building design and operation through national building codes, roadmaps and building rating systems. While moving toward energy-positive, carbon-neutral building performance targets, the use of on-site energy generation becomes compulsory (IEA-PVPS, 2015). Solar photovoltaic technologies are expected to play an important role in achieving these goals (Rekinger et al., 2014). More specifically, building integrated photovoltaic (BIPV) technologies are expected to be the main technology to generate on-site electricity in high performance buildings since it can be utilized to virtually cover any building surfaces that have access to direct sunlight. Commercial, institutional and high-rise residential buildings (commercial building installation costs can be up to 20% less expensive than residential due to larger scale installations) will be the niche market (Drachman and Adamson, 2012).

On the other hand, international architectural trends are moving toward highly glazed envelopes due to the fact that daylight and view to the outdoors has to some extent a positive effect on occupants' health, well-being and productivity (Farley and Veitch, 2001; Veitch and Galasiu, 2012). In addition, the presence of windows or skylights on buildings may have a positive effect on retailing (Heschong et al., 2002). Nonetheless, glazing typically has lower thermal resistance than opaque wall or roof constructions and can cause unwanted solar gains – particularly in cooling-dominated climates and/or buildings that have high internal gains. This creates an opportunity for BIPV technologies such as semi-transparent photovoltaic (STPV) windows to emerge in the marketplace (Figure 1.1).

In most commercial and high-rise residential buildings, where reducing the costs of cooling energy expenditures is important, an integrated strategy to control the transmission of solar radiation needs to be adopted. Rather than having reflective, tinted or fritted windows to reduce solar transmission (Figure 1.2), STPV windows may be used to reduce solar heat gains and generate solar electricity while still providing adequate daylight and view to the outdoors (Bahaj et al., 2008; James et al., 2009; Qiu et al., 2009; Vartiainen, 2001). The term STPV windows is used here to cover a broad range of PV technologies, from semi-transparent Si-based PV windows to translucent thin films such as a-Si/μc-Si (Klein et al., 2012; Sai et al., 2014), to fully transparent organic PV (Krebs, 2009; Li et al., 2012) and perovskites (Eperon et al., 2014; Snaith, 2013).

Figure 1.1 Existing semi-transparent photovoltaic window installations utilizing various PV technologies.

If designed and implemented properly, the use of STPV technologies may contribute to the climate-resiliency of the building or building cluster through distributed and localized energy generation and consumption. It may also eliminate grid transmission losses and reduce the need for specifically devoted land for solar energy generation (e.g. solar farms) by being an integral part of the building skin (Gaiddon et al., 2009; Temby et al., 2014).

1.2 Problem statement

Semi-transparent photovoltaics are new disruptive technologies that are being slowly introduced in the building industry and they are expected to be a major technology to generate on-site electricity in new and retrofit high performance buildings (Drachman and Adamson, 2012). STPV windows need to meet but are not limited to all expected functions of windows (the following functions are in no particular order as they are all essential to the reliability and performance of the technology):

- Maintain occupancy comfort (thermal, visual and acoustic) and view to the outdoors;
- Deliver high thermal performance (e.g. low U-values and regulate solar gains to minimize building energy expenditures);
- Meet technical requirements such as structural, weather proofing and condensation resistance;
- Provide durability (they should perform at least 20-30 years), fire protection and blast resistance;
- Generate solar electricity.

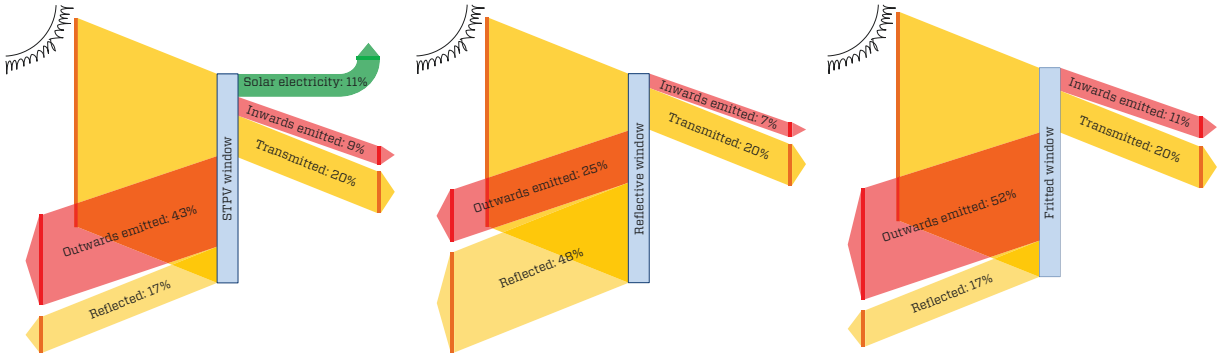

Figure 1.2 Sankey diagrams for solar energy transmission, reflection, absorption and electricity conversion for a STPV window (left), a reflective window (centre) and fritted window (right) under NFRC 100-2010 conditions (NFRC, 2014a). All windows have an average solar transmittance of 20%.

It is important that balance is attained between all functions by obtaining occupancy comfort, and minimizing energy and maintenance expenditures. In some cases, the aforesaid functions might compete with each other. e.g. lowering the optical transmittance of a STPV window integrated on a cooling-dominated building façade will result in an increase in solar electricity yield, reduction of solar gains, and also reduction of daylight availability (De Boer and van Helden, 2001; Miyazaki et al., 2005). Insufficient daylight leads to increased electric lighting energy consumption and possibly increased building cooling costs through sensible heat. In return, an increase in electric lighting might diminish any savings on cooling costs initially achieved due to reduced solar gains.

A deeper understanding of STPV technologies will allow the PV and window industry to provide the necessary materials and designs for high performance STPV windows. When solar radiation strikes a window surface, it is partly reflected (ρ), partly transmitted (τ) and partly absorbed (α):

$$\rho(\lambda,\theta)+\tau(\lambda,\theta)+\alpha(\lambda,\theta)=1 \tag{1.1}$$

where λ is the wavelength and θ the solar angle of incidence. In the case of a STPV window, a fraction of the energy absorbed is converted to solar electricity while the rest becomes thermal energy:

$$\alpha(\lambda,\theta,T_{STPV})=N_{out}\alpha(\lambda,\theta)+N_{in}\alpha(\lambda,\theta)+\eta_{el}(\lambda,\theta,T_{STPV}) \tag{1.2}$$

where T_{STPV} is the operating cell temperature, N_{out} is the fraction of absorbed solar energy reemitted outwards, N_{in} is the fraction reemitted inwards and η_{el} is the fraction of incident solar radiation that is absorbed and converted to solar electricity also known as electrical conversion efficiency. It is apparent that the electrical efficiency of a STPV window is strongly linked to its optical and thermal properties. The solar gains and daylight that comes through the window is also dependant on the optical and thermal properties of the window. Thus, balance should to be attained between electrical efficiency and solar and thermal transmittance of a STPV window in order to achieve a visually and thermally comfortable indoor environment while minimizing building energy expenditures (in the form of cooling, heating and electric lighting).

1.3. Thesis scope

The research presented on this thesis is based on the conviction that STPV window technologies (and BIPV in general) should be considered as an integral part of a broad strategy of energy-conserving, energy-efficient building design. The end goal is to transform buildings from energy consumers to energy producers without compromising on occupancy comfort. This cannot be achieved by studying STPV alone. All performance characteristics (e.g. electrical, thermal, daylighting and others) of the STPV windows should be studied and

quantified individually and in combination in order to capture the impact such technologies have on the building energy performance and occupancy comfort.

This thesis provides a systematic study of STPV windows through experimental work and simulations by addressing the following emerging issues that will allow STPV windows to become a ubiquitous building technology in the near future:

- the impact the various window design parameters have on the temperature profile and solar energy yield of STPV windows;
- the potential benefits of emerging STPV window technologies such as thin film Si, organic PV and perovskites;
- a general design methodology that could be easily followed by architects and engineers for the selection of ideal STPV window properties specific to climate, façade configuration and building typology;
- the development of low-order, easy-to-use and reliable thermal models for the prediction of cell operating temperatures that can be used to assess the solar energy yield of a STPV window systems during preliminary design stage;
- the development of an experimental standard test procedure suited to determine the solar heat gain coefficient and U-value of STPV windows based on existing PV and window test standards.

While the conducted research focuses on crystalline Si-based STPV windows for commercial building applications, the findings can be extended to emerging thin film technologies and other building typologies. We are hoping that through this effort, we will provide the reader with new insights and a better understanding of STPV window technologies and their impact on built environment.

1.4 Thesis overview

This thesis follows the manuscript-based format. Chapter 2 provides a technology overview on PV and window advancements suited to STPV window applications followed by a comprehensive literature review on STPV windows performance studies. Chapter 3 presents an experimental procedure for the determination of SHGC of STPV windows. It is important that current Solar Calorimetric Standards get updated to address current challenges and provide guidelines on how to test and characterize disruptive window technologies such as STPV windows. Chapter 4 takes a closer look on how STPV window assembly affects its cell operating temperatures. Experimentally-validated low-order thermal models are also developed. Chapter 5 investigates the potential benefits of STPV windows on the integral (energy, daylighting and thermal) performance of commercial buildings through the development of a building performance simulation methodology, while chapter 6 focuses on the visual comfort aspects and daylighting performance of various STPV façade configurations. Finally, chapter 7 summarizes the main contribution of this thesis and research needs.

Chapter 2
Literature Review

2.1 Introduction

This section provides an overview of major STPV technologies and studies on efforts to optimize the electrical, thermal and daylighting performance of STPV windows for cooling-dominated commercial building applications. Since there was no standard way on reporting results among the researchers, there are many instances where they cannot be directly compared to each other. Often, this inconsistency is due to modelling assumptions specific to the application studied or particularities to façade design. Furthermore, the studies are scattered across the globe, introducing a wide variety of climatic conditions.

2.2 Semi-transparent photovoltaic modules

Depending on the manufacturing process followed, STPV modules can be categorized on (Bizzarri et al., 2011): (i) matrix-based, where opaque PV cells are spaced each other allowing daylight to pass through the unfilled space between them, (ii) process-induced, where part of the semiconductor substrate is removed using laser-etching techniques thus creating voids that allow daylight to pass through and (iii) intrinsic-based, utilizing thin film transparent PV technologies (Figure 2.1).

Matrix-based STPV modules utilize conventional square-like (156 mm × 156 mm) crystalline Si PV cells. Other novel technologies utilize spaced micro spherical Si-based cells (Biancardo et al., 2007), mono-Si sliver cells (Deutsche Gesellshaft fur Sonnenenergie, 2005a) and concentrating photovoltaics (CPV) using transparent low-concentration prisms (Yamada et al., 2011). Typical process-induced STPV modules utilize a-Si/μc-Si thin film while intrinsic-based modules are been developed based on polymer-based, perovskites or a-Si/nc-Si thin films.

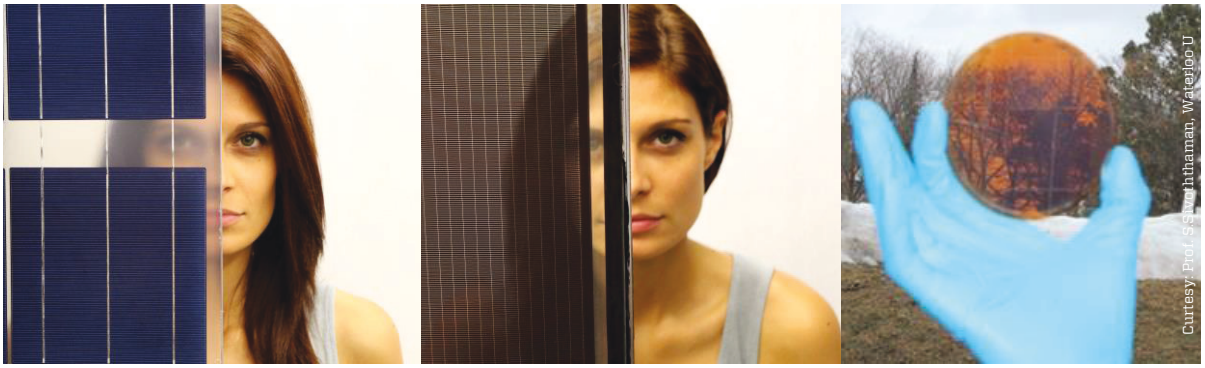

Figure 2.1. Matrix-based STPV windows using: poly-Si opaque spaced PV cells (left), induced-based "see-through" α-Si/μc-Si thin film (centre) and fully transparent α-Si/nc-Si thin film that can be used on intrinsic-based applications (right).

When it comes to appearance, matrix-based modules provide an interchange between transmitted light and shadows cast by opaque PV cells. By alternating the spacing between opaque PV cells, simple (e.g., equally spaced cells) to complex patterns (e.g., treating PV cells as pixels of an image drawn on the building façade) can be generated (Baum, 2011). When the opaque PV cells integrated on the STPV window come in the form of strips rather standard PV cells, they are perceived from the occupants as less obstructive to outdoor view (Markvart et al., 2012). On the other hand, both process-induced and intrinsic-based modules provide a"see-through" appearance with nominal or no obstruction to the outdoor view but may affect the colour rendering properties of the window (Lynn et al., 2012). Finally, emerging thin film technologies are being developed to harvest the near-infrared or ultraviolet spectrum of the sunlight and thus maximize transparency and colour neutrality under the visible spectrum (Betancur et al., 2013; Lunt and Bulovic, 2011).

2.2.1 PV technologies suited for STPV window applications

Advances in a range of relevant technologies, including the solar cells themselves, have made STPV an increasingly attractive option for building integration, replacing conventional windows and skylights. Various PV technologies can be utilized on STPV window applications with the most common being opaque, spaced crystalline Si PV cells and α-Si/μc-Si transparent thin films. Low-cost PV technologies with tuneable transparency and colour as well as mechanical flexibility are currently under development allowing the functional and architectural integration of PV technologies into the building skin.

Crystalline Silicon (Si)-based modules (first generation): Crystalline Si-based PV cells hold the lion's share – out 80% of the overall cell production are crystalline silicon cells (IEA-PVPS, 2015). Solar radiation is captured and converted into electricity by the PV cells based on the photovoltaic effect. Commercially available PV modules can convert up to 22% [and 25.6% on cell efficiency (National Renewable Energy Laboratory, 2016)] of the incident solar radiation into electricity while a major portion of the absorbed solar energy is converted into heat (roughly 30-70%, depending on the optical and thermal properties and PV technology used) and contributes to increase the temperature of the PV cells. As the PV temperature increases (primarily, due to increase on irradiance levels and secondarily, due to increase on the ambient air temperature) the diffusion current on the cells increases, leading to a reduction of the charges at the edges of the cells. As a result, the open circuit voltage significantly decreases while the short-circuit current slightly increases, causing an overall reduction of the power output and thus electrical efficiency of the module (Duffie and Beckman, 2006). In addition, as the solar radiation incident on the PV module increases, the short circuit current and thus power output of the module increases almost with a linear fashion (Figure 2.2). Since efficiency generally decreases as the PV cell operating temperature increases, this overheating is usually undesirable. Depending on the cell technology, the power of PV modules can be affected at a rate of as much as 0.55 %/°C. Less often, the PV cells are bifacial, making use of the secondary solar radiation that is reflected from the indoor space toward the rear side of the STPV window

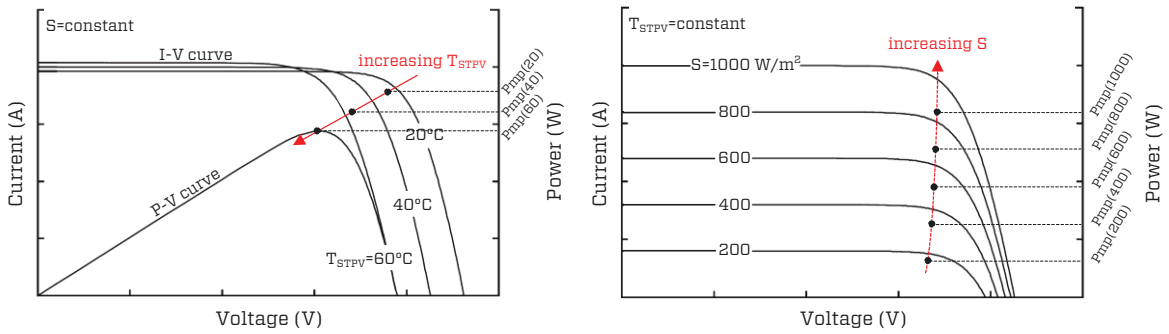

Figure 2.2. Current-Voltage curves under various operating cell temperatures with constant incident solar radiation (left) and under various incident solar radiation levels with constant operating cell temperature (right).

resulting to marginal increase on the power output of the module (up to 4%, when a highly reflective surface such as a roller shade is used).

α-Si/μc-Si and α-Si/nc-Si transparent thin films (second generation): α-Si/μc-Si and α-Si/nc-Si thin PV films are multi-junction (tandem cells) technologies utilizing a-Si as the front layer (1.7 eV), and μc-Si (or nc-Si) absorber layer (1.1 eV) deposited as a bottom layer complimenting the spectral response of the a-Si and thus increasing the cell efficiency (Green, 2007; Klein et al., 2012), while the frontsheet carries the electrodes (Figure 2.3). Currently, commercial products have module efficiencies of up to 9% [and 13.6% on cell efficiency (National Renewable Energy Laboratory, 2016)].

Emerging PV technologies (third generation): Transparent polymer-based (organic) PV (OPV) and perovskites are emerging thin film technologies, suited for window and skylight applications due to their tuneable transparency and colour as well as their foil form. Using low-cost raw materials (e.g., polymers, tin) and low-cost, low-temperature (<120°C) and scalable processes, they are expected to be a cost-effective, fully recyclable, visually attractive technologies well suited for STPV window applications. Perovskite-based cell efficiencies of up to 21% (not stabilized) and OPV of up to 11.5% have been reported under laboratory conditions (National Renewable Energy Laboratory, 2016).

Nevertheless, commercially available products are currently limited by low efficiency (≤5%) and experience quick degradation (≤3 years) from exposure to atmospheric conditions and sunlight (namely UV radiation). Moreover, due to the relatively low temperatures in manufacturing processes, prolonged operating temperatures above 75°C should be avoided due to accelerated film degradation and possibly permanent failure. Significant progress therefore needs to be made before they reach competitive efficiencies (above 5%) and operational lifetimes (25 years and above) on a commercial scale (Jørgensen et al., 2008; Snaith, 2013).

Despite the various cell architectures, OPV consists of at least five layers (Abdulrazzaq et al., 2013) (Figure 2.3): (i) a transparent substrate, (ii) a front transparent conductive oxide (TCO) layer that acts as a transparent anode to the photoactive layer, (iii) an electron-blocking hole transport layer (HTL) that separates the anode and the photoactive layer as well as prevents charge trap centres that will result in cell degradation, (iv) the active layer, where sunlight is absorbed, that consists of donor-acceptor interfacing as layer-by-layer or mixed

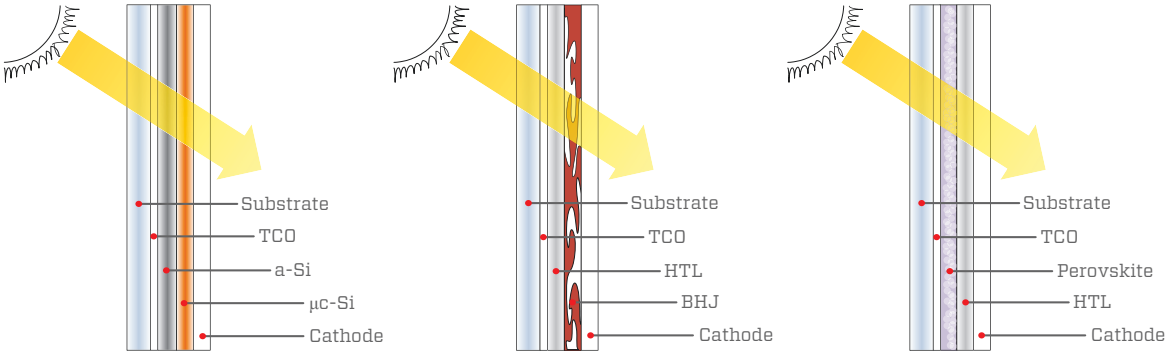

Figure 2.3. Conceptual architecture of α-Si/µc-Si (left), organic-based (centre) and perovskite (right) STPV modules.

together to create a bulk heterojunction (BHJ) with a bandgap as narrow as 1.4eV (Li et al., 2012), and (v) the cathode layer that acts as an electron collector. Up to 60% transparency on the visible spectrum has been reported but with significant reduction on conversion efficiency (≤4%) (C. C. Chen et al., 2012).

Initially developed within the field of dye sensitized solar cells (DSSC), perovskites-based cells share a similar-by-principal architecture with OPV cells (Snaith, 2013). In less than a decade, research developments resulted to up to 6 times increase on Perovskites conversion efficiencies (from 3.5% on 2009 to 21% on 2016), the steepest increase between all PV technologies. With tuneable bandgap (Green et al., 2014), perovskites are ideal for the development of tandem high efficiency PV devices (Bailie et al., 2014; Liu and Kelly, 2013).

2.2.2 Semi-transparent photovoltaic module assembly

Similar to PV modules, STPV modules consist of at least three layers: (i) the frontsheet, (ii) the STPV and encapsulation layer and (iii) the backsheet. STPV modules are most commonly frameless as they are meant to be integrated into a window, skylight or a curtain wall assembly, as the outermost layer of the multi-glazed insulating unit (Figure 2.4). However, framed STPV modules can be found and used on other building integrated applications such as overhangs and canopies. An extensive review on the performance characteristics of existing frontsheet/backsheet and encapsulation materials used on PV modules can be found at Willeke et al.(2013).

STPV module frontsheet: STPV frontsheet should maximize transmission in the spectral response range of the PV cell or film layer. Typical frontsheet used in commercial STPV modules is low-Fe white glass (also known as solar glass) with a solar transmittance of up to 92%. In order to increase even further the solar transmission, anti-reflective coating or surface texturing is applied, increasing solar transmission by up to 99.4% under AM1.5 (Deubener et al., 2009). Thickness of a typical solar glass frontsheet is 2 mm to 4 mm, always selected to provide the structural integrity required. Optically smart coatings are under development, increasing the solar radiation captured and converted into electricity. Down-shifting high energy photons (UV) through active photon conversion, plasmonic scattering (Gu et al., 2012; Zhao and Lunt, 2013) or harvesting NIR photons using luminescent solar concentrators (Zhao et al., 2014) can increase the range of solar spectrum harvesting and thus, increase the conversion

efficiencies. Such coatings can be applied on the frontsheet or directly on the photovoltaic cells. It should be noted that in the case of thin film technologies, the frontsheet plays the role of the substrate on the cell architecture.

Encapsulation layer: The encapsulation layer provides the necessary structural stabilization between frontsheet, PV layer and backsheet, and provides protection against weathering, humidity and corrosion. Typical encapsulation resins are ethylene vinyl acetate (EVA) mainly used on glass-backsheet modules and polyvinyl butyral (PVB) used on glass-on-glass modules. Similar to frontsheet, encapsulant should maximize solar transmission while provide electrical insulation, long term stability especially on UV-light (Kempe, 2010; Kempe et al., 2007), maximum adhesion and cross-linking (Jorgensen et al., 2006; Pern and Glick, 2000). A sealant is applied on the module's edges to porevent moisture penetration through cross-linking interface that might result to moisture intrusion, delamination and possibly degradation of the semiconductor device (Sharma and Chandel, 2013).

STPV module backsheet: The most common STPV backsheets are about 40 μm polyvinyl fluoride (PVF), polyvinylidene fluoride (PVDF) for glass-to-backsheet or 2 mm to 4 mm clear glass for glass-on-glass modules. In the case of bifacial cells, low-Fe white glass should be used as backsheet so as to make the most of the secondary (reflected) solar radiation incident on the rear side of the STPV module. When no STPV cooling strategy is applied such as natural or mechanical ventilated STPV/T system, highly absorptive backsheet (e.g., coloured or tinted) should be avoided as it results to PV cell overheating. Park et al. (2010) found that when coloured or tinted glass backsheet was used as a means to aesthetics and reduction of solar heat gains, the daily and seasonal electrical performance of the STPV skylights and windows was reduced when compared to clear glass backsheet. This was due to higher operating PV cell temperatures driven by the high solar absorbance of the coloured or tinted backsheet. An important observation was that the flash tests under STC were not able to capture these discrepancies.

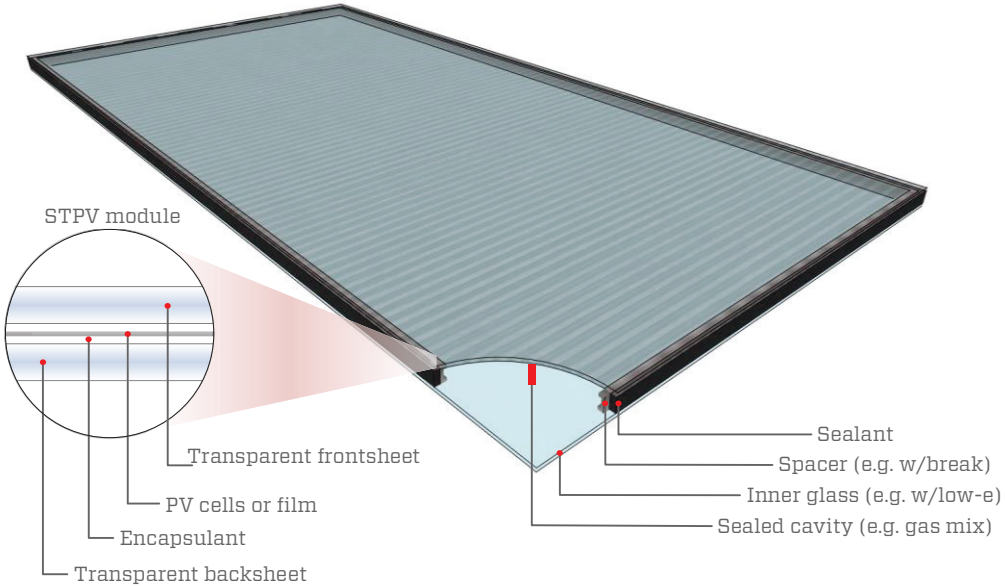

Figure2.4. Schematic of a double glazed STPV window assembly.

STPV module electronics: On matrix-based STPV modules, led-free ribbons are soldered between poles while on process-induced or intrinsic-based modules the connections are monolithic. A junction box located on the edge of the module is used to safely run the electrical supply wires. One positive and one negative polarity wire come out of the junction box. The wires carry plug-n-play weatherproof connections allowing modules to be connected on a "daisy chain" manner (Deutsche Gesellshaft fur Sonnenenergie, 2005a). Male and female connections are used avoiding incorrect connection that might damage the module or the module array. Commonly, a junction box house bypass diodes to prevent hot spots due to reverse current caused by total or partial shading (Mäki et al., 2012). Each diode is connected in parallel with half (2-diode module), one third (3-diode module) or one quarter (4-diode module) of the PV cells of the module, on reserve polarity to the one of the module.

2.2.3 Electrical performance models

Several models have been developed to estimate the electrical performance of PV systems(E Skoplaki and Palyvos, 2009). One of the simplest and most widely adapted model throughout literature is the Evan's model (Evans, 1981).The model assumes that the power generation (P_{PV}) of a PV module operating at the maximum power point is linearly dependent on the cell operating temperature (T_{PV}) and incident solar radiation (S):

$$P_{PV} = \eta_{ref} \cdot \left[1 + \mu_{P,mp} \cdot \left(T_{PV} - T_{ref}\right)\right] \cdot S \cdot A_{PV} \tag{2.1}$$

where η_{ref} and T_{ref} is nominal module efficiency and cell temperature (°C) under reference conditions, respectively, A_{PV} (m^2) is the surface area of the module and $\mu_{P,mp}$ is the maximum power point temperature coefficient (%/°C).

The maximum power point temperature coefficient is specific to every module. It is empirically-determined and is most likely provided by the manufacturer. While low-order electrical performance models are good for a preliminary analysis, they tend to overestimate the energy yield (E Skoplaki and Palyvos, 2009). When possible, more advanced electrical models should be adopted to capture the various effects design parameters (e.g., optical properties, cell technologies, module configuration) and climatic conditions (e.g., solar spectrum, quality of sunlight in terms of direct or diffuse irradiance, air mass) might have on the performance of STPV windows and PV systems in general. Other more accurate electrical models include the equivalent one-diode model and King's model.

The equivalent one-diode model (Figure 2.5) is typically used to describe the electrical performance of a cell, module or an array. The model is implemented in several simulation tools such as PVsyst (Pvsyst.SA, 2014) and EnergyPlus (U.S.DOE, 2012). Its detailed description can be found in various textbooks including Duffie and Beckman's "solar engineering and thermal processes (Duffie and Beckman, 2006). The module current (I) equals to the difference between light current I_L and, the diode current I_D and shunt current I_{sh}.

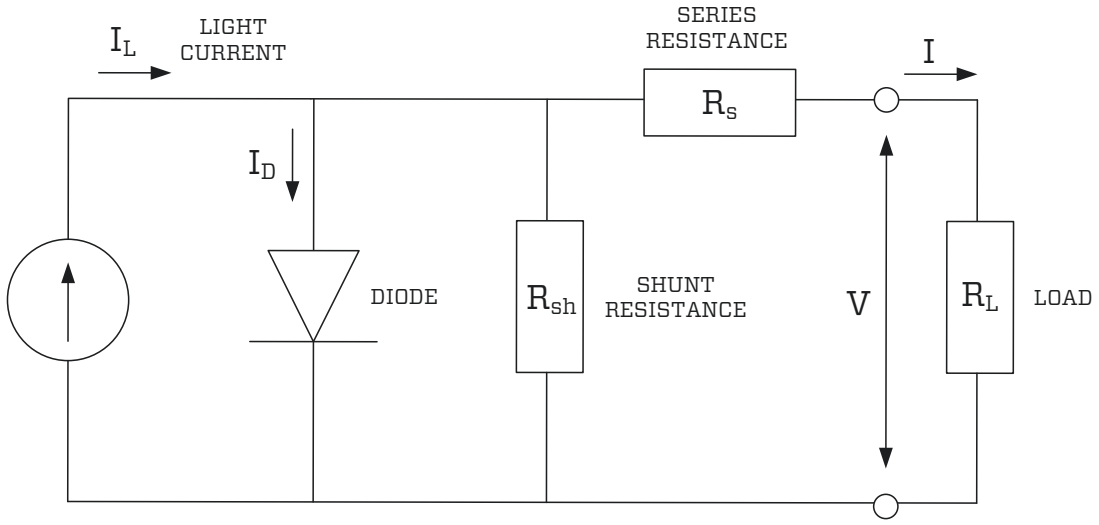

Figure 2.5. Equivalent circuit for the one-diode model.

It can be expressed as a function of five parameters (the model is also known as 5-parameter model):

$$I = I_L - I_D - I_{sh} = I_L - I_o\left(e^{(V+IR_S)/\alpha} - 1\right) - (V + IR_S)/R_{sh} \tag{2.2}$$

where I_o is the diode saturation current (A), R_s is the series resistance (Ω), R_{sh} is the shunt resistance (Ω) and α is the ideality factor (V). The shunt resistance expresses the leakage of current caused by defects, the series resistance expresses the voltage drop due to migration of charge carriers from the semiconductor to the contacts, and the ideality factor accounts for the thermal voltage and the various mechanisms accountable for moving carriers across the junction (Tian et al., 2012).

For given incident solar radiation and operating cell temperature, the five parameters need to be determined (I_L, I_o, R_s, R_{sh}, α) in order to calculate the module operating current and voltage. The power is calculated as the product of current I and voltage V:

$$P_{PV} = IV \tag{2.3}$$

Employing various approaches an implicit solution of eq.(2.2) is possible based on the information available by the module manufacturer's datasheet as follows (De Soto et al., 2006; Pvsyst.SA, 2014): (i) the short circuit current $I_{sc}(V=0)$, (ii) the open circuit voltage $V_{OC}(I=0)$, (iii) the maximum power point under reference conditions $P_{mp}(I_{mp},V_{mp})$, (iv) the temperature coefficient of the short circuit current $\mu_{I,SC}=\Delta I_{SC}/\Delta T_{PV}$ and (v) the temperature coefficient of the open circuit voltage $\mu_{V,OC}=\Delta V_{OC}/\Delta T_{PV}$. Table 2.1 provides average temperature coefficients for various PV module technologies available on the market that can be used when they are not provided by the manufacturer.

King's model (King et al., 2004) (also known as Sandia model) is a point-value mathematical model that is used to describe the electrical performance of a PV module or an array considering spectral correction. The model consists of various empirical equations and coefficients that are derived from experimental testing of the particular PV module. The coefficients of existing PV modules are available at the Sandia database and can be used to calculate five key points on the I-V curve (Figure 2.6): [0 , I_{SC}], [$V_{OC}/2$, I_x], [V_{mp} , I_{mp}], [$(V_{OC}+V_{mp})/2$, I_{xx}] and [V_{OC}, 0].

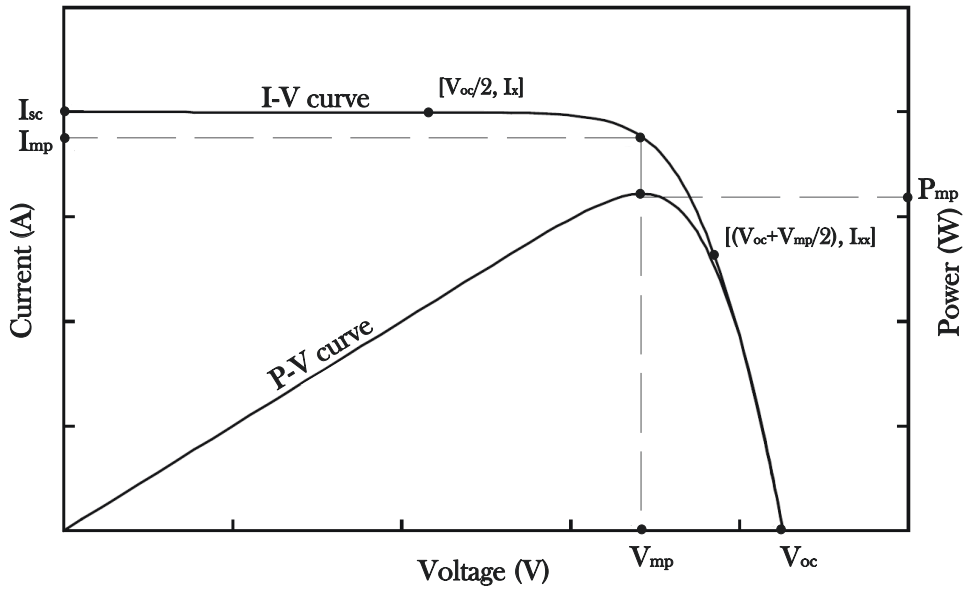

Figure 2.6. Five-key points with respect to the Current-Voltage and Power-Voltage curves.

Table 2.1.Average values for temperature coefficients of maximum power point ($\mu_{P,mp}$), short circuit current ($\mu_{I,SC}$) and open circuit voltage ($\mu_{V,OC}$) for cell technologies suited for STPV applications

Crystalline Si-based	$\mu_{P,mp}$ (%/°C)	$\mu_{I,SC}$ (%/°C)	$\mu_{V,OC}$ (%/°C)
mono-Si	-0.425	+0.046	-0.323
poly-Si	-0.443	+0.054	-0.332
Silicon Heterostructures (HIT)	-0.300	+0.032	-0.030
Bifacial Silicon structures	-0.312	+0.060	-0.271
Thin film	$\mu_{P,mp}$ (%/°C)	$\mu_{I,SC}$ (%/°C)	$\mu_{V,OC}$ (%/°C)
α-Si/μc-Si (micromorph)	-0.270	+0.071	-0.270
Organic-based (OPV)	+0.050	-0.210	-0.270

Note: Data generated based on specification datasheets of (up to) 50 PV module manufacturers

2.2.4 Thermal modelling

Besides the complexity or accuracy the various PV electrical performance models might provide, all have something in common: they require the incident solar radiation and the cell operating temperature as inputs. While the incident solar radiation can be estimated through meteorological data (Perez et al., 1990), weather satellite data or measured on site (Gueymard and Wilcox, 2011), the operating cell temperature can be either indirectly measured (e.g. by thermography or measuring back-surface temperatures) or estimated using PV thermal modelling. For the case of STPV windows, the cell temperature is influenced by the optical, thermal, electrical and physical properties of the STPV cells/module, the optical and thermal properties of the STPV window assembly and the prevailing climatic conditions such as air mass, solar spectrum, solar angle of incidence and wind speed (Duffie and Beckman, 2006).

When in-depth thermal study is required, energy balance equations can be employed expressing conductive, convective and radiative heat transfer phenomena (Fung and Yang, 2008; Wong et al., 2005). Depending on the model accuracy required, the STPV module layer can be treated as three layers: "frontsheet" layer, "STPV cell and encapsulant" layer and "backsheet" layer (Delisle, 2008; Wong et al., 2008). On STPV modules utilizing Si-based opaque spaced cells, the "STPV cell and encapsulant" layer can be separated into two parts: "STPV cells" part and "encapsulant" part (Fung and Yang, 2008). The latter approach could provide a more accurate estimation of the PV cell operating temperature. Nonetheless, Robinson (2011) measured the temperature gradient across a double glazed, low-e (surface-3), poly-Si STPV window installed in a typical office. Through a year of monitoring data, temperature gradients of less than 1°C were observed. Similar experimental observations were made throughout the literature independent of the STPV packing factor, electrical efficiency, window assembly and size, reinforcing the notion of treating the "STPV cell and encapsulant" layer as an isothermal surface (Infield et al., 2006; Notton et al., 2005; Yoon et al., 2011).

Depending on the cavity geometry and characteristics (non-vented or ventilated cavity, isothermal or anisothermal surfaces), the convective heat transfer coefficients can be approximated using existing correlations or studied in detail using computational fluid dynamics (CFD) methods (Gan, 2009; Han et al., 2013, 2010, 2009; Koyunbaba and Yilmaz, 2012). Thermal bridging occurs due to spacer separating the various window layers as well as due to window frame (Ge and Fazio, 2004; Gustavsen et al., 2007). The edge-of-window might have significantly higher thermal conductance than the centre-of-window thus frame and spacer effects should be accounted on the energy balance equations. Depending on the component complexity, the analysis could be carried out using one-dimensional, two-dimensional of three-dimensional heat transfer.

However, it has been shown that low-order models can be used to predict the operating cell temperature (E. Skoplaki and Palyvos, 2009). The simplest model considers the impact incident solar radiation and (S) and outdoor ambient air temperature (T_o) has on cell temperature (TSTPV) through a linear correlation (Ross, 1976):

$$T_{STPV} = k \cdot S + T_o \tag{2.4}$$

where k is the slope of line $(T_{STPV}-T_o)=k\cdot S$, determined through experimental measurements. A typical value for STPV window is $k=0.0455\ m^2K/W$.

King's model uses an implicit correlation between the measured back-surface temperature (T_{back}) and operating cell temperature (King et al., 2004):

$$T_{STPV} = T_{back} + \frac{S}{S_{ref}} \cdot \Delta T \tag{2.5}$$

where S_{ref} is the reference solar radiation (1000 W/m^2) and $\Delta T=T_{STPV} - T_{back}$. For practical reasons, the back-surface temperature on a STPV window assembly should be the inner surface of the innermost layer of the insulating glazed unit (e.g. surface-4 on a double-glazed window unit) rather than the back of the STPV module.

When the back-surface temperature cannot be measured, it can be estimated using the following empirical model:

$$T_{back} = S \cdot e^{a+b\cdot WS} + T_o \tag{2.6}$$

where a is an empirically-determined coefficient determining the upper temperature limit under low wind speeds and high solar irradiance; b is an empirically-determined coefficient determining the rate at which the back-surface temperature drops with the rise of the wind speed; WS is the wind speed measured at standard 10-m height (m/s), available on meteorological weather data. The empirically-determined coefficients are influenced by the STPV window assembly and mounting arrangement and location.

2.3 Materials and technologies suited for STPV window applications

Existing fenestration materials and technologies can be employed on the STPV window assemblies to enhance their integral performance. An effort is made to present the most promising ones as well as current challenges in the application of such materials and technologies.

2.3.1 Coatings and suspended films

Low-emissivity (low-e) coatings are applied on the glass surfaces facing the window cavities to reduce radiative heat transfer (Han et al., 2010) and thus reduce the U-value and SHGC of the window. Low-e coatings can be categorized on hard and soft coatings (Jelle et al., 2012). Hard coatings are doped metal oxide coatings deposed during glass float line production while soft coatings are dielectric-metal-dielectric coatings applied on the glass surface after manufacturing. As hard coatings are embedded on the glass surface, they are more durable and they are preferred for applications where window handling or degradation due to outdoor air exposure (e.g., STPV/T application) might be an issue (Ando and Miyazaki, 2008).

Suspended films with low-e properties can be used to replace the in-between glass layers of a multi-glazed STPV window (Jelle et al., 2012; Stamenic and Lubun, 2007) effectively reducing the overall thickness and weight of the window assembly as well as its U-values (as low as 0.28 $W/m^2/K$) and SHGC. Despite the wide use of low-e coatings and suspended films on windows, their impact on the electrical performance and temperature profile of the STPV window applications has not been systematically studied.

Self-cleaning film coatings can be adopted and used on the outer surface of the STPV window (surface-1) to reduce accumulation of debris and possibly snow (Midtdal and Jelle, 2013) and thus increase electricity production. A photocatalytic reaction on the titanium dioxide (TiO_2) coating, triggered by UV-radiation, deteriorates the debris that then is removed from rain or atmospheric water vapour.

2.3.2 Cavity gas fills

An additional improvement on the thermal performance of a STPV window can be achieved by replacing the air in the sealed window cavities with noble gases (Ar, Kr and Xe) or mixes (e.g., 90% Ar and 10% air) reducing the convective heat transfer and thus the U-value of a STPV window, without affecting the SHGC (Carmody et al., 2004; Jelle et al., 2012). The optimal thickness of the cavity varies based on the gas or mix used as well as emissivity of glass surfaces facing the cavity.

2.3.3 Window spacers and frames

As in any other window assembly, the importance of highly insulating window spacers and frames is recognized and special attention needs to be given during design and assembly (Figure 2.7). Spacers and framing systems should allow pressure equalization and thermal movement of the STPV window layers while minimize thermal bridging (Ge and Fazio, 2004). An extensive technology and literature review on state-of-the-art window frame systems and spacers can be found at Gustavsen et al., (2007). When STPV windows are installed, minimal re-tooling is required while an additional capping system is used to house the cables and junction boxes and facilitate maintenance (Roberts and Guariento, 2009; Stamenic and Lubun, 2007).

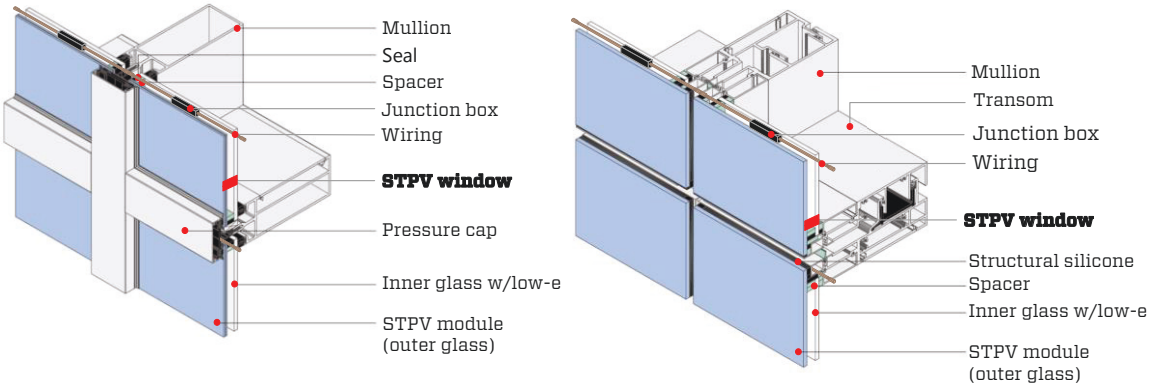

Figure 2.7. Schematics of stick (left) and unitized (right) curtain wall systems integrating STPV windows (Roberts and Guariento, 2009)

2.4 STPV window design and performance studies

For comparative purposes, all existing studies are converted and reported in relation to the total visible transmittance (τ_{vis}) of the insulating STPV window unit under normal angle of incidence. A wide range of design parameters have been studied through experiments or simulations (namely optical properties of STPV window, SHGC, U-value and electrical conversion efficiencies) many of which are strongly linked.

The electrical efficiency of STPV windows is inversely proportional to transmittance and solar heat gain coefficient. As the transmittance of the STPV window increases, less sunlight is captured by the photovoltaic layer and converted to solar electricity and more is transmitted indoors, increasing the solar gains and daylight within the indoor space.

Independently of the design parameters of the STPV window and the building application (e.g., window, skylight, canopy), it is imperative that the STPV module should be the outermost glass layer of the window assembly. Delisle (2008) demonstrated through simulations that by moving the semiconductor layer from outermost glass to the middle glass of a triple glazed window (both assemblies had a low-e coating on surface-5), electrical generation reduction of up to 22% was predicted caused mainly by the reduction of transmitted solar radiation to the PV cells. In addition, operating cell temperatures of up to 16°C higher were anticipated despite the fact that the cavity between outermost glass and STPV layer was naturally vented to outdoors to avoid high temperatures.

2.4.1 STPV window orientation

Façade orientation plays a major role on the potential annual STPV power production, solar heat gains and daylight availability. In general, near equatorial facing façades (e.g., south facing for northern hemisphere) have the highest annual solar potentials for electricity generation, depending of the local weather (Figure 2.8). Equatorial facing skylights with a tilt angle near to the altitude of the building site will maximize the electrical power generation. Whenever optimal orientation is not possible due to site constrains, the STPV façade orientation should be maintained preferably anywhere between ESE and WSW (for the northern hemisphere) while self-shading or shading from adjacent structures should be minimal. When considering the impact STPV windows have on the building energy performance, it was shown that the selection of the ideal STPV optical properties was independent of the building orientation within this orientation range of SE to SW (Chow et al., 2007; Miyazaki et al., 2005; Robinson and Athienitis, 2009).

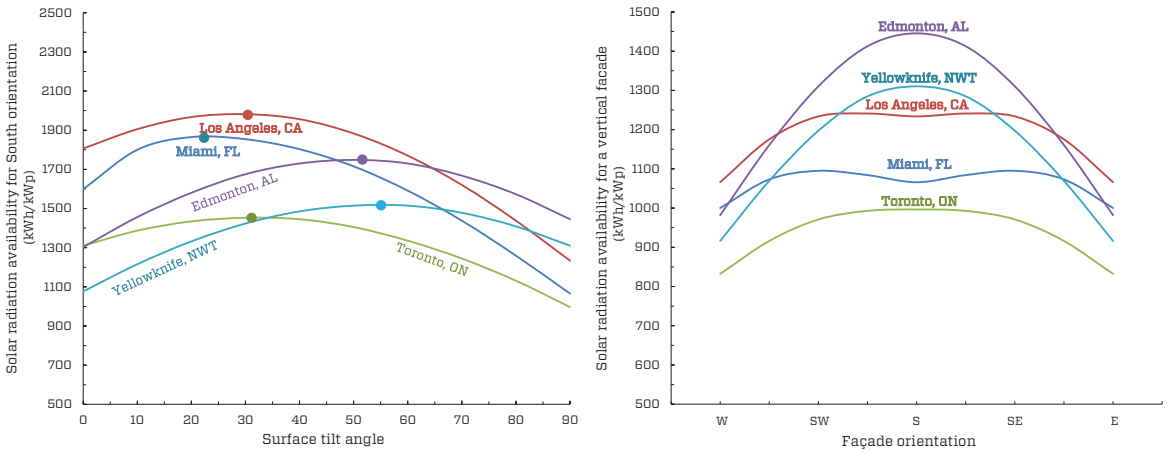

Figure 2.8. Annual solar energy availability for various North American cities under various tilt angles (left) and surface orientations (right). No debris or snow accumulation was taken into account.

2.4.2 Window-to-wall ratio

When it comes to an effective façade design, modestly-sized windows with an integrated strategy to control the transmission of solar radiation (e.g., fixed or dynamic shades, electrochromic windows, STPV windows) are the preferred configuration to simultaneously optimize energy performance and occupancy comfort. Lam, Ge, & Fazio (2016) demonstrated through a simulation-based sensitivity analysis that WWR is the design parameter that has the most significant impact on achieving net-zero energy performance targets for a typical office. Façades with more than a 60% window-to-wall ratio (WWR) should be avoided as they tend to cause visual and thermal discomfort due to excess daylight and solar gains (Dubois and Flodberg, 2012; Tzempelikos and Athienitis, 2007; Vartiainen, 2001).

A simulation-based parametric study was performed for an office building in Japan (Miyazaki et al., 2005). The study used an EnergyPlus model calibrated with a reference building performance data. A shade controlled to block direct sunlight when glare occurred was used. For a south facing façade, the study found that the selection of ideal STPV window optical properties was sensitive to the WWR. For WWR=30%, 40% and 50% the ideal visible transmittance of STPV window was found to be τ_{vis}=63%, 48% and 32%, respectively.

Olivieri et al. (2014) used COMFEN simulation tool to study the impact of STPV windows on an office building in Madrid, Spain. For 33%≤WWR≤66% the ideal visible transmittance was found to be τ_{vis}=16% to 25% while for WWR<33% and WWR>66% it was found to be τ_{vis}=32% and 10%, respectively. In addition to the energy performance analysis, a glare assessment was carried out for the various transmittances under CIE clear and overcast sky conditions (for summer solstice, winter solstice and equinox). During clear sky conditions, the maximum surface illuminance did not exceed 2000 lx, for all cases. However, the possibility for glare to occur during the winter solstice (low solar altitude) was rather high. This was due to the fact that the study considered no shading devices.

2.4.3 STPV facade design

An effective building façade design can reduce building operating costs while creating a pleasant, glare-free, indoor environment (Carmody et al., 2004). The three-section façade concept is one example. The three-section façade consists of: (i) a bottom "spandrel section" that extends up to workplane height (0.8 m above the floor) and it is opaque as it contributes little to daylight (Dubois and Flodberg, 2012), (ii) a middle "view section" which normally extends from the workplane to about 2.0m above the floor and it allows a view to the outdoors (Boyce et al., 2003) and (iii) a top "daylight section" that admits daylight deep into the room and it should be designed to protect occupants from direct solar radiation and glare (Galasiu et al., 2004).

When the three-section façade design incorporates STPV windows on the "daylight" and "view" sections, it could also turn the building façade into a solar power plant. A simulation study was performed for a STPV façade on a typical south-facing office using the DeLight simulation tool (Vartiainen, 2001). Nine curtain wall configurations were simulated based on the three-section façade concept for five European cities (latitudes from 38°N to 67°N). The model was experimentally validated (Vartiainen et al., 2000). The study found that a façade configuration with translucent STPV windows (τ_{vis}=18.4%) on the "daylight section: and clear STPV windows (τ_{vis}=18.4%) covering part of the "view section" maximized annual daylight utilization and solar electricity yield, independently of the geographic location. Venetian blinds were used on the "view section", controlled to block direct sunlight at all times, while no blinds were necessary for the "daylight section" due to diffuse nature of transmitted light through the translucent STPV windows.

A similar simulation study was performed for five Canadian cities (latitudes from 43°N to 63°N) using a radiosity-based model validated with experimental data (Robinson, 2011). The study was differentiated by the fact that the "view section" fully incorporated clear glass windows rather STPV ones. The analysis showed that STPV windows installed on the "daylight section" with τ_{vis}=9% to 18% maximized the daylighting and electrical performance of the STPV façade, independently of office orientation, geographic location and STPV efficiency.

As a counterexample, a simulation study utilizing Adeline simulation tool suggested that the optical properties of the STPV window (simulated for τ_{vis}=7% to 34%) integrated on the "daylight section" had little impact on the daylight performance of an office in Madrid, Spain (De Boer and van Helden, 2001). This is possibly due to the fact that the "view section" alone, incorporating clear glass windows, provided adequate daylight into the office.

2.4.4 Optical properties of STPV windows

Experimental studies have demonstrated that the colour rendering of STPV windows partly depends on the PV technology utilized (Lynn et al., 2012). STPV windows integrating a-Si thin film and crystalline Si-based cells provide colour neutrality and excellent colour rendering. On the other hand, a-Si/μc-Si and organic STPV currently available in the market, yield red, blue or green shift in colour.

In regards to window tint, one-direction colour shift is less preferable when compared either to a two-direction colour shift or colour neutrality (Pineault and Dubois, 2008). Thus, STPV window technologies that yield one-direction shift should be avoided on façades where visual comfort and view to the outdoors is of a major importance (e.g., offices, classrooms). Such STPV technologies can still be exploited as elements on façades, skylights and canopies where colour neutrality and rendering is not of a major concern (e.g., atria, corridors). Besides the visual environment, the spectral properties of STPV windows also impact the solar heat gains (Gueymard and DuPont, 2009) and its electrical performance (Park et al., 2010).

2.4.5 Thermal properties of the STPV windows

The thermal performance of STPV is an area that needs urgent attention because it exerts a significant influence on the durability of the STPV and other window components such as spacers, sealants and framing. Excessively high temperatures need to be predicted either through testing and/or simulation. The allowable temperature rise depends on the STPV technology implemented (e.g., organic, Si-based, etc.). Despite the common use of low-e coating and suspended films on window assemblies, no systematic study has been made to investigate their impact into the PV cell temperature and power output of a STPV window. When PV cell overheating is of a concern, the window sealed cavity can be replaced with a ventilated one, turning the façade into an active thermal collector (STPV/T) in addition to the electricity generation and daylight transmission (Gaillard et al., 2014a). The absorbed solar energy that is converted into heat is recovered either actively, using a fan or pump, or passively by a heat removal fluid flowing on the rear side of the STPV module. As the fluid circulates behind the PV cells, it cools down the cells through convection and increasing their electrical efficiency.

Measurements on Mataro library, in Madrid, Spain, showed STPV cell temperatures of up to 50°C for a mechanically ventilated double skin STPV façade, while inner glass surface temperatures of up to 32°C were measured with top to bottom temperature gradient of less than 1°C (Infield et al., 2006). Gaillard et al. (2014) reported cell temperatures up to 60°C for a naturally ventilated double skin façade installation in Toulouse, France, with a cell temperature gradient up to 10°C on the vertical axis. Peng et al. (2013) measured the thermal performance of double skin STPV façade under various air flow modes (non-ventilated, naturally ventilated and mechanically ventilated), in Hong Kong, China. It was found that as the nature of the air flow changed, the U-value increased (3.4, 3.8 and 4.6 $W/m^2 \cdot K$, respectively), while the SHGC decreased (0.13, 0.12 and 0.1, respectively). In addition, compared to non-ventilated mode, naturally ventilated cavity resulted to a reduction of up to 1.5°C PV module temperature while mechanically ventilated to a reduction of up to 6.3°C. Guardo et al. (2009) investigated a similar configuration using CFD. The authors concluded that the reduction on SHGC was due to the increase on air mass flow rather than turbulence mixing effects.

When it comes to integration of STPV technologies on insulated glazing units, De Boer and van Helden (2001) predicted STPV window temperatures of up to 65°C while Wong et al. (2008) predicted STPV skylight temperatures of up to 75°C. Up to 60°C PV cell operating

temperatures were measured, with no significant temperature gradient, for a STPV office installation in Yongin, South Korea (Yoon et al., 2011). Delisle (2008) found that U-value had little impact on the STPV annual electrical performance. The STPV window assemblies were considered on the "spandrel" section of an office building located in three major Canadian cities, assuming that the daylight transmitted through it was not significant (maximum possible packing factor). The simulations (using TRNSYS) revealed that when the STPV module is the outermost glass of the window assembly (a double glazed and triple glazed STPV window were studied, with low-e coating on surface-3 and surface-5, respectively), the electrical performance and operating cell temperatures were very similar, while there was a decrease of 6 percentage points on the annual space heating energy consumption when upgrading from a double glazed STPV window to a triple glazed one, mainly due to the decrease of the U-value of the STPV window.

Vats et al. (2012) compared the PV cell operating temperatures of a STPV and a mechanically ventilated STPV/T system for roof and façade applications. The simulations showed that the PV cell temperatures on a STPV/T can be up to 5.5°C higher compared to a STPV depending on the mass flow rate. This was due to the fact that the inlet air drawn through the STPV/T façade was from the indoor environment.

2.4.6 Test and characterization of STPV windows

Considering the current advancements on the window industry such as electrochromic windows, STPV windows or windows incorporating angular selective coatings (Fernandes et al., 2015; Jelle et al., 2012), Solar Calorimetric Standards should be updated to address current challenges and provide guidelines on how to test such technologies. Another important consideration is the thermal behaviour of such windows. Excessively high temperatures for prolonged periods should be predicted and, if possible, avoided. Few studies have addressed the need for new testing standards for the determination of the SHGC, U-value, and electrical performance of STPV systems (and building integrated photovoltaic technologies in general).

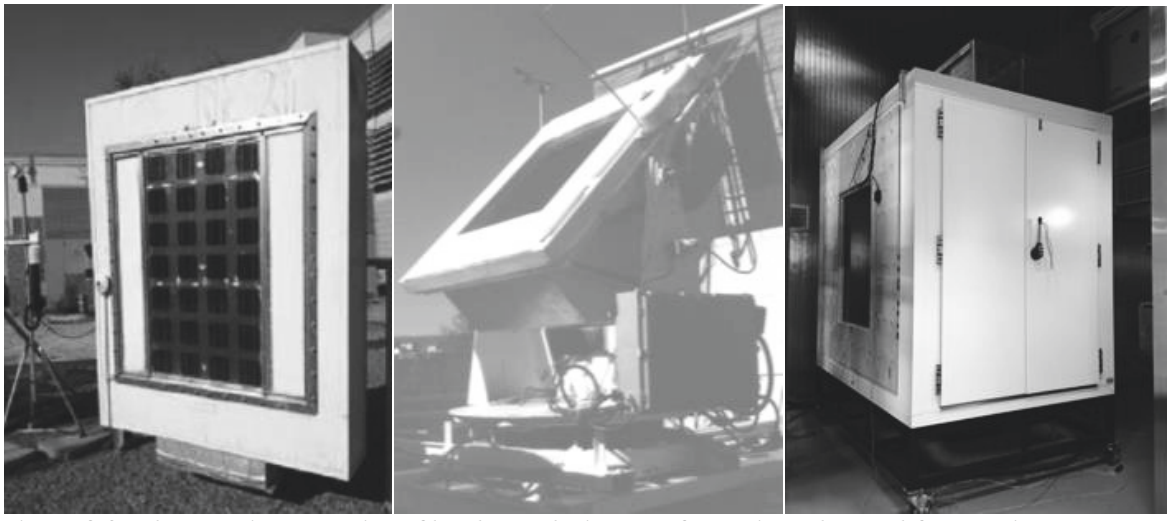

Figure 2.9. Three main categories of hot box calorimeters for testing advanced fenestration systems: an outdoor solar fixed (Bloem et al., 2012), an outdoor solar tracking (Harrison and Collins, 1999) and an indoor calorimeter utilizing a solar simulator at Concordia University.

Fully controllable conditions, repeatability and the ability to reach and maintain steady-state conditions are necessary to determine performance parameters such as SHGC and U-value of advanced fenestration systems. While the use of outdoor solar calorimeters (Figure 2.9) provide the ability to test window technologies under realistic and dynamic climatic conditions, repeatability has proved to be challenging due to variation of the outdoor temperature, wind speed and direction, sky conditions, air mass, solar spectrum and solar angle of incidence (Marinoski et al., 2012; Pereira and Sharples, 1991). Olivieri et al. (2014; 2013) proposed a methodology for the optical electrical and thermal characterization of STPV windows utilizing an outdoor calorimeter. In order to reduce measurement uncertainties due to dynamic conditions, a comparative analysis with a reference specimen of known properties was performed, tested side-by-side with the STPV specimen.

Solar tracking calorimeters have been utilized in order to achieve quasi-steady conditions by maintaining normal incidence. However, it has been shown that the tilt angle of the window might introduce uncertainties on the surface heat transfer coefficients and possibly distort the measurements while the view factor of the window-to-ground varies as the tilt angle of the calorimeter changes (Harrison and Collins, 1999; Tseng and Goswami, 2001). Bloem et al. (2012) developed an outdoor calorimeter to determine the electrical and thermal output of STPV/T windows. Free-rack mounted and rear-insulated reference modules were used for a comparative analysis.

On the other hand, there are efforts to develop an international standard (ISO/DIS 19467) for the determination of SHGC of conventional and advanced fenestration systems such as STPV windows, using a solar simulator (ISO, 2015). Indoor calorimetry utilizing a solar simulator provides the necessary control and test repeatability under steady state or dynamic conditions. However, solar spectrum mismatch should be taken into account while high collimation and uniformity are necessary for the test and characterization of STPV windows. Chen et al. (2012) introduced an indoor calorimetric facility for STPV window testing and determination of the SHGC and electrical performance. The facility utilized a continuous single-lamp solar simulator. In order to achieve high uniformity and light collimation under variable angle of incidence, the lamp was located 10 m away from the specimen while a correction factor was applied to accommodate for the spectral mismatch.

2.4.7 Occupancy behaviour on the control of motorized shades

It has been shown that the patterns of manually controlled shades have a decisive impact on the appropriate selection of façade optical and thermal properties – including STPV windows – due to "effective" available daylight and heat gains in the space. The current approach on designing a STPV façade is either assuming that there are no shades (design based on worst case scenario) or assuming a simplified control strategy (e.g. fully closed shades, when glare occurs). Occupant observational studies demonstrate that both scenaria are unrealistic (Gunay and O'Brien, 2016; O'Brien et al., 2013; Van Den Wymelenberg, 2012) resulting to suboptimal façade design and performance.

Occupants tend to be inactive shade users (less than one shade adjustment per day) (Inoue et al., 1988; Kapsis et al., 2013; Lindsay and Littlefair, 1992; Sutter et al., 2006). Instead of being highly-responsive to glare conditions, occupants tend to leave their shades in a position that "causes the least trouble" (Bordass et al., 2001). Moreover, they reposition themselves when glare occurs (Osterhaus, 2005). As a result, buildings tend to have much higher shade occlusions than instantaneous weather conditions would suggest. This might lead to suboptimal façade design that in-return might result to unnecessary electric lighting use and ultimately inflates energy use relative to what building designers might expect.

More than a dozen researchers have studied dynamic shade use in real buildings for duration of days to six years. The studies have generally concluded that for mechanically (HVAC) conditioned spaces, solar-related factors are the greatest motivators for shade movement and that indoor or outdoor temperature has little impact on it. Occupants in naturally conditioned spaces do use shades to help regulate thermal comfort as the indoor temperature and skin temperature is strongly related to the solar gains (Inkarojrit, 2005; Reinhart and Voss, 2003; Sutter et al., 2006).

Façade orientation and solar penetration depth into an office are among the best predictors of shades position. The literature consistently reports that near south-facing façades have the greatest mean shade occlusion and near north-facing façades have the least (Inkarojrit, 2008; Mahdavi et al., 2008), while for near east and west, it falls in between (Pigg et al., 1996; Zhang and Barrett, 2012). However, there is a considerable variation between studies. Many researchers have acknowledged that their results are skewed by unique building characteristics or occupancy patterns, including: façade design, multiple sets of shades per space, multiple occupancy, views and privacy, and automated lighting controls, to name a few. On the contrary , Inoue et al. (1988), and Reinhart and Voss (2003) found that solar penetration depth is a good predictor for the shade position (when the direct solar radiation exceeds about 50W/m^2), with their results to be in a good agreement.

Rubin, Collins, and Tibbott (1987) has shown that occupants put significant thought into shade position, while when they have easier access to shades control (e.g., shades controlled with a wall-mounted switch instead of a manual rod) or there is an automated artificial lighting control system, they tend to be more active users (Pigg et al., 1996; Sutter et al., 2006). Haldi and Robinson (2010) noted that occupants do not specifically control their shades to improve future anticipated conditions. This finding is very important, as it indicates the value in automated shade controls with a predictive element. With only a few exceptions, the studies indicate that shade occlusion and shade movement increase with higher levels of solar radiation, which supports the notion that universally-accurate shade use models can be created. Currently, there is a sufficient lack of understanding in manually controlled shade use to justify further and more extensive studies.

2.4.8 HVAC system and daylighting/lighting controls

In general, the building typology and energy systems have an impact on the selection of the ideal STPV properties. De Boer and van Helden (2001) found that façade orientation, tilt

angle and building internal loads had stronger impact into the energy performance of the building than the selection of optical and electrical properties of the STPV window. Miyasaki et al. (2005) found that the selection of ideal double glazed STPV window optical properties was not sensitive on the Coefficient of Performance (COP) values assumed for the HVAC system. Chow (2007) drew similar conclusions for a double glazed STPV window naturally vented to the outdoors, a design solution proposed to reduce operating PV cell temperatures and heat gains to indoors.

Miyasaki et al. (2005) and Robinson (2011) found that depending on the electric lighting control strategy applied (on/off versus continuous dimming), the parametric analysis led to different selection of STPV window optical properties in order to maximize the energy benefits. Both studies considered shades controlled to maintain visual comfort. On the other hand, the selection of the optical properties of the roller shade was shown to have little impact on the selection of ideal optical properties for the STPV window (Robinson, 2011).

Wong el al. (2008, 2005) conducted the only study that investigated the integral energy performance of poly-Si STPV skylights (south facing roof on a tilt angle of 30°) on residential applications, for five Japanese cities. The study found that the use of unshaded double glazed STPV skylight increased the building energy consumption when compared to an opaque BIPV roof system. The increase was attributed to undesirable heat gains during cooling season and night heat losses during heating season. However, when a controlled shade with U-value of 0.13 $W/m^2 \cdot K$ (namely cellular shades) was used, energy savings of up to 9% were attained for an STPV skylight of τ_{vis}=0.5. It should be noted that no measures to reduce the thermal conductance of the STPV window assembly were considered (e.g., use of low-e coating, sealed cavity filled with Ar), while the lighting needs were mainly satisfied from the existing windows.

2.4.9 STPV window economic feasibility studies

Despite the various studies on BIPV and BIPV/T economic appraisals, only a few have focused on STPV applications. Moreover, the PV average module prices have decreased by 85% in six years (end of 2008, the average crystalline-Si module price was USD 4.05/Wp while end of 2014, it was USD 0.6/Wp) (IEA-PVPS, 2015), while the system price widely varied, depending mainly on the nature and size of the installation. The price reductions on PV module and systems have been so rapid that many of the studies could be considered obsolete (Figure 2.10). James et al. (2009) carried out an economic analysis investigating the capital and annual operational costs for five shading solutions (fritted glass, STPV windows, automatic interior roller shades, exterior fixed louvers and exterior one-axis tracking louvers) for an atrium application in Southampton, England. The analysis showed that STPV had the highest capital cost at the time, mainly due to USD 4-4.5/Wp mono-Si PV module prices, but the lowest building operational cost due to the ability to generate electricity and reduce the electricity imported from the grid. In addition, a future scenario was analysed, for when STPV module prices reach USD 1/Wp and estimated that only fritted glass would have lower nominal cost than STPV windows while all other shading solutions had significantly higher nominal and operational costs. The analysis did not consider the energy savings on heating,

cooling and electric lighting consumption, affected and varied from system to system. Nevertheless, it demonstrated that STPV applications can be a cost effective solution when it comes to new or retrofit commercial and institutional buildings.

Bizzarri (2011) performed a preliminary economic analysis for a double skin façade retrofit for an office building. A payback period of 57 years was estimated when no incentives were considered. Taken into account the Italian national feed-in tariff, the payback period was reduced to 16 years. It should be noted that no optimization on the selection of optical and thermal properties of the STPV double skin façade was delivered. Instead, the use of an existing STPV product was considered. Li et al. (2009b) estimated a simple monetary payback of 18 years considering the electricity tariff only for an office building in Hong Kong, China. It should be noted that the analysis was delivered with the assumption of utilizing a market available single glazed STPV window product. However, if the optical and thermal properties of such a product are optimized to reduce heating/cooling loads and maximize power production, the payback could be reduced even further.

Finally, an economic feasibility study of STPV window integrated on greenhouse roofs in Sardinia, Italy, showed a payback period to vary between 10-13 years (depending on the STPV roof configuration) when the local feed-in tariff was considered (Cossu et al., 2010).

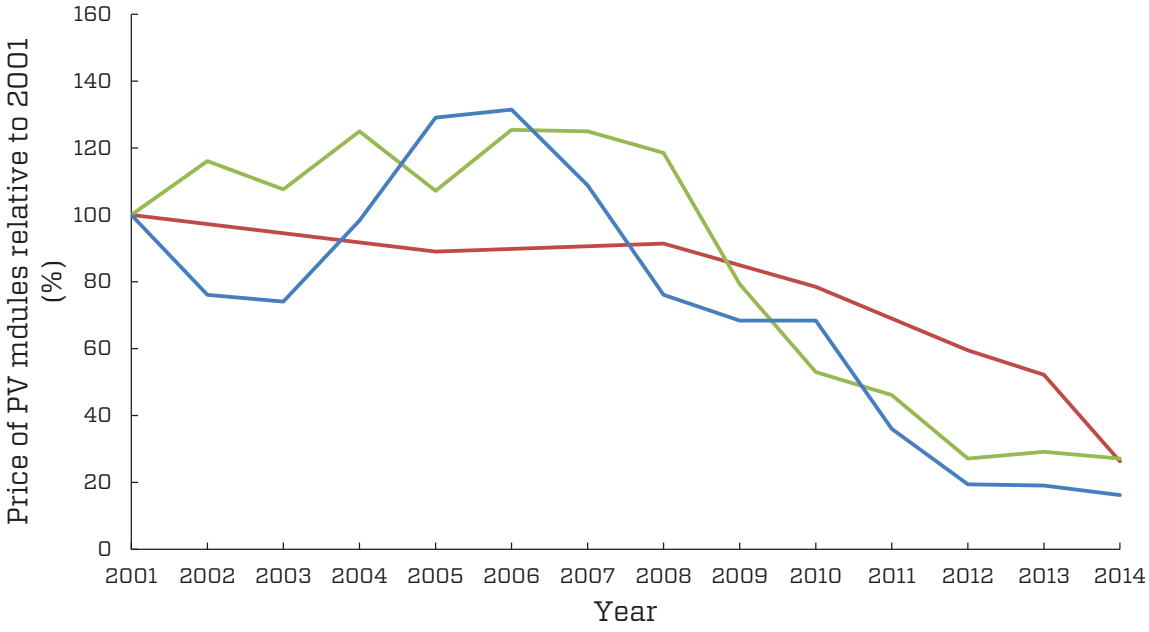

Figure 2.10. PV modules prices normalized to 2001 for three indicative countries (IEA-PVPS, 2015).

2.5 STPV windows and other advanced fenestration technologies

Various comparative studies have been performed between STPV windows and other advanced fenestration technologies in efforts to identify advanced window technologies suited to specific applications. STPV windows and skylights can significantly lower building cooling peak loads on cooling dominated climates, when compared to tinted glass (Li et al., 2009a, 2009b). Chow et al. (2010) investigated the potential impact fenestration technologies such as reflective glazing, electrochromic windows, vacuum windows and STPV windows have on the reduction of heat gains on cooling dominated buildings. The authors exhibited that the integration of STPV technologies can be as effective as reflective window with the additional benefit of electricity generation. Bahaj et al. (2008) simulated the impact electrochromic glazing, holographic optical elements, aerogel glazing and STPV windows have on highly glazed buildings in Dubai, UAE. The study concluded that STPV window is potentially a promising solution. By covering 40% of the glass façade with STPV windows, the electricity consumption for air conditioning can be reduced by 31% (including electricity offset due to solar electricity generation) when compared to state-of-the-art double glazed low-e window.

Bizzarri et al. (2011) simulated the performance of a double-skin façade retrofit for an office building in Ferrara, Italy. For a SW-facing STPV façade, an 82% reduction on annual solar heat gains was estimated when compared to a clear glass double skin façade retrofit. This reduction resulted to a significant increase on annual heating demand (from 4.7 kWh/m^2/yr to 31.9 kWh/m^2/yr), while annual cooling demand was reduced by 52% (from 67.5 kWh/m^2/yr to 32.2 kWh/m^2/yr). Qiu et al. (2009) simulated the thermal and electrical performance of a double skin STPV façade (non-ventilated and natural ventilated) and compared to a single absorptive glazing typically used in Shanghai, China. The non-ventilated configuration resulted to a reduction on end-use electricity consumption of 10%, while the natural ventilated configuration to a reduction of 13%, with no significant difference on STPV annual electrical performance between the two STPV configurations. The authors noted that a mixed mode might be preferable in order to maximize the energy benefits by ventilating the cavity during cooling season while maintaining the cavity closed during heating season.

2.5.1 STPV electrochromic windows

A novel window technology is stand-alone STPV electrochromic windows (Baetens et al., 2010; Bullock et al., 1996). STPV electrochromic windows combine the main benefits of STPV devices and electrochromic one: generation of solar electricity and control of SHGC and visible transmittance (Moeck et al., 1998). STPV electrochromic windows can be found as (Deb et al., 2001; Dyer et al., 2014): (i) side-by-side devices with the STPV module being the outer glass layer and the electrochromic device being the inner one or (ii) a monolithic device utilizing a-Si or DSC. The current limitation on the monolithic device is that when the electrochromic layer is dimmed down, it shades the STPV layer resulting to significant reduction of electricity generation.

2.6 Research opportunities

Through an extensive literature and technology review, the following major research needs were identified and tackled through this thesis:

- *STPV windows design and performance*: The majority of STPV window products in the market tend to be optimized primarily for power generation, overlooking particularly thermal and daylighting requirements. There has been limited work on the integral (solar electricity, thermal and daylighting) performance of STPV window systems and their passive and active interaction with building energy performance and occupants' comfort, especially for cold climates. In addition, no robust methodology exists to guide PV, window and building industries to develop near optimal STPV window designs that can incorporate some of the positive attributes of traditional glazing and reduce or even neutralize its negative impacts;
- *Thermal behaviour of STPV windows:* The thermal performance of STPV windows is an area that needs urgent attention because it exerts a significant influence on the durability of the STPV and other window components such as spacers, sealants and frames. Excessively high temperatures need to be predicted either through testing and/or simulation. The allowable temperature rise depends on the STPV technology implemented. Despite the common use of low-emissivity coatings and suspended films, no systematic study has been made to investigate their impact on STPV cell operating temperature and its solar energy yield;
- *Development of STPV window test procedures*: Few studies have addressed the need for new testing standards for the determination of the solar heat gain coefficient (SHGC), thermal conductance (U-value), and electrical performance of STPV windows (F. Chen et al., 2012; Olivieri et al., 2013). STPV windows should be treated and tested as PV and fenestration technologies. Further experimental research is required to develop a new standard test procedure. The new standard should combine together – but not limited to – existing test standards for window systems and PV modules.

Chapter 3
Determination of Solar Heat Gain Coefficient for Semi-Transparent Photovoltaic Windows: an Experimental Study[1]

Abstract

Semi-Transparent Photovoltaic (STPV) windows integrate transparent photovoltaic film technologies or spaced opaque solar cells on the exterior glass layer. As these technologies are being developed and eventually adopted in the building and window industry, the evaluation of key performance parameters such as the solar heat gain coefficient (SHGC), thermal conductance (U-value) and electrical power output is required. These performance parameters are interdependent and they have a direct impact on the building cooling, heating, electric lighting loads, solar electricity generation and occupancy comfort. Thus, STPV windows should be treated as integrated photovoltaic and fenestration technologies. This study focuses on the experimental determination of the SHGC of STPV windows under maximum power point operation, utilizing an indoor solar simulator and calorimeter facility. The objective of this work is to provide input on the development of an experimental procedure suited to the determination of the SHGC of STPV windows. The results indicate that the solar electricity generation of the STPV window must be considered during the experimental determination of the SHG). Failure to do so may lead to up of 23% (for a STPV window with visible transmittance of 6% and nominal conversion efficiency of 15%) higher SHGC measured values compared to a STPV window operating under maximum power point tracking conditions.

3.1 Introduction

Semi-transparent PV (STPV) windows have a great potential for integration in fenestration systems, adding the option of solar electricity production while still fulfilling daylighting needs. In commercial and high-rise residential buildings where trends in architecture already include large glazed façades and lighting loads constitute a significant portion of the overall energy consumption, the integration of this technology is promising.

A typical STPV glass consists of a PV layer laminated between a transparent frontsheet and backsheet (Figure 3.1). Depending on the PV technology used, the PV layer may be located between the encapsulation resin or it is monolithically deposited on the transparent conductive oxide (TCO) frontsheet or backsheet. Various PV technologies are used for STPV glass applications, with the most common being opaque crystalline Si PV cells arranged in a way

[1] Kapsis, K., Athienitis, A.K., & Harrison, S., 2016. Determination of solar heat gain coefficient for semi-transparent photovoltaic windows: an experimental study. ASHRAE Transactions 125.

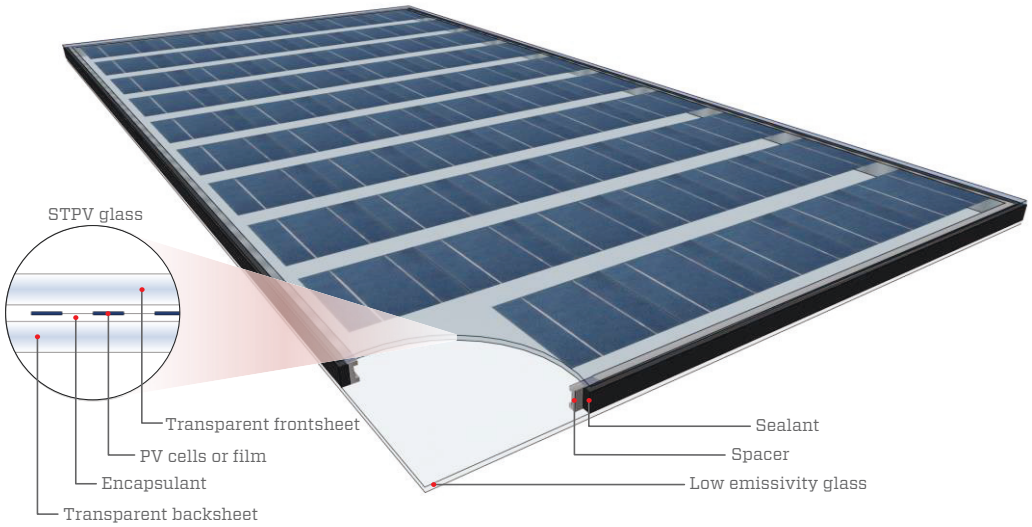

Figure 3.1. Schematic of a double glazed STPV window integrating a crystalline Si STPV glass as the outer layer.

which allows light to pass through the resulting space between the cells, and a-Si/μc-Si "see-through" thin PV films. Other emerging technologies include fully transparent polymer-based PV (Li et al., 2012) and perovskites (Snaith, 2013).

STPV glass can be integrated as the outer layer of insulated glazing units (referred to as "STPV window" herein). STPV windows can then be installed in new or retrofitted commercial and high-rise residential building façades and skylights. Their utilization has the potential to reduce building energy consumption through solar electricity generation, reduce solar gains by partial shading (Miyazaki et al., 2005; Ng et al., 2013) while still allow daylight transmission and partial or full view to the outdoors (Markvart et al., 2012; Vartiainen, 2001).

A deeper understanding of STPV technologies will allow the PV and window industry to provide the necessary materials and designs for high performance windows. When solar radiation strikes a window surface, it is partly reflected (ρ), partly transmitted (τ) and partly absorbed (α):

$$\rho(\lambda,\theta)+\tau(\lambda,\theta)+\alpha(\lambda,\theta)=1 \tag{3.1}$$

where λ is the wavelength and θ the solar angle of incidence. In the case of a STPV window, a fraction of the energy absorbed is transformed to solar electricity while the rest is transformed to thermal energy:

$$\alpha(\lambda,\theta)=N_{out}\alpha(\lambda,\theta)+N_{in}\alpha(\lambda,\theta)+\eta_{el}(\lambda,\theta) \tag{3.2}$$

where N_{out} is the fraction of absorbed solar energy reemitted outwards, N_{in} is the fraction reemitted inwards and η_{el} is the fraction of incident solar radiation that is absorbed and converted to solar electricity also known as electrical conversion efficiency.

Commercially available STPV windows can convert between 5-20% of the incident solar radiation into electricity, while the portion of solar energy that is converted into heat (roughly 30-70%, depending on the optical and thermal properties and PV technology used) contributes to the increase in temperature of the PV cells. Electrical efficiency is dependent on the optical, thermal and electrical characteristics of the STPV window, as well as the climatic conditions, air mass, solar spectrum and solar angle of incidence (Duffie and Beckman, 2006). STPV window efficiency generally decreases as the operating temperature increases, almost in a linear fashion of up to -0.55%/°C, depending on the STPV technology used (Athienitis and O'Brien, 2015). Operating temperatures exceeding 75°C have significant influence on the durability of the PV cells or films and window components such as spacers, sealants and framing. The optical and thermal properties of the STPV window as well as the presence of low emissivity coatings or suspended films have a direct impact on operating temperatures, window electrical performance and durability (Chow et al., 2010; Gaillard et al., 2014b; Park et al., 2010).

Of particular importance is the solar heat gain coefficient (SHGC) which is the fraction of the solar radiation entering the space through the window assembly, consisting of the solar transmittance and the inward-flowing fraction of absorbed solar energy (ASHRAE, 2013):

$$SHGC(\lambda,\theta) = \tau(\lambda,\theta) + N_{in}\alpha(\lambda,\theta) \tag{3.3}$$

The SHGC depends on the optical and thermal properties of the window assembly, the climatic conditions, air mass, the solar spectrum and solar angle of incidence (Klems, 2000; Kuhn et al., 2001). In a STPV window, it is also influenced by the electrical conversion efficiency of the STPV glass; the higher the efficiency, the lower the SHGC — more absorbed solar energy is transformed to electricity rather than into heat. Thus, a systematic study is required to experimentally determine and predict such interactions. It is essential to measure key properties (namely SHGC and U-value) of advanced fenestration systems as they have a direct impact on building energy performance and occupancy comfort.

Considering the current advancements on the window industry such as electrochromic windows, STPV windows or windows incorporating angular selective coatings (Fernandes et al., 2015; Jelle et al., 2012), Solar Calorimetric Standards should be updated to address current challenges and provide guidelines on how to test such technologies. The objective of this paper is to provide input on the development of an experimental procedure suited to determine the SHGC of STPV windows. Another important consideration in the performance of such windows is determining the temperature distribution so as to find ways to avoid excessively high temperatures for prolonged periods. Few studies have addressed the need for new testing standards for the determination of the SHGC, U-value, and electrical performance of STPV systems (and building integrated photovoltaic technologies in general).

Fully controllable conditions, repeatability and the ability to reach and maintain steady-state conditions are necessary to determine the SHGC and U-value of fenestration systems. While the use of outdoor solar calorimeters provides the ability to test window technologies under realistic and dynamic climatic conditions, repeatability has proved to be challenging. Variation

of the outdoor temperature, wind speed and direction, sky conditions, air mass, solar spectrum and solar angle of incidence (Marinoski et al., 2012; Pereira and Sharples, 1991) result to transient or quasi-steady test conditions. Olivieri et al. (2014; 2013) proposed a methodology for the optical electrical and thermal characterization of STPV windows utilizing an outdoor calorimeter. In order to reduce measurement uncertainties due to dynamic conditions, a comparative analysis with a reference specimen of known properties was performed, tested side-by-side with the STPV specimen.

Solar tracking calorimeters have been utilized in order to achieve quasi-steady conditions by maintaining normal incidence. It has been shown that the tilt angle of the window might introduce uncertainties on the surface heat transfer coefficients and possibly distort the measurements (Harrison and Collins, 1999; Tseng and Goswami, 2001). The view factor of the window-to-ground also varies as the tilt angle of the calorimeter changes impacting the radiative heat exchange between the window and skydome. Bloem et al. (2012) developed an outdoor calorimeter to determine the electrical and thermal output of STPV/T windows. Free-rack mounted and rear-insulated reference modules were used for a comparative analysis.

On the other hand, there are efforts to develop an international standard (ISO/DIS 19467) for the determination of SHGC of conventional and advanced fenestration systems such as STPV windows, using a solar simulator (ISO, 2015). Indoor calorimetry utilizing a solar simulator provides the necessary control and test repeatability under steady state or dynamic conditions. However, solar spectrum mismatch should be taken into account while high collimation and uniformity are necessary for the test and characterization of STPV windows. Chen et al. (2012) introduced an indoor calorimetric facility for STPV window testing and determination of the SHGC and electrical performance. The facility utilized a continuous single-lamp solar simulator. In order to achieve high uniformity and light collimation under variable angle of incidence, the lamp was located 10 m away from the specimen while a correction factor was applied to accommodate for the spectral mismatch.

3.2 Experimental setup and methodology

The characterization and performance tests of the STPV windows were performed at the Solar Simulator and Environmental Chamber (SSEC) laboratory at Concordia University, Montreal, Canada. The experimental study presented below allows the determination of solar, thermal and electrical performance of STPV windows.

3.2.1 Solar simulator

The Concordia University indoor solar simulator is a continuous lamp field that consists of eight metal halide (MHG) lamps emulating the sunlight and a test bench where the solar calorimeter is attached (Figure 3.2). The solar simulator is located in a space where room temperature (T_{amb}) is regulated at 21°C ±1°C and relative humidity of 30% ±5%. It can be positioned from 0° (horizontal position to e.g., emulate a flat roof) to 90° (vertical position to e.g., emulate a vertical façade) and virtually to any tilt angle in-between (e.g., at 30° - 45° to

emulate the slope of a roof). For this study, all tests were performed in a vertical position and at normal incidence angle.

Spectrum: The spectral quality of the lamps fulfils the specifications of the standard ISO 9806:2013 (ISO, 2013), with approximately 80% of the emitted radiation lying in the range in which the incidence angle modifier varies by no more than 2%. An UV/Vis/NIR spectroradiometer with a spectral range of 200 nm to 2500 nm was used to measure the solar simulator spectrum. Figure 3.3 shows the normalized solar simulator spectrum in comparison to the AM 1.5 reference spectrum (NFRC, 2014b). A spectral mismatch correction factor is applied to accommodate for the difference between the solar simulator spectrum and the AM 1.5 reference spectrum (F. Chen et al., 2012; Harrison and Wonderen, 1994).

Irradiance uniformity: The solar simulator irradiance intensity (S) can vary from 500 W/m^2 to 1200 W/m^2 with a uniformity of up to 97% (depending on the dimensions of the window) and a temporal stability of ±1% during the testing period (Appendix A). A calibrated pyranometer (temperature compensated detector) with a cosine response and a spectral range of 285 nm to 2800 nm is used to scan the window area on a scanning grid of maximum spacing 0.15 m (NFRC, 2010). The spatial mean is deduced by a simple average. In addition, a calibrated mono-Si reference solar cell is also used to measure the irradiance intensity available to the poly-Si based PV glass for electricity conversion (Dunn et al., 2012).

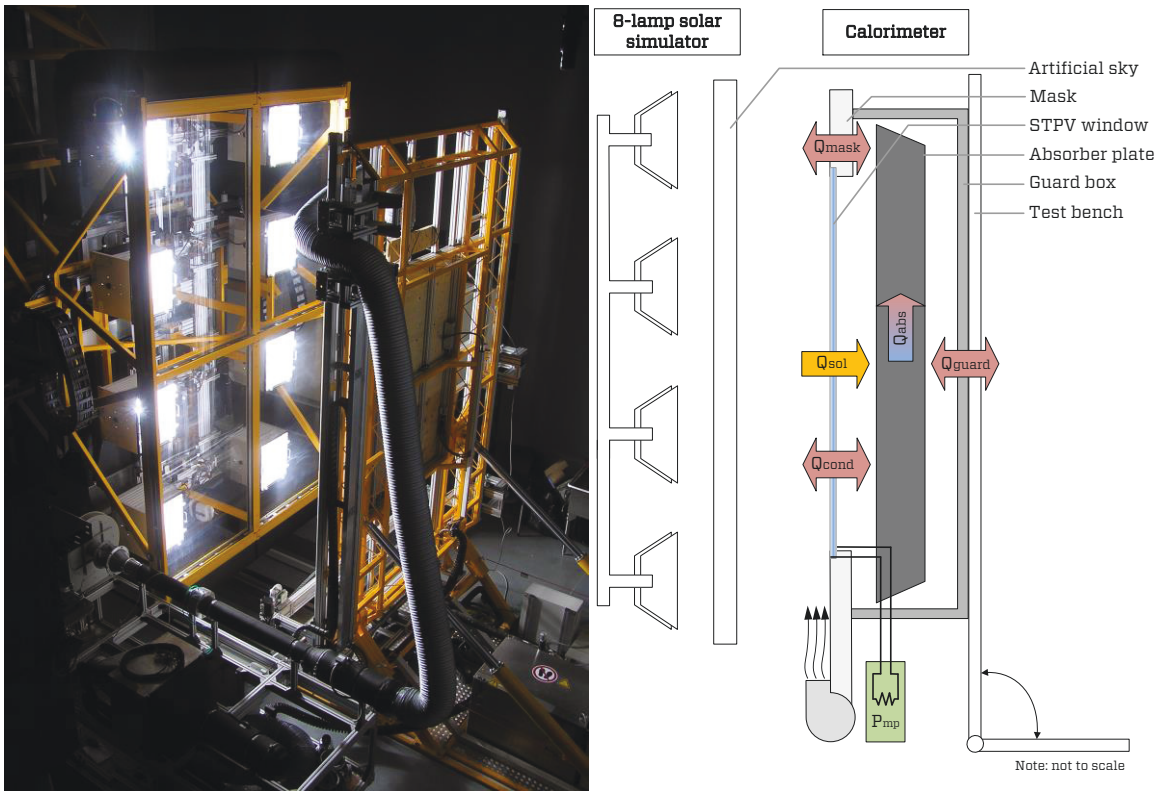

Figure 3.2. Test of STPV window prototypes using the solar calorimeter apparatus at Concordia University solar simulator laboratory (left) and schematic of the experimental setup (right).

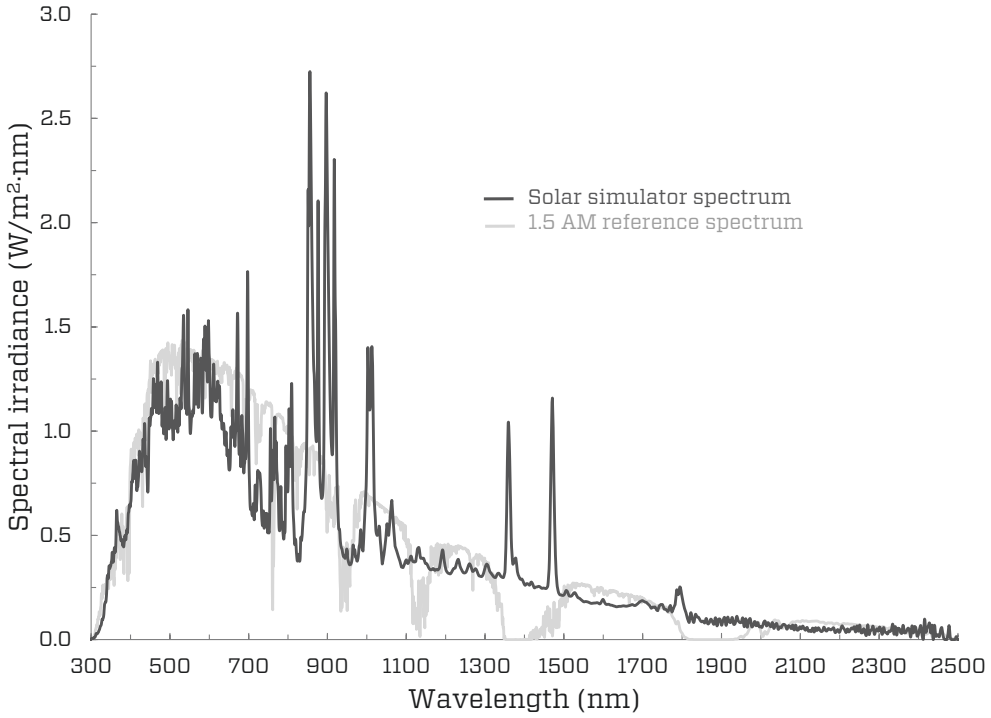

Figure 3.3. Comparison of normalized solar simulator spectrum (including the artificial sky) and AM1.5 reference spectrum.

Artificial sky: An artificial sky apparatus, located in front of the lamps, maintains a surface temperature (T_{sky}) of 13°C ±2°C. Its primary function is to remove the IR radiation generated by the lamps while minimizing the influence of thermal irradiance from the adjacent surfaces to the window.

Wind effect: A linear, variable-speed fan is used to reproduce the wind-induced convection for still air to 14 m/s. The fan blows ambient air parallel to the surface of the window. (Appendix A).

In addition, the convective heat transfer coefficient is measured directly with a hot plate apparatus. The hot plate is heated with an integrated electric heater. The power output (P_{pla}) of the heater is controlled with a PID controller to maintain constant plate surface temperature (T_{pla}) under a given wind speed. The exterior convective film coefficient ($h_{o,meas}$) is then calculated as follows:

$$h_{o,meas} = \frac{P_{pla}}{\left(T_{pla} - T_{amb}\right) \cdot A_{pla}} \tag{3.4}$$

where A_{pla} is the surface area of the plate. The exterior convective film coefficient is measured using a scanning grid of spacing 0.3 m. Electroplated copper is chosen due to its smooth surface (similar to glass) and low emissivity. The emissivity of the plate (ε_{pla}) was measured at 0.030 ±0.01 using an emissivity meter with a spectral range of 5 μm to 40 μm, resulting to an

estimated radiative heat transfer coefficient of 0.020 W/(m^2·K). Knowing the exterior convective heat transfer coefficient under the testing conditions, allows for the correction of the measured thermal conductance of the STPV window to a value under a standard exterior convective film coefficient (NFRC, 2014c) as follows:

$$U_{st} = \frac{1}{\frac{1}{U_{meas}} - \frac{1}{h_{o,meas}} + \frac{1}{h_{o,st}}} \tag{3.5}$$

where U_{st} and U_{meas} is the thermal conductance of the STPV window under standard conditions (e.g., NFRC 102) and test conditions, respectively, and $h_{o,st}$, $h_{o,meas}$ is the exterior convective film coefficient under standard conditions and test conditions, respectively.

3.2.2 Solar calorimeter

An indoor calibrated solar calorimeter apparatus is used to mount and test the STPV windows. The calorimeter was developed, characterized and calibrated based on NFRC 201 standard (NFRC, 2010). The dimensions of the calorimeter are 2.2 m long × 1.2 m wide × 0.2 m thick, excluding the mask wall. The front (mask wall) surface of the calorimeter, where the test specimen is mounted, has dimensions of 2.6 m × 1.6 m × 0.06 m, with a solar reflectance of 78%. It protrudes from the perimeter of the solar calorimeter in order to shade the rear surfaces (guard box) of the calorimeter and minimize the effects of direct solar irradiation. The mask wall and guard box are insulated and sealed to minimize thermal losses to the ambient environment [≤0.561 W/(m^2·K)].

An absorber plate housed within the calorimeter is connected to a water-based closed loop. The closed loop is connected to a water-to-water heat exchanger capable of extracting heat in order to maintain the average absorber plate temperature (T_{abs}) at desired levels. The calorimeter is attached at the test bench and placed under the solar simulator. Measurements are conducted on a tilt angle of 90° (vertical) when the apparatus reaches steady state conditions (temperatures and emulated solar radiation levels are kept constant throughout the test period). The time constant of the calorimeter was experimentally determined at 18 min, based on NFRC 201 standard.

The Harrison and Dubrous method is used to determine the SHGC of the window tested (Harrison and Dubrous, 1993; Harrison and Wonderen, 1994). An energy balance performed on the STPV window (Figure 3.2) shows that the net energy rate through the window into the calorimeter (Q_{net}) can be calculated as the sum of the solar heat gains resulting from exposure to the solar radiation (Q_{sol}) and the net heat flow (Q_{cond}) due to temperature gradient across the window (ΔT_{STPV}).

$$Q_{net} = Q_{sol} - Q_{cond} = \left(SHGC \cdot S \cdot A_{STPV}\right) - \left(U \cdot \Delta T_{STPV} \cdot A_{STPV}\right) \tag{3.6}$$

where S is the solar irradiance incident on the window, A_{STPV} is the surface area of the STPV window, and SHGC and U are the solar heat gain coefficient and the thermal conductance of the STPV window, respectively.

Treating the solar calorimeter apparatus as a solar thermal collector, the thermal performance factor (η_{th}) of the window is then defined as:

$$\eta_{th} = \frac{Q_{net}}{A_{STPV} \cdot S} \tag{3.7}$$

The SHGC of the STPV window can be determined by substituting eq.(3.6) on eq.(3.7).

$$\eta_{th} = -U \cdot \frac{\Delta T_{STPV}}{S} + SHGC \tag{3.8}$$

Through linear regression of the performance data, the SHGC is determined as the intercept of the regression line with the axis of ordinates. It should be noted that the U-value is sensitive to window properties and assembly as well as indoor and outdoor conditions (e.g., wind speed, turbidity and direction, indoor and outdoor temperatures). While current solar calorimetric standards opt to derive the U-value of the window tested using validated simulation tools (U_{st}) in order to determine the SHGC value from eq.(3.8), the use of the Harrison and Dubrous method allows the measurement of the actual U-value under the test conditions (U_{meas}) thus, reduces uncertainties when determining the SHGC value. When compared to the standard single point measurement, the proposed method requires multiple point measurements (under various irradiance and temperature conditions) resulting in increased overall test period.

The net energy flow through the STPV window into the enclosure is experimentally measured based on an energy balance on the calorimeter enclosure. The net energy flow through the window into the calorimeter is the sum of the energy rate extracted by the absorber plate (Q_{abs}), the heat conducted through the mask (Q_{mask}) and guard box (Q_{guard}) and the heat lost due to air leakage (Q_{lkg}).

$$Q_{net} = Q_{abs} + Q_{mask} + Q_{guard} + Q_{lkg} \tag{3.9}$$

where Q_{abs} is the product of the mass flow rate ($\dot{m}$), the specific heat of the circulating water (C_P) and the temperature rise between inlet and outlet of the absorber plate (ΔT_{abs}).

$$Q_{abs} = \dot{m} \cdot C_P \cdot \Delta T_{abs} \tag{3.10}$$

All front and back surface temperatures (namely the guard box, the mask, the absorber plate and the STPV window tested) as well as air temperatures (ambient and inside the calorimeter) are measured using T-type thermocouples. In addition, during the assembly of each STPV window, a T-type thermocouple was installed in direct contact with the back surface of a PV cell (within the encapsulation resin). The inlet and outlet temperature of the absorber plate are measured using 1/10 DIN Resistance Temperature Detectors (RTDs), while the water flow is measured with an electromagnetic flow sensor with an accuracy of ±0.5 % of the measured value. Finally, an uncertainty analysis is contacted after each test (Appendix B).

Electronic load and current-voltage curve: The STPV windows or arrays of windows installed on a building façade are connected to a micro-inverter or central inverter, respectively. The inverter uses maximum power point tracking (MPPT) to extract maximum power from the STPV system and feed-in to the building or the grid (Deutsche Gesellshaft fur Sonnenenergie, 2005a). It is critical that during the testing period (prior and during steady state conditions) the STPV window tested is connected to an electronic load (or a resistor load) that functions as a current sink performing at the maximum power point (P_{mp}) to emulate realistic operation conditions. If there is no-load (open circuit), the STPV glass will perform as heat-absorbing glass; the solar radiation absorbed by the PV cells or film is converted to heat only, increasing the STPV glass temperature. As the temperature increases, the SHGC rises due to increase of the inward-flowing fraction of absorbed solar energy [see eq.(3.3)]. Consequently, testing under an open circuit will produce a higher SHGC value than that observed under operating conditions with an applied load (F. Chen et al., 2012). An electronic load operating under MPPT is connected to the window. A current-voltage curve is also taken to characterize the electrical performance of each specimen under test conditions.

Infrared (IR) thermography: A thermal imaging camera is used to capture the temperature profile of the STPV window under steady state conditions. The camera is calibrated based on the surface emissivity of the STPV window while the temperature profile is verified using five surface point temperature measurements conducted with T-type thermocouples. The IR thermography allows the detailed study of the STPV window temperature profile as well as the identification of any faults (e.g., air leakage, thermal bridging and defective PV cells) through hot-spot detection.

3.3 Characterization of the STPV glass prototypes and windows

Four STPV glass prototypes were assembled (Figure 3.2). The prototypes utilize poly-Si PV cells arranged in such a way as to allow light to pass through the resulting space between the opaque cells. Each STPV glass assembly (Figure 3.1) consists of (outer-to-inner layer): (i) 3.2 mm tempered, antireflective-coated, White glass, (ii) Ethylene-Vinyl Acetate (EVA) encapsulant layer, (iii) poly-Si spaced PV cells layer, (iv) EVA encapsulant layer and (iv) Polyvinyl Fluoride (PVF) transparent backsheet. All prototypes are frameless having dimensions of 1948 mm × 976 mm. Various packing factors are used — packing factor (f) is the fraction of the glass area occupied by PV cells — resulting to various optical and electrical properties for each STPV prototype glass.

Solar-optical characterization: The multilayer optical properties of each STPV glass are measured based on the NFRC 300 standard (NFRC, 2014b) using a UV/Vis/NIR spectrophotometer with a spectral range of 200nm to 2500nm and equipped with an integrating sphere. Each STPV glass can be spatially-separated into two parts: an opaque "PV cells" part and a "transparent encapsulant" part (Fung and Yang, 2008; Zondag et al., 2002). Then, the spatially-averaged "effective" optical properties of the STPV glass are determined as:

$$\tau_{STPV} = f \cdot \tau_{cell} + (1-f) \cdot \tau_{enc} \tag{3.11}$$

$$\rho_{STPV} = f \cdot \rho_{cell} + (1-f) \cdot \rho_{enc} \tag{3.12}$$

where τ_{STPV}, ρ_{STPV} are the total effective transmittance and reflectance (front or back) of the STPV glass, τ_{cell}, ρ_{cell} is the transmittance and reflectance of the "PV cell" part, and τ_{enc}, ρ_{enc} is the transmittance and reflectance of the "encapsulant" part, respectively. While it was found that the above equations can sufficiently express the spatially-averaged "effective" optical properties of the STPV glass utilizing opaque PV cells, they are not suitable for STPV glass that integrates transparent PV thin film, translucent glass or translucent encapsulant. Instead, the ASHWAT method is recommended to calculate the effective solar-optical properties of the STPV glass (Wright et al., 2009).

The solar-optical properties are imported into LBNL OPTICS6 (Lawrence Berkeley National Laboratory, 2015a) to calculate the total optical properties of each STPV glass (Figure 3.4) summarized in Table 3.1.

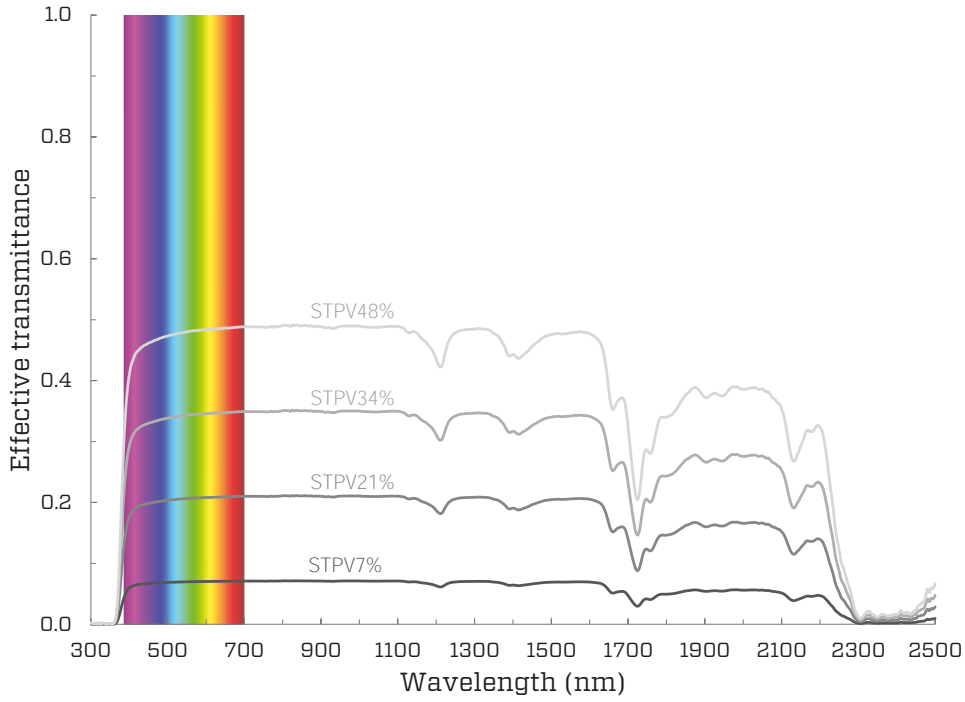

Figure 3.4. Effective spectral transmittance of each STPV glass prototype.

Each STPV prototype glass is then integrated as the outer glass layer of a double-glazed STPV window. Each STPV window (Figure 3.1) consists of (outer to inner layer): (i) 6 mm STPV glass, (ii) 25.4 mm sealed air cavity and (iii) 5.64 mm commercial clear glass with low emissivity coating (ε_3=0.157). The thickness of the air cavity on the windows was not selected for optimal thermal performance but rather to accommodate the junction box located on the rear side of each STPV glass. The optical file of each STPV glass are imported to LBNL WINDOW7.1 (Lawrence Berkeley National Laboratory, 2014a) to calculate the total optical properties of the STPV windows (Table 3.2).

Electrical characterization: Table 3.3 summarizes the electrical properties measured under standard testing conditions (STC) of AM 1.5 global irradiance, 1000 W/m^2 and 25°C PV cell temperature. This data is provided for reference purposes. However, STPV windows are unlikely to perform under these conditions. Thus, a current-voltage curve is taken under the various test conditions to study the electrical performance of STPV windows and ensure operation at maximum power point. Figure 3.5 illustrates the current-voltage curves for the four STPV windows.

Table 3.1. Optical and thermal properties of the four STPV glass prototypes.

Name of glass	Optical properties				Thermal properties		
	Solar		Visible				
	τ_{front}	ρ_{front}	τ_{front}	ρ_{front}	e_{front}	e_{back}	U-value W/(m^2·K)
STPV7%	0.066	0.092	0.070	0.059	0.920	0.950	6.111
STPV21%	0.195	0.088	0.206	0.062			
STPV34%	0.324	0.084	0.342	0.064			
STPV48%	0.453	0.080	0.479	0.066			

Note: τ: transmittance; ρ: reflectance; e: emissivity. The STPV glass prototypes are named based on their (front) visible transmittance.

Table 3.2. Optical and thermal properties of the four corresponding STPV windows.

Name of window	Optical properties				Thermal properties			STPV glass used as the outer layer
	Solar		Visible					
	τ_{front}	ρ_{front}	τ_{front}	ρ_{front}	e_{front}	e_{back}	U-value W/(m^2·K)	
STPV_WIN6%	0.046	0.198	0.058	0.205	0.920	0.840	2.011	STPV7%
STPV_WIN17%	0.135	0.181	0.172	0.188				STPV21%
STPV_WIN29%	0.223	0.168	0.285	0.176				STPV34%
STPV_WIN40%	0.312	0.158	0.398	0.167				STPV48%

Note: τ: transmittance; ρ: reflectance; e: emissivity. The STPV windows are named based on their (front) visible transmittance.

As the solar radiation incident on the STPV window increases, the short circuit current and thus power output of the window increases almost with a linear fashion. At the same time, the PV temperature increases due to the increase on irradiance levels. In return, the diffusion current on the cells increases, leading to a reduction of the charges at the edges of the cells and reduction of the open circuit voltage (Duffie and Beckman, 2006).

3.3.1 Measurement of the SHGC of STPV windows

The SHGC value (and STPV window efficiency, profile temperatures and U-value) varies depending on the test conditions under which the STPV window is tested. The test conditions (Table 3.4) used at the SSEC laboratory are different than the NFRC 200 standard (NFRC, 2014d), resulting in different SHGC values. A simulation-based correction method was proposed to obtain SHGC values under a standard AM1.5 spectrum (F. Chen et al., 2012; Van Wonderen, 1996). Besides spectrum mismatch, the method can be extended to include measurement result correction due to variation on test conditions (namely outdoor/indoor temperatures, outdoor/indoor convective heat transfer coefficient and irradiance intensity) and thus, producing SHGC values under NFRC 200 standard conditions and spectrum. An additional challenge is that existing simulation tools for the determination of the SHGC and U-value of window systems do not have the ability to simulate the solar electricity generation of STPV windows (Mitchell et al., 2013). Hence, the following method is proposed to measure the SHGC values of STPV windows (operating at maximum power point) under SSEC conditions and calculate the SHGC values under NFRC 200 standard conditions:

Step 1: The solar-optical properties of the STPV window layers are measured based on NFRC 300 and imported to LBNL WINDOW7.1 as presented above. The software simulates the SHGC value of the STPV window assembly under NFRC 200 standard conditions ($SHGC_{oc\_sim}$);

Step 2: The SHGC value of a STPV window under open circuit ($SHGC_{oc\_meas}$) is experimentally determined using the Harrison and Dubrous method;

Step 3: The correction factor (c) from SSEC test conditions to NFRC 200 standard conditions is calculated as follows:

$$c = \frac{SHGC_{oc\_sim}}{SHGC_{oc\_meas}} \tag{3.13}$$

Step 4: The SHGC value of a STPV window operating at the maximum power point ($SHGC_{mp\_meas}$) is experimentally determined using the Harrison and Dubrous method;

Step 5: The SHGC value of a STPV window operating under maximum power point under NFRC 200 standard conditions is then calculated:

$$SHGC_{mp\_standard} = c \cdot SHGC_{mp\_meas} \tag{3.14}$$

The four STPV windows were tested and characterized following the aforementioned methodology. The temperature difference between the inlet and outlet of the absorber plate was kept at 2°C±0.5°C to minimize the temperature differential on the STPV window as it might affect the PV electricity generation (De Vries, 1998; Tina et al., 2010). For all cases, the difference between simulated and measured SHGC values are within measurement uncertainty estimates (Table 3.5). Applying a correction factor, the SHGC values can then be calculated under NFRC 200 standard for the various STPV windows operating under maximum power point conditions (Table 3.6).

Table 3.3. Electrical properties of the four STPV windows under STC.

Name of window	Number of PV cells	Cell technology	Electrical efficiency η_{mp}	Nominal maximum power P_{mp}(W)	Open circuit voltage V_{oc}(V)	Short circuit current I_{sc}(A)	Temperature coefficient $\mu_{P,mp}$(%/°C)
STPV_WIN6%	72	Poly-Si	0.15	294.10	45.2	8.56	-0.43
STPV_WIN17%	60		0.13	240.40	37.61	8.52	
STPV_WIN29%	48		0.10	187.90	29.98	8.57	
STPV_WIN40%	36		0.07	133.30	22.28	8.48	

Note: The STPV windows are named based on their (front) visible transmittance.

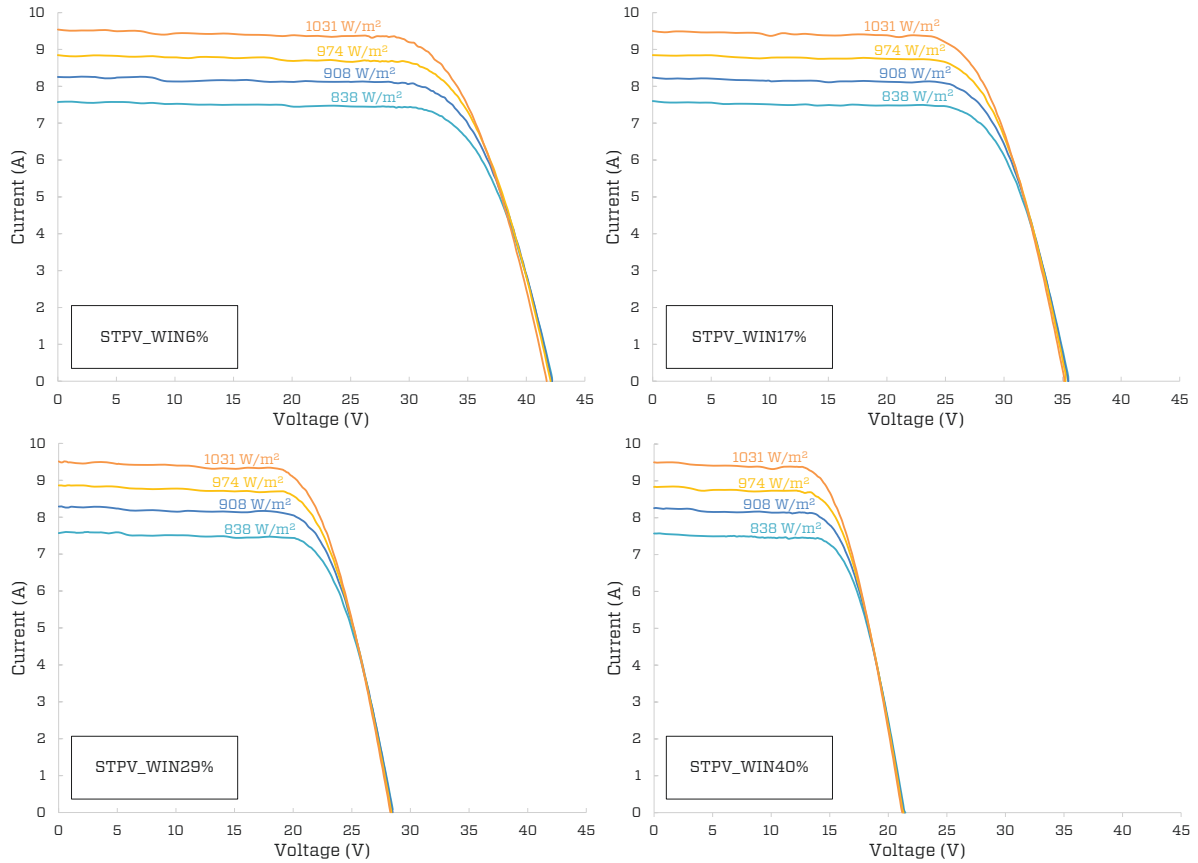

Figure 3.5. Current-voltage curves for the four STPV windows under indoor/outdoor temperatures of 21°C ± 1°C, exterior convective film coefficient of 20 W/(m²·K) and various irradiance intensities (from 838 W/m² to 1031 W/m²).

Table 3.4. Environmental conditions for the determination of the SHGC value through simulation and experiment

Parameter	NFRC 200 standard conditions (simulation using WINDOW7.1)	SSEC conditions (initial test conditions)
Irradiance intensity (W/m^2)	783	838
Solar spectrum	ASTM AM1.5	Atlas MHG lamps
Interior air temperature (°C)	24	21
Exterior air temperature (°C)	32	21
Wind speed (m/s)	5.5	5

The correction factor is strongly influenced by the spectral mismatch between the test spectrum and the standard AM1.5 due to spectral response of the PV cells (F. Chen et al., 2012). As the area covered by PV cells increases, so does their spectral effect on the transmittance and solar heat gains (Gueymard and DuPont, 2009). As a result, the correction factor is also increased. Finally, when the solar electricity generation of the STPV window is taken into account by operating the STPV windows at the maximum power point rather than assuming open circuit conditions, the SHGC is reduced between 2% (for STPV window with visible transmittance of 40%, STPV_WIN40%) and 23% (for STPV window with visible transmittance of 6%, STPV_WIN6%)(Figure 3.6). The reduction is expected to be even higher in a STPV window with no low-e coating due to significant increase of the inward-flowing absorbed solar energy.

3.3.2 Temperature profile measurements for the STPV windows

The thermal performance of STPV windows is an area that needs urgent attention because it exerts a significant influence on the durability of the PV cells or films and other window components. Operating temperatures exceeding 75°C have significant influence on the durability of the PV cells or films and other window components and need to be predicted either through testing or validated simulation tools. For this reason, the temperature profile of the STPV windows was measured under various irradiance intensities and wind conditions. The inner air and surface temperatures of the calorimeter PV cell operating temperatures of up to 46.2°C to 55.3°C were observed for STPV_WIN40% and STPV_WIN6% respectively, under 1000 W/m^2 and exterior convective film coefficient of 20 $W/(m^2 \cdot K)$. The average STPV window temperature is strongly affected by the solar absorbance of the STPV glass (outer layer). As the absorbance of the STPV glass increases (resulting to an increase on the electrical efficiency and reduction on the transmittance), only a small fraction (around 20% of the absorbed solar energy) is transformed to electricity while the rest (around 80% of the absorbed solar energy) contributes to the increase of the PV cell operating temperature.

In addition, a temperature differential between "PV cell" part and "encapsulant" part of up to 13°C was measured. This high differential temperature was observed on STPV_WIN40% caused by the increased spacing between the opaque PV cells (a low packing factor of f=0.46). This differential temperature is mainly driven by the variation of the solar absorbance between the "PV cell" part (α_{cell}=0.991) and "PV encapsulant" part (α_{enc}=0.165).

However, as the spacing between the PV cells is reduced, the temperature differential is also reduced to less than 0.5°C (for STPV_WIN6% the packing factor is f=0.92). Such differential temperatures are specific to STPV windows utilizing opaque PV cells (due to variation of optical properties between "PV cells" part and "encapsulant" part) and it has not observed on STPV windows utilizing thin film PV technologies with uniform optical properties throughout the window surface (Yoon et al., 2011).

Table 3.5. SHGC values of the four STPV windows, under open circuit, simulated under NFRC 200 standard conditions ($SHGC_{oc\_sim}$) and measured under SSEC conditions ($SHGC_{oc\_meas}$).

Name of window	$SHGC_{oc\_sim}$ Simulated (open circuit)	$SHGC_{oc\_meas}$ Measured (open circuit)	Difference $SHGC_{oc\_sim}$ - $SHGC_{oc\_meas}$	Correction factor c
STPV_WIN6%	0.145	0.125±0.022	0.020	1.160
STPV_WIN17%	0.242	0.225±0.023	0.017	1.076
STPV_WIN29%	0.339	0.331±0.028	0.008	1.024
STPV_WIN40%	0.436	0.438±0.031	-0.002	0.995

Note: The STPV windows are named based on their total visible transmittance.

Table 3.6. SHGC values of the four STPV windows under maximum power point measured under SSEC conditions ($SHGC_{mp\_meas}$) and calculated under NFRC 200 standard conditions ($SHGC_{mp\_sim}$).

Name of window	$SHGC_{mp\_meas}$ Measured (under MPPT)	$SHGC_{mp\_sim}$ Calculated (under MPPT)
STPV_WIN6%	0.096±0.017	0.111±0.018
STPV_WIN17%	0.203±0.022	0.218±0.022
STPV_WIN29%	0.314±0.027	0.322±0.027
STPV_WIN40%	0.428±0.030	0.426±0.030

Note: The STPV windows are named based on their total visible transmittance.

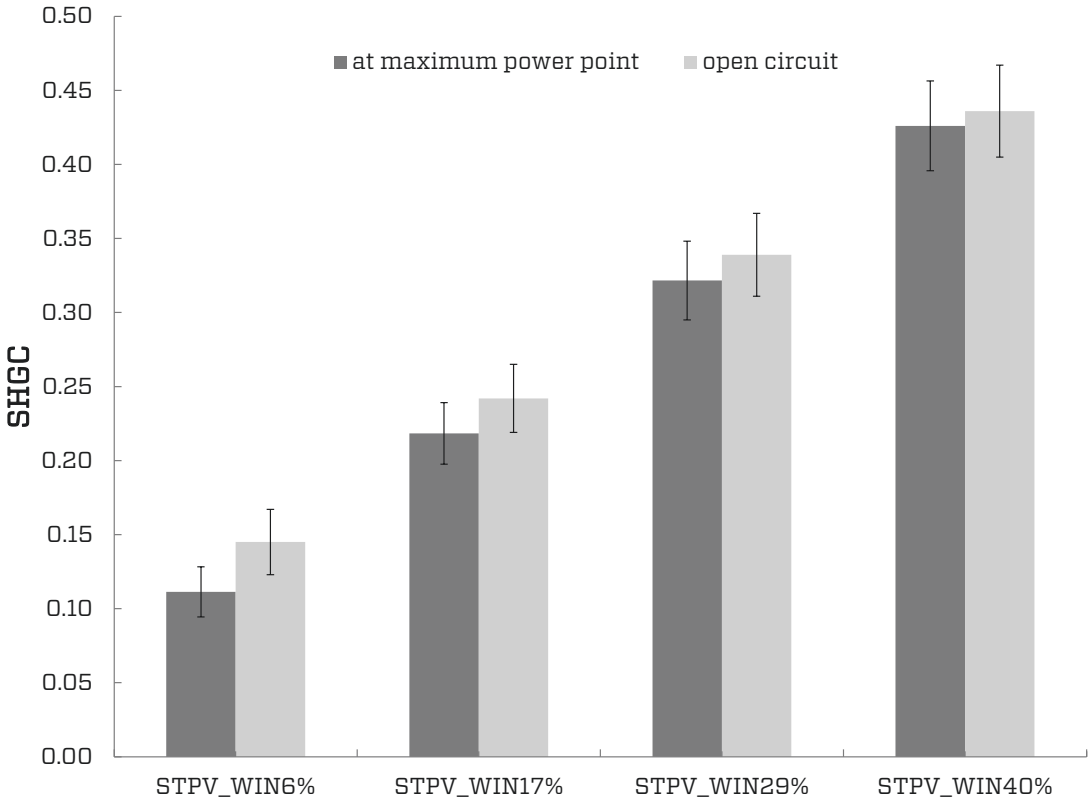

Figure 3.6. SHGC values for the four STPV windows for maximum power point and open circuit operation, under NFRC200 environmental conditions.

3.4 Conclusions

An experimental study on the determination of Solar Heat Gain Coefficient (SHGC) for Semi-Transparent Photovoltaic (STPV) windows has been presented. An indoor solar simulator and solar calorimeter facility is utilized to test and characterize four STPV prototype windows. Currently, there is no commercially available simulation tool or standard test procedure able to estimate the SHGC of STPV windows when operating at maximum power point conditions. A common practice in the building and window industry is to test or simulate STPV windows under open circuit, a condition that is witnessed only under fault operation of such a system. This study shows that when the solar electricity generation of the STPV window is taken into account by operating the STPV windows at the maximum power point rather than assuming open circuit conditions, the SHGC is reduced between 2% (for STPV window with visible transmittance of 40%, STPV_WIN40%) and 23% (for STPV window with visible transmittance of 6%, STPV_WIN6%). The need to update the existing standards to provide guidelines on how to test and certify STPV window technologies is apparent. It was found that the electricity generation from the STPV windows can result in up to 23% reduction of SHGC in comparison to a heat-absorbing (e.g., tinted or fritted glass) window with the same optical and thermal properties.

In addition, cell operating temperatures of up to 55.3°C were observed with a temperature differential between "PV cell" part and "encapsulant" part of up to 13°C. This demonstrates the need to predict the operating temperatures of STPV window through testing or simulations.

The three-dimensional heat transfer phenomena that take place on a STPV window should be further studied and understood as they impact the durability of the PV cells and window components such as spacers, sealants and framing. The development of experimentally-validated heat transfer and electrical performance models for STPV windows is also required in order to provide the right tools to the building and window industry to predict their overall performance and their impact on the building energy and occupancy comfort. Such model can then be extended to windows integrating different PV technologies such as "see-though" thin films.

Chapter 4
Semi-Transparent Photovoltaic Windows Performance Modelling: on the Prediction of Cell Operating Temperatures[2]

4.1 Introduction

Semi-transparent PV (STPV) windows are PV technologies that fall under the broader category of building integrated photovoltaics (BIPV). STPV can replace conventional windows and skylights in new or retrofit commercial, institutional and high-rise residential buildings. In highly-glazed buildings where reducing cooling energy expenditures are important, insulated glazing units with low-emissivity coatings are generally adopted to reduce heat transfer by long-wave radiation. The outer glass layer often requires low solar transmittance to reduce transmission of solar radiation. STPV windows have the capability to reduce solar heat gains, generate solar electricity (Fung and Yang, 2008; Miyazaki et al., 2005) while still providing satisfactory daylighting levels and views to the outdoors (Olivieri et al., 2013; Vartiainen, 2001). However, STPV windows & skylights tend to operate at higher temperatures than open rack systems (De Boer and van Helden, 2001; Wong et al., 2008). High operating temperatures (75°C and above) impact adversely the electrical conversion efficiency and lifespan of the window. Prolonged exposure to high operating cell temperatures can result in failure of the window components (e.g. sealants, gaskets) and possibly cell degradation or damage (in the case of thin film polymer-based STPV technologies).

The objective of this work is to study and predict the thermal response of insulated glazing units integrating STPV technologies on their outer glass layer (Figure 4.1). A deeper understanding of the impact of various window assembly parameters (namely low-emissivity coatings or suspended films and thermal conductance) is necessary to predict and prevent prolonged overheating that might result to accelerated PV cell degradation, delamination and window component or assembly failure. An experimental study of four STPV prototype windows is performed and the measurements are used to develop a numerical thermal model.

The model is then used to perform climate-based simulations and predict the temperature profile of the STPV window on a yearly basis. The proposed model can be extended to any multi-layered c-Si STPV window with various electrical, thermal and optical properties. A low-order thermal model is also developed based on the King's thermal model (King et al., 2004). This model can be used during the preliminary design stages, when the detailed STPV window assembly design and properties are not known.

---

[2] Kapsis, K., Athienitis, A.K., 2016. Semi-Transparent Photovoltaic Windows Performance Modelling: on the Prediction of Cell Operating Temperatures. Renewable Energy (Submitted).

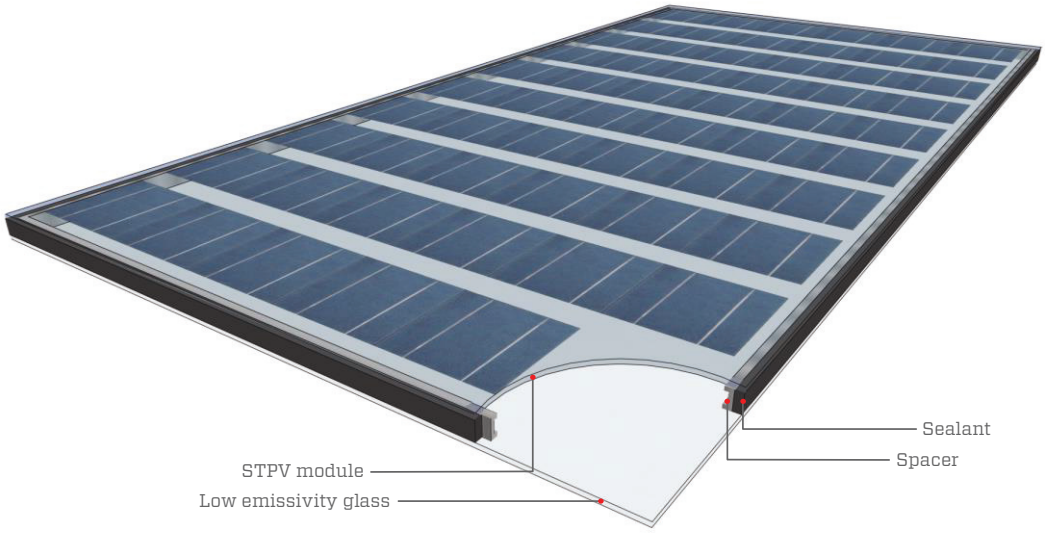

Figure 4.1. Typical double-glazed STPV window utilizing poly-Si PV spaced PV cells.

4.1.2 Thermal behaviour of STPV windows

Despite the common use of low-e coating and suspended films on window assemblies, no systematic study has been made to investigate their impact on PV cell temperature and power output of a STPV window. When PV cell overheating is of concern, the window sealed cavity can be replaced with a ventilated one, turning the façade into an active thermal collector (STPV/T) in addition to the electricity generation and daylight transmission (Gaillard et al., 2014a). The absorbed solar energy that is converted into heat is recovered either actively, using a fan or pump, or passively by a heat removal fluid flowing on the rear side of the STPV module. As the fluid circulates behind the PV cells, it cools down the cells through convection and increasing their electrical efficiency.

Measurements on Mataro library, in Madrid, Spain, showed STPV cell temperatures of up to 50°C for a mechanically ventilated double skin STPV façade, while inner glass surface temperatures of up to 32°C were measured with top to bottom temperature gradient of less than 1°C (Infield et al., 2006). Gaillard et al. (2014) reported cell temperatures up to 60°C for a naturally ventilated double skin façade installation in Toulouse, France, with a cell temperature gradient up to 10°C on the vertical axis. Peng et al. (2013) measured the thermal performance of double skin STPV façade under various air flow modes (non-ventilated, naturally ventilated and mechanically ventilated), in Hong Kong, China. It was found that as the nature of the air flow changed, the U-value increased (3.4, 3.8 and 4.6 $W/m^2 \cdot K$, respectively), while the Solar Heat Gain Coefficient (SHGC) decreased (0.13, 0.12 and 0.1, respectively). In addition, compared to non-ventilated mode, naturally ventilated cavity resulted to a reduction of up to 1.5°C PV module temperature while mechanically ventilated to a reduction of up to 6.3°C. Guardo et al. (2009) investigated a similar configuration using computational fluid dynamics (CFD). The authors concluded that the reduction on SHGC was due to the increase of air mass flow rather than turbulence mixing effects.

When it comes to integration of STPV technologies in insulated glazing units, De Boer and van Helden (2001) predicted STPV window temperatures of up to 65°C while Wong et al. (2008) predicted STPV skylight temperatures of up to 75°C. Up to 60°C PV cell operating temperatures were measured, with no significant temperature gradient, for a STPV office installation in Yongin, South Korea (Yoon et al., 2011). Delisle (2008) found that U-value had little impact on the STPV annual electrical performance. The STPV window assemblies were considered on the "spandrel" section of an office building located in three major Canadian cities, assuming that the daylight transmitted through it was not significant (maximum possible packing factor, where packing factor is the ratio of the window surface area covered with PV cells). The simulations (using TRNSYS) revealed that when the STPV module is the outermost glass of the window assembly (a double glazed and triple glazed STPV window were studied, with low-e coating on surface-3 and surface-5, respectively), the electrical performance and operating cell temperatures were very similar, while there was a decrease of 6 percentage points on the annual space heating energy consumption when upgrading from a double glazed STPV window to a triple glazed one, mainly due to the decrease of the U-value of the STPV window.

Vats et al. (2012) compared the PV cell operating temperatures of a STPV and a mechanically ventilated STPV/T system for roof and façade applications. The simulations showed that the PV cell temperatures on a STPV/T can be up to 5.5°C higher compared to a STPV depending on the mass flow rate. This was due to the fact that the inlet air drawn through the STPV/T façade was from the indoor environment.

4.2 Thermal modelling of STPV windows

Besides the complexity or accuracy the various PV electrical performance models might provide, all have something in common: they require the incident solar radiation and the cell operating temperature as inputs. While the incident solar radiation can be estimated through meteorological data (Perez et al., 1990), weather satellite data or measured on site (Gueymard and Wilcox, 2011), the operating cell temperature can be either indirectly measured (e.g. by thermography or measuring back-surface temperatures) or estimated using PV thermal modelling. For the case of STPV windows, the cell temperature is influenced by the optical, thermal, electrical and physical properties of the STPV cells/module, the optical and thermal properties of the STPV window assembly and the prevailing climatic conditions such as air mass, solar spectrum, solar angle of incidence and wind speed (Duffie and Beckman, 2006).

When in-depth thermal study is required, energy balance equations can be employed expressing heat transfer through conduction, convection and radiation (Fung and Yang, 2008; Wong et al., 2005). In many instances, the thermal models take into account the thermal capacity of the various window layers (namely thermal capacity of glass and cells) (Fung and Yang, 2008; Infield et al., 2006; Notton et al., 2005). However, when STPV windows are integrated on a building façade, the thermal mass of the window assembly is negligible when compared to the thermal mass of the building walls and indoor air volume (within two orders of magnitude) and thus can be excluded from the energy balance (Gaillard et al., 2014a). On STPV modules utilizing Si-based opaque spaced cells, when the packing factor and/or spacing

between cells is substantial, the "STPV module" layer can be separated into two parts: "STPV cells" part and "encapsulant" part (Fung and Yang, 2008). Depending on the cavity geometry and characteristics (non-vented or ventilated cavity, isothermal or anisothermal surfaces), the convective heat transfer coefficients can be approximated using existing correlations or studied in detail using CFD methods (Gan, 2009; Han et al., 2013, 2010, 2009; Koyunbaba and Yilmaz, 2012). Thermal bridging occurs due to spacer separating the various window layers as well as to window frame (Ge and Fazio, 2004; Gustavsen et al., 2007). The edge-of-window might have significantly higher thermal conductance than the centre-of-window thus frame and spacer effects should be accounted for in the energy balance equations. Depending on the component complexity, the analysis could be carried out using one-dimensional, two-dimensional of three-dimensional heat transfer.

It has been also shown that low-order models can be used to predict the operating cell temperature (E. Skoplaki and Palyvos, 2009). The simplest model considers the impact incident solar radiation and (S) and outdoor ambient air temperature (T_o) have on cell temperature (T_{STPV}) through a linear correlation (Ross, 1976):

$$T_{STPV} = k \cdot S + T_o \tag{4.1}$$

where k is the slope of line $(T_{STPV}-T_o)=k \cdot S$, determined through experimental measurements. A typical value for a STPV window is k=0.0455 m^2K/W (Nordmann and Clavadetscher, 2003).

King's model uses an implicit correlation between the measured back-surface temperature (T_{back}) and operating cell temperature (King et al., 2004):

$$T_{STPV} = T_{back} + \frac{S}{S_{ref}} \cdot \Delta T \tag{4.2}$$

where S_{ref} is the reference solar radiation (1000 W/m^2) and $\Delta T=T_{STPV} - T_{back}$. For practical reasons, the back-surface temperature of a STPV window assembly should be the inner surface of the innermost layer of the insulated glazing unit (e.g. surface-4 on a double-glazed window unit) rather than the back of the STPV module.

When the back-surface temperature cannot be measured, it can be estimated with using the following empirical model:

$$T_{back} = S \cdot e^{a+b \cdot WS} + T_o \tag{4.3}$$

where a is an empirically-determined coefficient determining the upper temperature limit under low wind speeds and high solar irradiance; b is an empirically-determined coefficient determining the rate at which the back-surface temperature drops with the rise of the wind speed; WS is the wind speed measured at standard 10-m height (m/s), available on

meteorological weather data. The empirically-determined coefficients are influenced by the STPV window assembly and mounting arrangement and location.

4.3 Thermal modelling of STPV windows using finite difference method

Energy balance equations are employed to predict the thermal behaviour of a STPV window using finite difference method. Figure 4.2 presents the energy transfer within a double-glazed STPV window assembly. Each layer consists of an inner and an outer surface. The finite difference model presented below assumes: (i) one-dimensional heat transfer normal to each layer (ii) each layer is thin enough to neglect any thermal capacitance (iii) absorbed solar radiation (and transformed to thermal or electrical energy) in each layer is equally distributed between inner and outer surface of the layer (ISO, 2003a).

STPV module (surface 1)

$$\left(E_o\varepsilon_1 - \varepsilon_1\sigma T_1^4\right) + h_o(T_o - T_1) + \left[\frac{\alpha_1 S}{2} - \frac{P_{STPV}}{2A_{STPV}}\right] = U_{STPV}(T_1 - T_2) \tag{4.4}$$

STPV module (surface 2)

$$U_{STPV}(T_1 - T_2) + \left[\frac{\alpha_1 S}{2} - \frac{P_{STPV}}{2A_{STPV}}\right] = \left[\sigma\frac{\varepsilon_2\varepsilon_3}{1-(1-\varepsilon_2)(1-\varepsilon_3)}(T_2^4 - T_3^4)\right] + h_{cav}(T_2 - T_3) \tag{4.5}$$

Inner glass (surface 3)

$$\left[\sigma\frac{\varepsilon_2\varepsilon_3}{1-(1-\varepsilon_2)(1-\varepsilon_3)}(T_2^4 - T_3^4)\right] + h_{cav}(T_2 - T_3) + \frac{\alpha_2 S}{2} = U_{glass}(T_3 - T_4) \tag{4.6}$$

Inner glass (surface 4)

$$U_{glass}(T_3 - T_4) + \frac{\alpha_2 S}{2} = \left[\varepsilon_4\sigma T_4^4 - E_{in}\varepsilon_4\right] + h_i(T_4 - T_{in}) \tag{4.7}$$

where S is the solar irradiance incident on the STPV window (W/m^2); E_o, E_{in} is the exterior and interior thermal radiation incident on innermost and outermost window surfaces, respectively (W/m^2); P_{STPV} is the electrical power output of the window under maximum power tracking (MPPT) mode (W); A_{STPV} is the window surface area (m^2); T_i is the average temperature of surface i, with $T_{STPV}=T_1$ (K); T_o, T_{in} are the outdoor air and indoor air temperature, respectively (K); ε_i is the emissivity of surface i; h_o, h_{in} are the outdoor and indoor air film convective heat transfer coefficient, respectively ($[W/(m^2\cdot K)]$; h_{cav}, is the convective heat transfer coefficient of the sealed cavity $[W/(m^2\cdot K)]$; U_{STPV}, U_{glass} are the thermal conductance of

the STPV module and inner glass, respectively [W/(m^2·K)]; σ is the Stefan-Boltzmann constant [5.6703·10^{-8} W/(m^2·K^4)]. Analogous equations can be used for multi-layered STPV windows.

Assuming non-absorbing gas (e.g. air, Ar, Kr or Xe gas/mix) in the sealed window cavity, the solar transmission (τ), reflection (ρ) and absorption (α) within the STPV window can be calculated as follows (ISO, 2003b):

Solar transmission of layer i to j

$$\tau_{i,j} = \frac{\tau_{i,j-1}\tau_{j,j}}{1-\rho^{f}_{j,j}\rho^{b}_{j-1,i}} \tag{4.8}$$

Front solar reflection of layer i to j

$$\rho^{f}_{i,j} = \rho^{f}_{i,j-1} + \frac{\tau^{2}_{i,j-1}\rho^{f}_{j,j}}{1-\rho^{f}_{j,j}\rho^{b}_{j-1,i}} \tag{4.9}$$

Back solar reflection of layer i to j

$$\rho^{b}_{j,i} = \rho^{b}_{j,j} + \frac{\tau^{2}_{j,j}\rho^{b}_{j-1,i}}{1-\rho^{b}_{j-1,i}\rho^{f}_{j,j}} \tag{4.10}$$

Solar absorption in layer j

$$\alpha_{j} = \frac{\tau_{1,j-1}\left(1-\tau_{j,j}-\rho^{f}_{j,j}\right)+\tau_{1,j}\rho^{f}_{j+1,N}\left(1-\tau_{j,j}-\rho^{b}_{j,j}\right)}{1-\rho^{f}_{j,N}\rho^{b}_{j-1,1}} \tag{4.11}$$

where for eq.(4.11) $\tau_{i,j}=1$ and $\rho_{i,j}=0$ when $i<0$ or $j>N$. It should be noted that each variable is a function of wavelength (λ).

Depending on the model accuracy required, the electrical power output of the window (P_{STPV}) can be approximated using the following PV electrical models [listed in ascending order of accuracy (Deutsche Gesellshaft fur Sonnenenergie, 2005b)]: (i) Evan's model (Evans, 1981) (ii) equivalent one-diode model (De Soto et al., 2006) or (iii) King's model (King et al., 2004). Other electrical models exist providing various levels of accuracy and complexity (E Skoplaki and Palyvos, 2009).

4.4 Experimental verification of the thermal model

An experimental study was performed utilizing an indoor solar simulator to evaluate the aforementioned thermal model. Four double-glazed STPV window prototypes were assembled and tested utilizing poly-Si spaced cells.

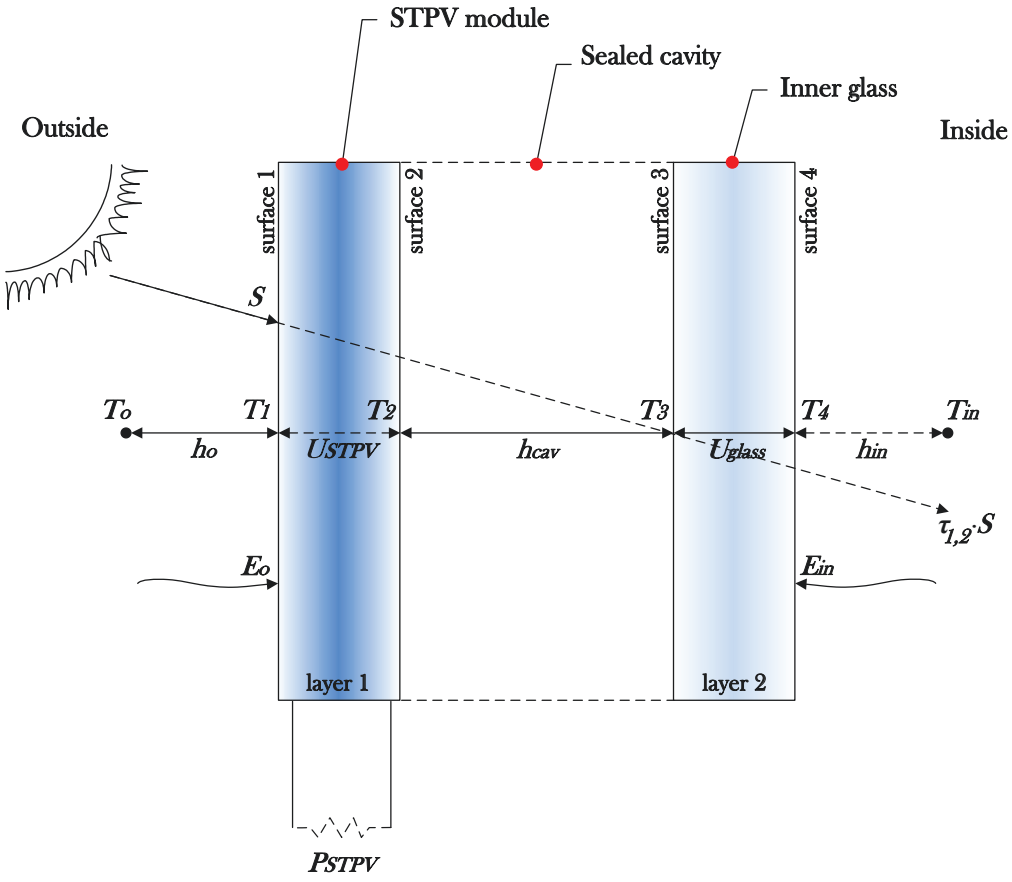

Figure 4.2. Energy balance schematic for a double glazed STPV window.

4.4.1 Description of the experimental setup

The solar simulator is located in the Solar Simulator and Environmental Chamber (SSEC) laboratory, at Concordia University, Montreal, Canada. The solar simulator is a continuous lampfield able to emulate sunlight. It is coupled with an artificial sky apparatus to minimize the influence of thermal irradiance from adjacent surfaces to the tested window and a linear variable-speed fan to reproduce wind-induced convection on the exterior window surface (Kapsis et al., 2016). The test conditions are summarized in Table 4.1.

Each STPV window was mounted on a thermally-calibrated solar calorimeter apparatus used to emulate the indoor thermal environment of a typical office building (Figure 4.3). A thermally-calibrated IR camera was used to measure the temperature distribution on the outermost window surface (surface-1). T-type thermocouples were also used to measure surface (on STPV window and calorimeter) and air temperatures (exterior and within the calorimeter) during the test period. The STPV window was connected to an electronic load, functioning at the maximum power point, to measure and anticipate the power generated by the STPV. All tests were performed under steady-state conditions. Thus, no transient thermal effects were studied. The results of this study should be considered as bearing this limitation.

Table 4.1 Experimental conditions.

Variable	Average test conditions	Spatial (temporal) variation
Incident solar irradiance (W/m^2)	750, 800, 850, 900, 950 & 1000	±3% (±1%)
Wind-induced convective heat transfer coefficient [$W/(m^2 \cdot K)$]	20, 25, 30, 35 & 40	±3.2
Ambient air temperature (°C)	21	(±1)
Calorimeter indoor air temperature (°C)	21	(±1)
Calorimeter indoor surface temperatures (°C)	21	±2 (±1)
Artificial sky temperature (°C)	13	±2 (±1)

4.4.2 Description of the STPV window prototypes

Four double-glazed STPV window units were assembled. Each STPV prototype window is frameless with dimensions of 1948 mm × 976 mm. It comprises of a STPV module as the outer layer and a 6mm glass (incorporating a low emissivity coating on surface-3) as the inner one. A 25 mm sealed air cavity separates the two glass layers. The thickness of the cavity was selected to take into account the junction box located on the rear side of each STPV module. The number and spacing of the opaque poly-Si cells integrated on each window varied, resulting to various optical and electrical properties. The solar spectral transmittance of each window layer was measured using a UV/Vis/NIR spectrophotometer (Figure 4.4). The total optical, thermal and electrical properties of each STPV window prototype are summarized in Table 4.2. T-type thermocouples were used to measure the operating cell temperature – embedded within the module encapsulation resin, the thermocouples were in direct contact with the rear side of PV cells.

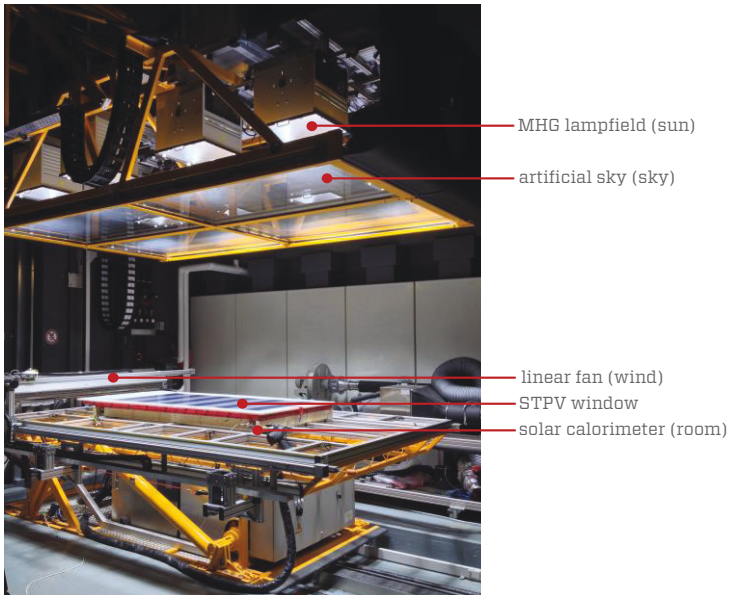

Figure 4.3. Experimental setup for the study of the thermal behaviour of STPV windows at Concordia University solar simulator laboratory.

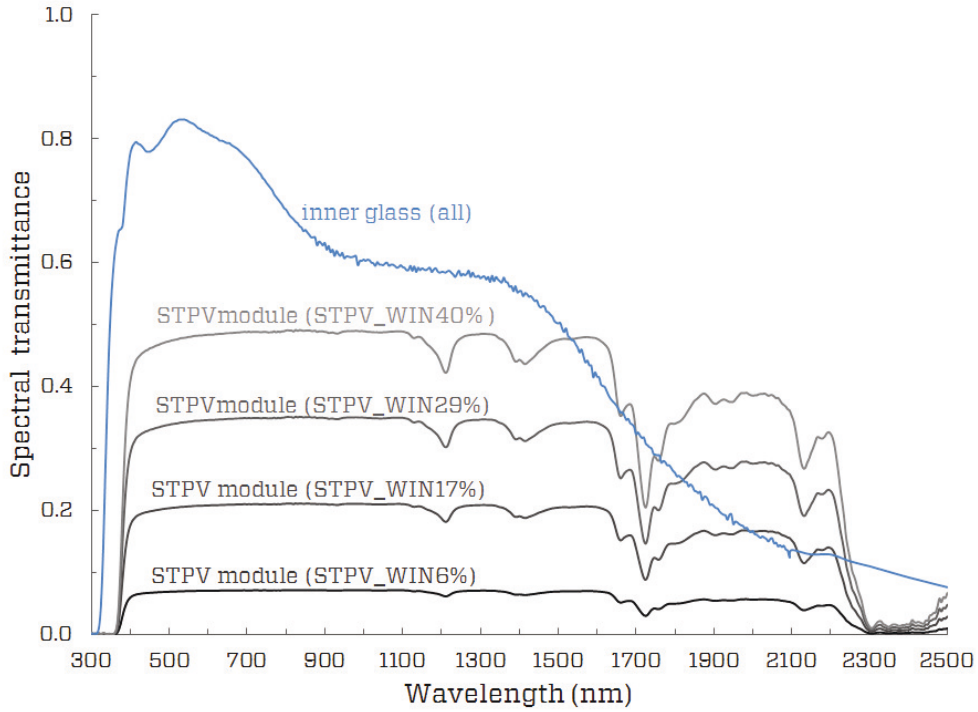

Figure 4.4. Measured solar spectral transmittance of STPV window layers. Note that "STPV module" refers to the outer layer of each window. All STPV windows have identical inner glass.

Table 4.2. Total optical, thermal and electrical properties of the four STPV windows.

Name of window	Optical properties				Thermal properties			Nominal maximum power under STC P_{mp}(W)	Packing factor (%)
	Solar		Visible						
	τ_{front}	ρ_{front}	τ_{front}	ρ_{front}	ε_{front}	ε_{back}	U-value W/(m^2·K)		
STPV_WIN6%	0.046	0.198	0.058	0.205	0.920	0.840	2.011	294.10	92.2
STPV_WIN17%	0.135	0.181	0.172	0.188				240.40	76.8
STPV_WIN29%	0.223	0.168	0.285	0.176				187.90	61.4
STPV_WIN40%	0.312	0.158	0.398	0.167				133.30	46.1

Note: τ: transmittance; ρ: reflectance; e: emissivity. The STPV windows are named based on their (front) visible transmittance.

4.4.3 Thermal model verification

A comparative study on the STPV window prototypes was performed between experimental measurements and model predictions. The measured optical [namely $\tau(\lambda)_i$ and $\rho(\lambda)_i$] and thermal (namely U_{STPV}, U_{glass} and ε_i) properties as well as the electrical power output of each STPV window (P_{STPV}) were imported to the thermal model.

PV cell operating temperatures of 46.2°C (for STPV_WIN40%) to 55.3°C (for STPV_WIN6%) were measured under 1000 W/m^2 and wind-induced convective heat transfer

coefficient of 20 W/(m^2·K). The thermal model was able to predict cell temperatures within accuracy of ±4°C (for STPV_WIN6%). Though, the model accuracy reduced as the packing factor increased (up to ±7°C for STPV_WIN40% with a packing factor of 46.1%) (Figure 4.5). This is due to the fact that the model assumed uniform spatial optical and thermal properties. IR thermography revealed a temperature differential between "PV cell" part and "encapsulant" part of up to 13°C (for STPV_WIN40%) due to increased spacing between the opaque PV cells (Figure 4.6). The temperature differential reduced to less than 0.5°C (0.9°F) for STPV_WIN6%. Such differential temperatures are specific to STPV windows utilizing opaque PV cells (due to variation of optical properties between "PV cells" part and "encapsulant" part) and it is not apparent on STPV windows utilizing thin film PV technologies (Yoon et al., 2011). In order to increase the accuracy of the model, the STPV module layer under eq.(4.4) and eq.(4.5) can be separated into two parts: "STPV cells" part and "encapsulant" part (Fung and Yang, 2008).

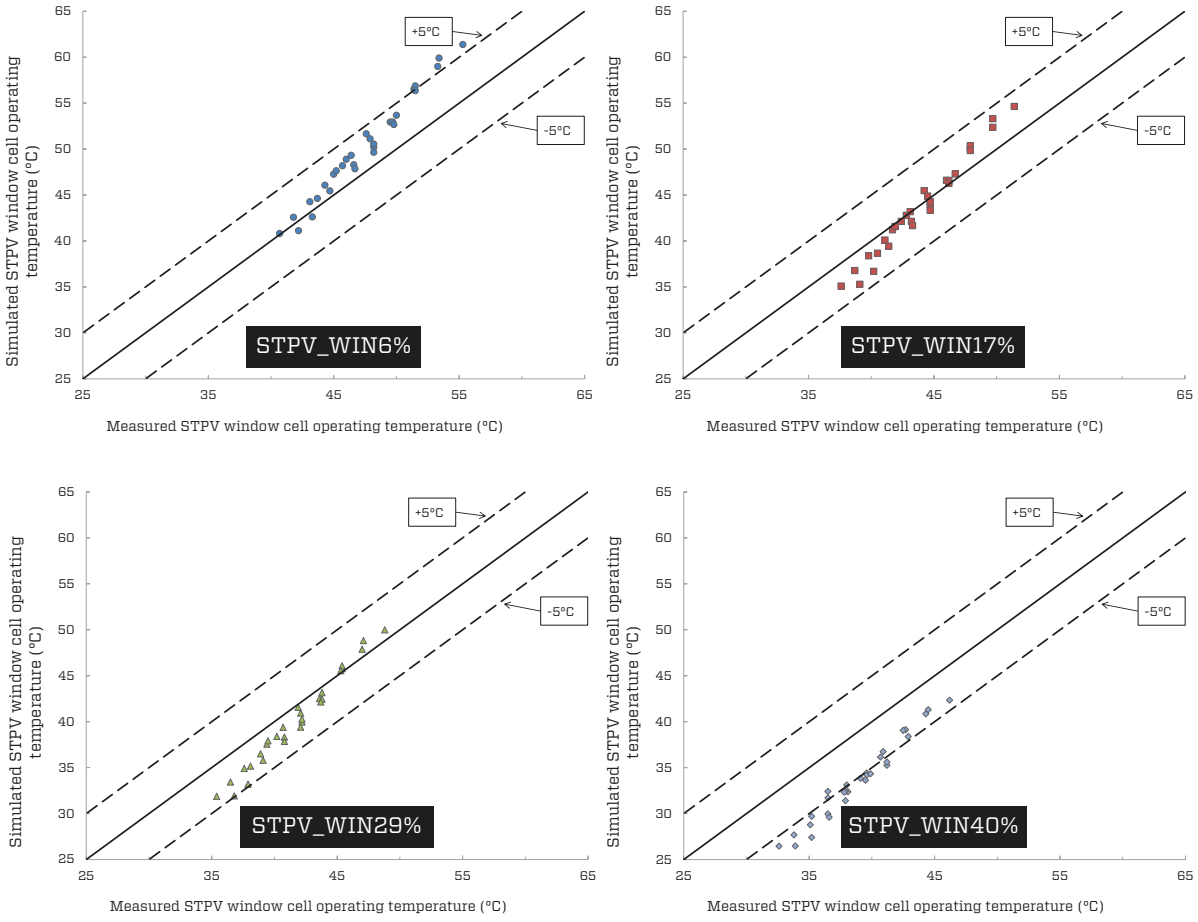

Figure 4.5. Simulated over measured cell operating temperatures for the four STPV window prototypes.

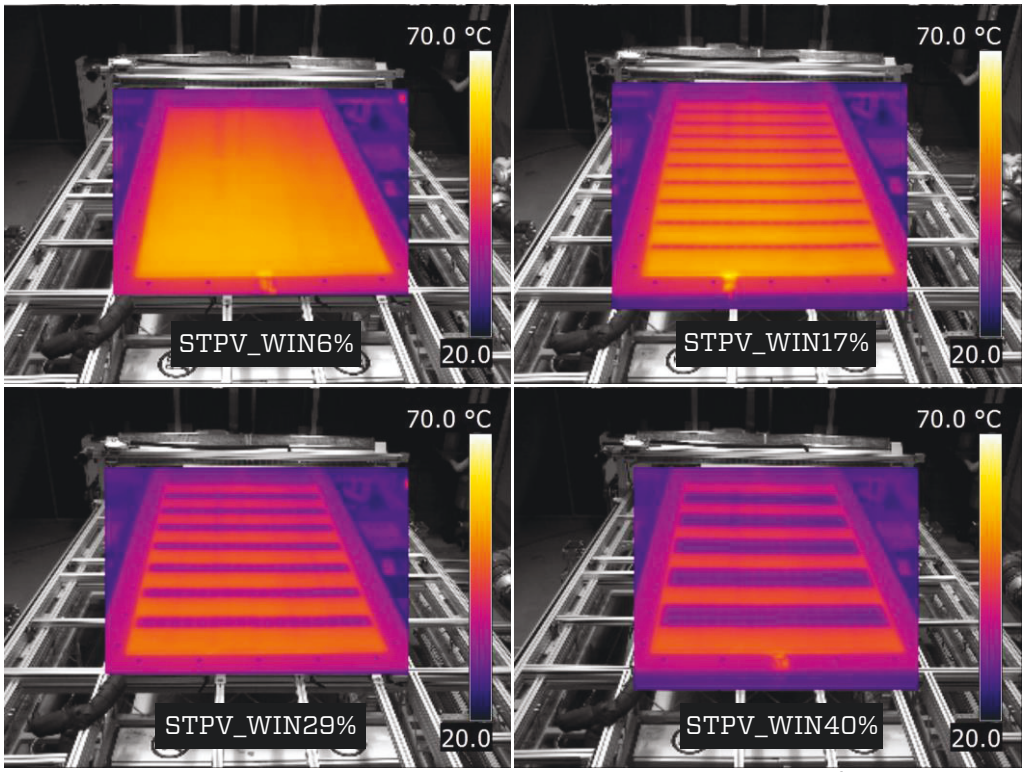

Figure 4.6. Temperature profile for the four STPV windows, under 1000W/m^2, exterior convective film coefficient of 20 W/(m^2·K) and emulated indoor temperatures of 21°C.

The latter approach could provide a more accurate estimation of the cell operating temperature. Finally, operating cell temperatures of up to 80.5°C were observed under 1000 W/m^2 irradiation, still air and ambient air temperature of 21°C for the STPV_WIN6% window assembly, representing the upper cell temperature limit under low wind conditions.

4.5 Parametric analysis

The proposed thermal model was also coupled with an equivalent one-diode electrical model through EnergyPlus simulation software (Lawrence Berkeley National Laboratory, 2015b) to predict the thermal behaviour of various STPV window configurations (Kapsis and Athienitis, 2015). In a given cell temperature and incident solar irradiance, the current-voltage relationship is defined as follows (De Soto et al., 2006):

$$I = I_L - I_D - I_{sh} = I_L - I_o\left(e^{(V+IR_S)/\alpha_I} - 1\right) - (V + IR_S)/R_{sh} \tag{4.12}$$

and

$$\alpha_I = \frac{N_s n_I k T_{STPV}}{q_e} \tag{4.13}$$

where I_o is the diode saturation current (A), R_s is the series resistance (Ω), R_{sh} is the shunt resistance (Ω), α_I is the ideality factor (V), N_s is the number of cells in series, n_I is the usual ideality factor (V) and q_e is the electron charge ($1.60218 \cdot 10^{-19}$ C).

The objective of this parametric study was to understand how STPV window assembly affects the operating cell temperature. For comparative purposes, a building-added STPV module naturally ventilated on both its front and rear side ("free-standing" system) was also simulated. The aforementioned electrical model was used to predict the electrical output of the system while the operating cell temperature was approximated by eq.(4.2) where a=-3.56, b=-0.075 and ΔT=3°C, empirically determined for an open rack system (King et al., 2004).

The simulated STPV windows were integrated on a south-oriented perimeter office façade located in Toronto, ON, Canada (latitude 43.7°N). The Perez model was adopted to predict the beam and diffuse irradiance incident on the window (Perez et al., 1990). Standard EnergyPlus weather data (epw) was used as input while the simulations were performed at a 5-min timestep. Five STPV window assemblies were simulated (Figure 4.7). All assemblies integrated identical STPV modules (Table 4.3).

4.5.1 Presence and location of low-emissivity coating

Low-emissivity coatings are commonly used on window assemblies to reduce heat transfer through radiation exchange between layers and thus enhance the window thermal performance by reducing its overall conductance (Jelle et al., 2012). The location of coating (for "low-e@2" and "low-e@3" assemblies) does not impact the thermal conductance (U-value) of the assembly but does affect the solar heat gains through the window (Figure 4.7). Moreover, when a low-e coating is applied, the SHGC is reduced up to 18% (from 0.274 for "no low-e" to 0.225 for "low-e@3"). The simulations suggest that the presence of low emissivity coating (ε=0.157) on a double-glazed STPV window assembly could increase the operating cell temperatures up to 3°C during spring and summer season (from 59°C for "no low-e" to 62°C for "low-e@3") (Figure 4.8). Though, the location of the low emissivity coating between surface-2 ("low-e@2" assembly) and surface-3 ("low-e@3" assembly) has no impact on the thermal behaviour of the window (less than 0.5°C difference between the two assemblies). Furthermore, when compared to an open-rack system, the operating cell temperatures can be up to 24°C higher (from 38°C for "free-standing" system to 62°C for "low-e@3" window assembly).

Table 4.3. Total optical and electrical properties of the STPV module utilized in all simulated window configurations. The same module was used on the STPV_WIN17% window assembly.

Name of module (outer layer)	Cell technology	Packing factor (%)	Optical properties				Electrical properties under STC			
			Solar		Visible					
			τ_{front}	ρ_{front}	τ_{front}	ρ_{front}	P_{mp}(W)	V_{oc}(V)	I_{sc}(A)	η_{mp}
STPV21%	poly-Si	76.8	0.195	0.088	0.206	0.062	240.40	37.61	8.52	0.13

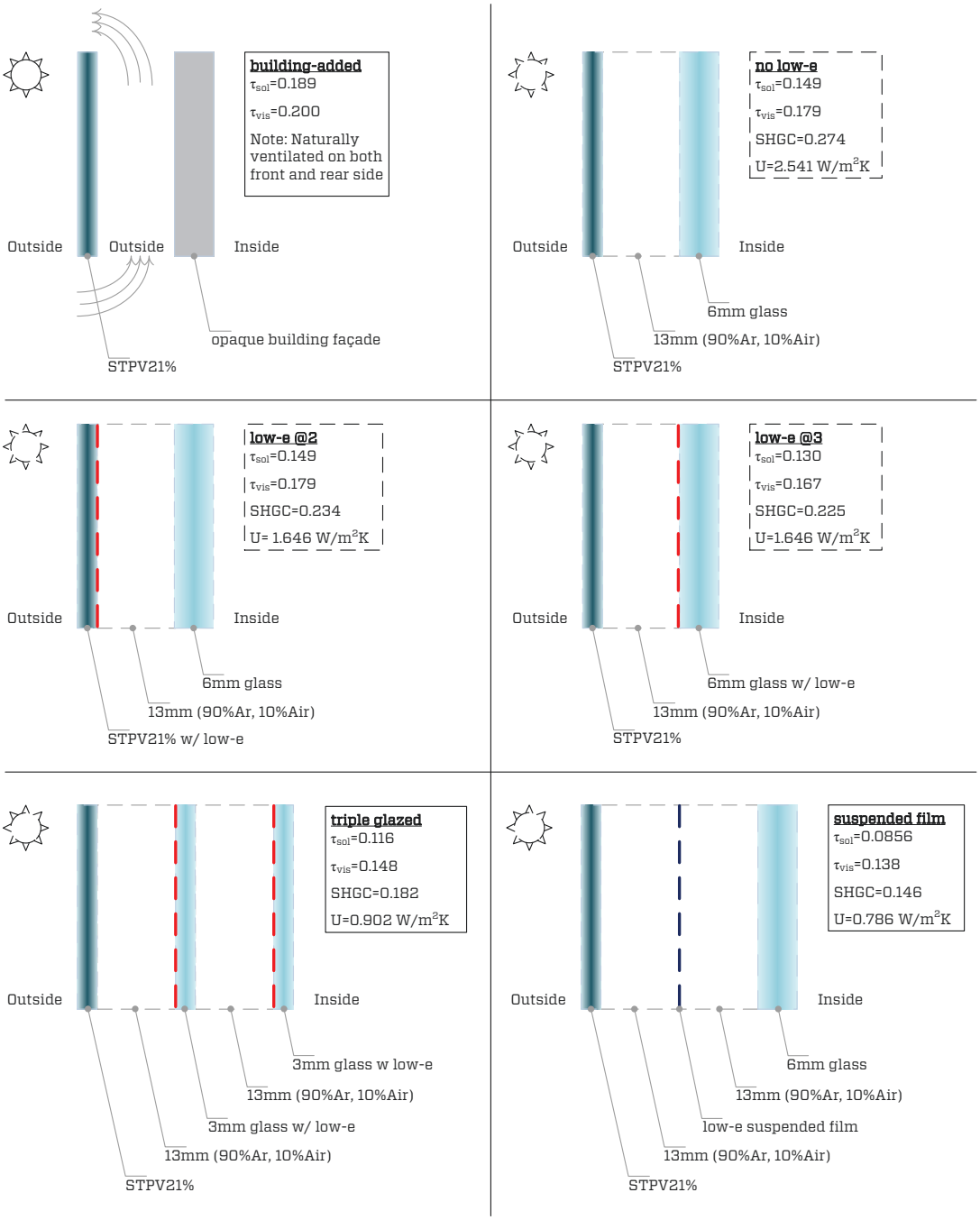

Figure 4.7. Simulated STPV window configurations. A building-added STPV module was also simulated for comparative purposes.

4.5.2 Impact of thermal conductance of the window

When it comes to the thermal performance of modern building envelope, windows are the weakest link as they have significantly higher U-value than the insulated walls (within one order magnitude) (Lyons et al., 2000). In recent years, in order to reduce the window thermal conductance and conserve thermal (cooling and heating) energy, multi-layered windows incorporating low-emissivity properties are used. Once STPV technologies are integrated in high performance window assemblies, high operating cell temperatures might lead to: (i) significant reduction of the annual electricity yield but also (ii) thermal stress of the window

components and STPV devices that might result to component or assembly failure (Deutsche Gesellshaft fur Sonnenenergie, 2005b; Sharma and Chandel, 2013). Upgrading to a triple-layer assembly, the predicted operating cell temperatures can be as high as 65°C for the "suspended film" assembly (up to 31°C higher than the "free-standing" system)(Figure 4.8). For the day presented, up to 9% reduction of the electricity yield is predicted (from 760 kWh/kW for the "free-standing" system to 692 kWh/kW for the "suspended film" assembly) (Figure 4.9). Finally, the annual frequency of cell operating temperatures is presented for the whole year (Figure 4.10).

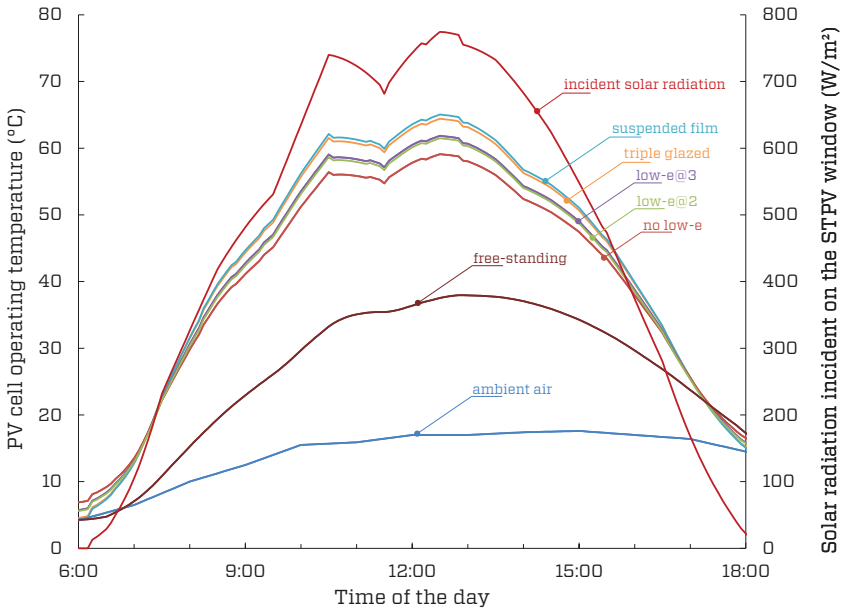

Figure 4.8. Simulated operating cell temperatures of various STPV window assemblies during a typical warm and sunny day for Toronto, Canada.

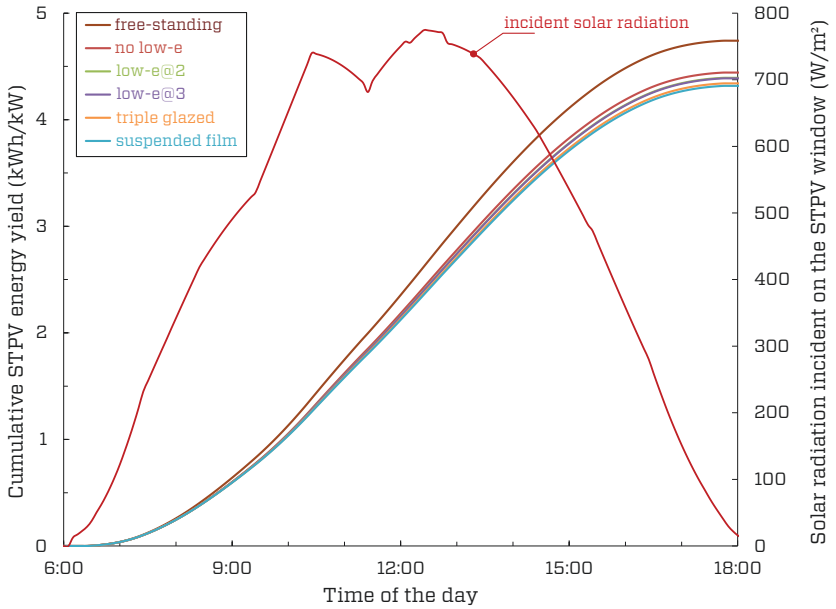

Figure 4.9. Estimated electricity yield of the various STPV window assemblies during a typical warm and sunny day for Toronto, Canada.

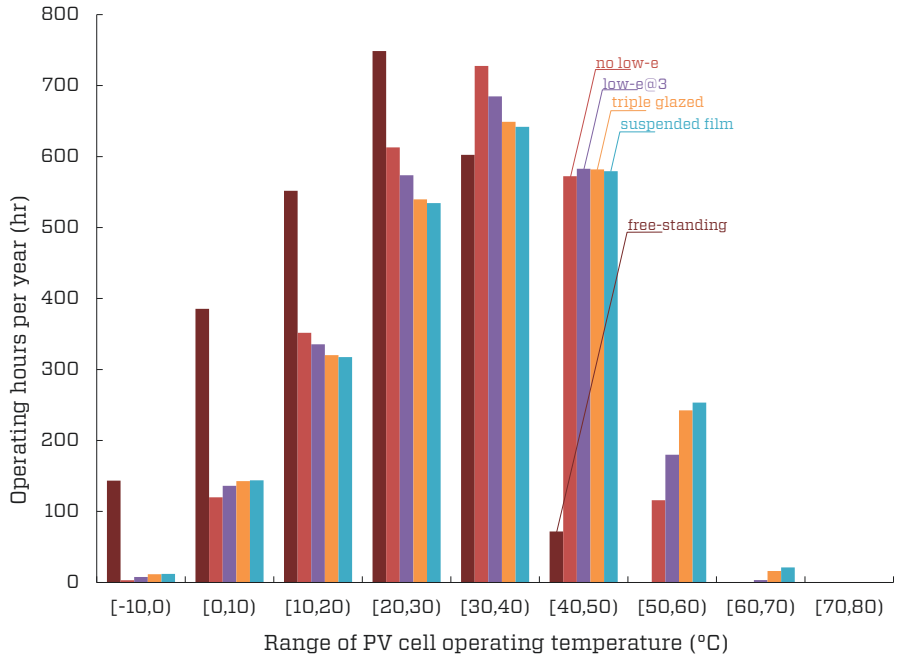

Figure 4.10. Annual frequency of operating cell temperatures for the various STPV window assemblies.

Despite the fact that the data is climate-specific, it provides insight into what is the likelihood for high cell temperatures to occur. For the climate of Toronto, where summer season is relatively mild, no cell temperatures above 70°C occur. However, if the analysis is performed for warmer climates (e.g. Houston or Los Angeles), the occurrence of high temperatures (>70°C) is expected to be evident if not significant.

4.6 Low-order thermal models of STPV windows

Simplified thermal models were also developed based on King's empirical model (King et al., 2004) presented on eq.(4.2) end eq.(4.3). The low-order models can be used when the detailed STPV window assembly design and properties are not known. The annual performance data produced by the detailed numerical thermal model and coupled with one-diode electrical model was used to train a non-linear regression model (numerical experiment) and obtain the empirically-determined coefficients for two STPV window archetypes (Table 4.4): (i) a double-glazed STPV window assembly with low-emissivity coating on surface-2 or surface-3 and (ii) a triple-glazed STPV window assembly with low-emissivity coatings on surface-3 and 4 or surface-3 and 5. Figure 4.11 illustrates the empirically-determined cell temperatures over numerical experiment and the corresponding histograms of residuals. The respective coefficients of determination are R^2 = 0.891 (for double-glazed) and R^2 = 0.939 (triple-glazed). While the models are trained with irradiance data about 500 W/m^2 (red data points), they can also be used to predict operating cell temperatures for irradiance conditions below 500 W/m^2 (blue data points) within an accuracy of about ±5°C. However, low order models tend to underestimate the operating cell temperatures under low irradiance levels.

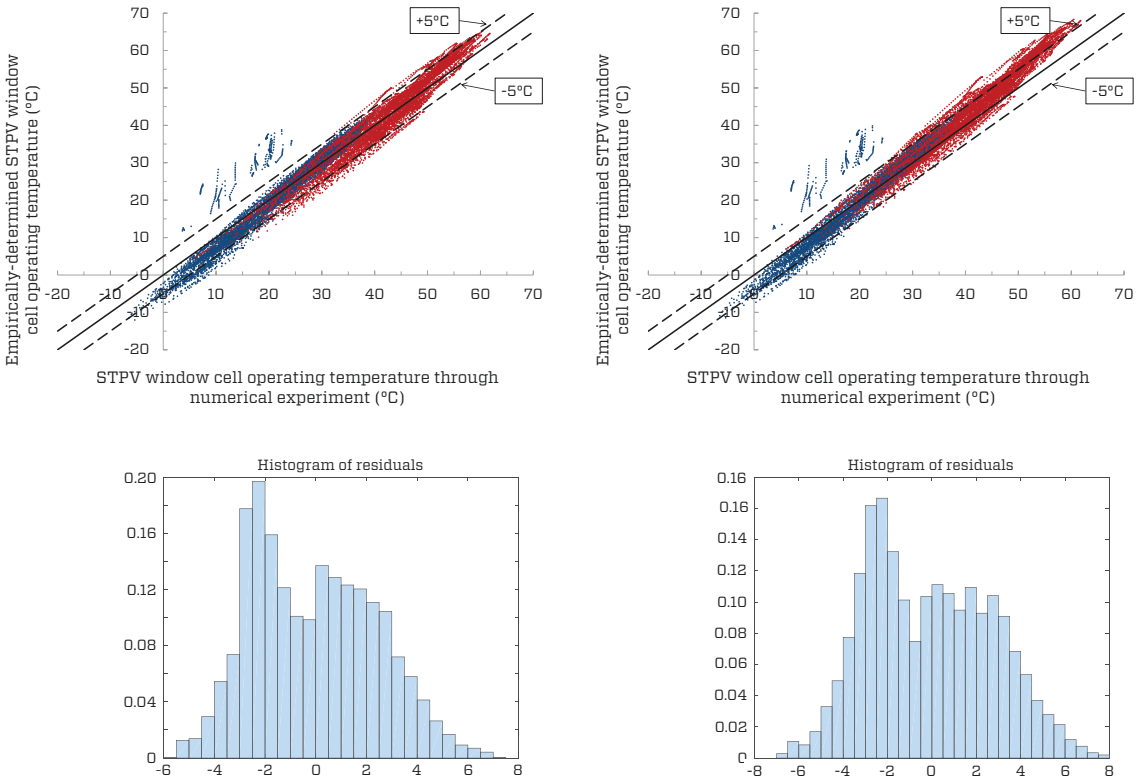

Figure 4.11. Empirically-determined cell temperatures over numerical experiment data and corresponding histograms of residuals for a double-glazed (left) and triple-glazed (right) STPV window assemblies.

Table 4.4. Empirically determined coefficients used to predict the back surface temperature of a building integrated STPV window as a function of irradiance, ambient temperature, and wind speed measured at the meteorological height of 10 m.

STPV window assembly	Mount	a	b	ΔT
Double-glazed with low-e coating (surface-2 or surface-3)	Building integrated	-2.85	-0.0351	9
Triple-glazed with low-e coatings (surface-3 and 4 or surface-3 and 5)		-2.88	-0.0319	11

4.6 Conclusions

The present study focuses on the thermal behaviour of Semi-Transparent Photovoltaic windows (STPV). STPV windows & skylights tend to operate at higher temperatures than open rack systems. High operating temperatures (75°C and above) impact adversely the electrical conversion efficiencies and lifespan of the window and they may result in failure of the window components (e.g. sealants, gaskets) and possibly cell degradation or damage. For this reason, an experimentally-verified numerical thermal model was developed to study the impact of low-e coating, suspended films and overall thermal conductance (U-value) on the operating cell temperatures.

The model was verified with full-scale experiments under the Concordia University Solar Simulator facility. Four double-glazed STPV prototypes windows were assembled and tested. The tests revealed that the STPV module packing factor plays a significant role on the operating cell temperatures (operating cell temperatures rise proportionally to the packing factor) resulting to measured cell temperatures of up to 55.3°C under 1000 W/m^2 and wind-induced convective heat transfer coefficient of 20 W/(m^2·K). The proposed numerical thermal model is able to predict the cell temperatures with an accuracy of about ±5°C (for packing factor >50%) and about ±7°C (for packing factor <50%).

A simulation-based parametric analysis was also carried out for various STPV window configurations. The simulations suggest that the presence of a low-emissivity coating on a double-glazed STPV window assembly has some impact (up to 3°C increase when compared to a double-glazed STPV window with no low-e coatings) on the cell temperatures. However, the location of the coating (either surface-2 or surface-3) has negligible influence on the thermal behaviour of the window. Upgrading to a triple-layer assembly, the predicted operating cell temperatures can be as high as 65°C and up to 31°C higher than the "free-standing" system. This increase resulted to up to 9% reduction on the daily solar electricity yield (from 760 kWh/kW for the "free-standing" system to 692 kWh/kW for the "suspended film" assembly) indicating that the thermal conductance (U-value) of the STPV window impacts the thermal behaviour of the STPV window and thus, the expected power output: the operating cells temperature on a STPV window are inversely proportional to the U-value of the window.

Finally, low-order thermal models were also developed for the following archetype STPV windows: (i) a double-glazed assembly with low-emissivity coating on surface-2 or surface-3 and (ii) a triple-glazed assembly with low-emissivity coatings on surface-3 and 4 or surface-3 and 5. The models can be used during the preliminary design, when the detailed STPV window assembly design and properties are not known.

Chapter 5
A Study of the Potential Benefits of Semi-Transparent Photovoltaics in Commercial Buildings[3]

Abstract

This study investigates the potential benefits of semi-transparent photovoltaic windows on the energy, daylighting and thermal performance of commercial buildings. A general simulation methodology is proposed and utilized, integrating thermal, electrical and daylighting analysis. The impact of various building design parameters on the selection of ideal optical properties of semi-transparent photovoltaics is examined. The potential performance of poly-Si, a-Si/μc-Si and organic cell technologies is also studied. The selection of the module optical properties is shown to be sensitive on the daylight and lighting controls applied and photovoltaic cell technology utilized. The selection of a semi-transparent photovoltaic module with 10% visible effective transmittance resulted in the lowest annual end-use electricity consumption (as low as 5 kWh/m^2/yr). Finally, simulation results suggest that high cell operating temperatures of up to 64°C could occur that might cause accelerated degradation when organic thin film technologies are used.

5.1 Introduction

Effective building façade design should contribute to the creation of a pleasant, glare-free, thermally comfortable environment that will reduce building energy expenditures and optimize daylight utilization (Boyce et al., 2003). In most commercial and high-rise residential buildings, where reducing the costs of cooling energy is important, an integrated strategy to control the transmission of solar radiation needs to be adopted. Rather than having reflective, tinted or fritted windows to reduce solar transmission, Semi-transparent photovoltaic windows may be used to reduce solar heat gains and generate solar electricity (Bahaj et al., 2008; James et al., 2009; Qiu et al., 2009), while still provide adequate daylighting and view to the outdoors (Vartiainen, 2001). The term Semi-transparent photovoltaic (STPV) is used here to cover a broad range of PV technologies, from Si-based cells (arranged in such a way as to allow light to pass through the resulting space between the opaque cells) (Baum, 2011) to "see-through" thin films (Lynn et al., 2012), such as a-Si/μc-Si (Klein et al., 2012; Sai et al., 2014), organic PV (Krebs, 2009; Li et al., 2012) and perovskites (Eperon et al., 2014; Snaith, 2013). As STPV

[3] Kapsis, K., & Athienitis, A.K., 2015. A study of the potential benefits of semi-transparent photovoltaics in commercial buildings. Solar Energy, 115, pp.120–132.

technologies are penetrating the building industry, they are expected to play a key role in on-site electricity generation of new and retrofitted high-performance commercial and institutional buildings; on-site electricity generation can partly offset daily electricity consumption, eliminate grid transmission losses and potentially contribute to grid "peak demand shaving", resulting in reduced need for peak-capacity power plants (Athienitis and O'Brien, 2015).

STPV windows can be utilized to cover large skylight and façade surfaces and regulate solar heat gains and daylight (Bizzarri et al., 2011; Roberts and Guariento, 2009). In order for this to be done effectively, and to ensure market acceptance of this technology within the building industry, the solar, optical and thermal properties of STPV windows and their effect on a building energy performance need to be studied and quantified. Issues such as heat management (STPV cells overheating and non-uniform temperature distributions between cells located near centre-of-the-window and cells located near-the-edge results in electrical efficiency reduction and STPV window thermal stress), visual and thermal performance as well as cost and durability (at least twenty years of performance) have been shown to be as important as STPV electricity production (Chow et al., 2007; Fung and Yang, 2008; Vats et al., 2012). E.g. the selection of STPV optical properties has a direct impact on STPV electrical performance, solar heat gains and daylight availability within the building (Figure 5.1). Improper quantification of such interactions will not only affect the predicted energy use but also misguide the designer towards a suboptimal design, which will impact ease of functionality, ease of installation and result in an unfavourable adoption of this technology by the end-user.

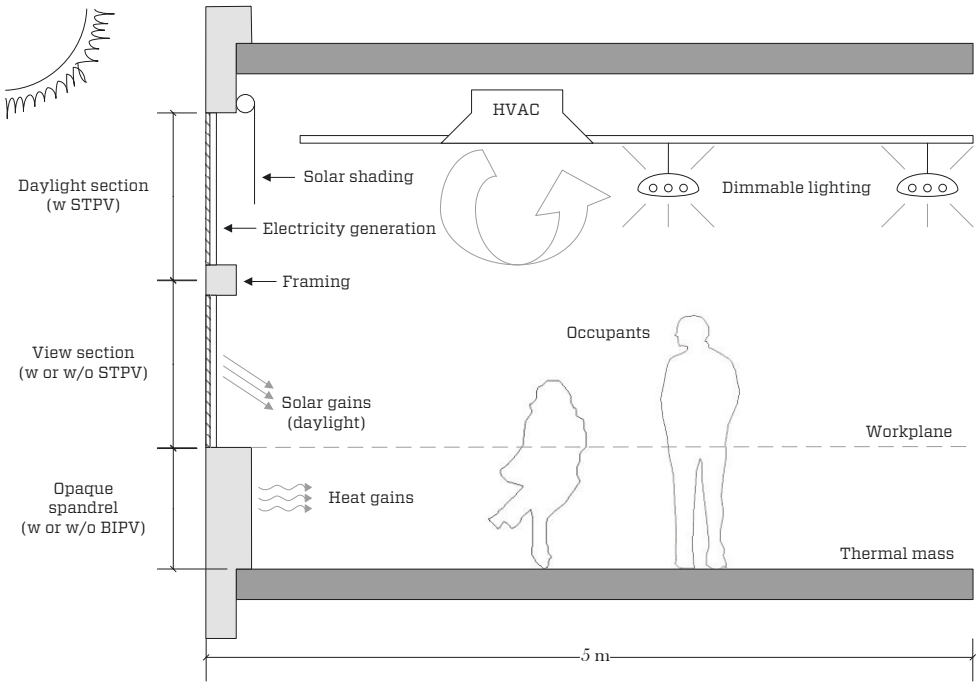

Figure 5.1. Schematic of major interactions between the STPV windows, the office space and the occupants.

The objective of this study is to investigate the potential benefits of STPV windows on the building energy, daylighting and thermal performance through the selection of the STPV optical properties. The study focuses on cooling dominated commercial building perimeter zones in a continental climate region (South-eastern Canada and North-eastern United States). The end goal of this work is to provide input to the design of cost effective, high performance STPV windows with optical, electrical, and thermal properties suited to commercial building façade applications through a general design methodology that could be easily followed by architects and engineers during the preliminary design stage, when there is an opportunity to have the greatest impact on the final design. This differs from standard practice which typically involves the use of energy modelling at the end of the design process when there is little opportunity to make design changes.

5.1.1 Brief overview of existing STPV performance studies

Façade orientation and window-to-wall ratio (WWR) play major roles on the annual STPV electricity yield, solar heat gains and daylight availability. In general, near equatorial facing façades have the highest annual solar potentials for electricity generation. Equatorial facing skylights with a tilt angle near to the altitude of the building site tend to maximize the electricity yield. Whenever optimal orientation is not possible due to site constrains, the STPV windows should face preferably anywhere between ESE and WSW for the north hemisphere (between ENE and WNW for the south hemisphere). When considering the impact STPV windows have on the building energy performance, it was shown that the selection of the ideal STPV optical properties was independent of the building orientation (Chow et al., 2007; Miyazaki et al., 2005; Robinson and Athienitis, 2009), within this orientation range. Though, Miyasaki et al. (2005) and Ng et al. (2013) showed, through simulations, that the WWR has an impact on the selection of ideal STPV optical properties.

Independently of the façade configuration and orientation, it is imperative that the STPV module should be the outermost glass layer of a window assembly. Delisle (2008) demonstrated that by moving the STPV module from being the outermost glass to the middle glass layer of a triple glazed window, electrical yield reduction of up to 22% was predicted, caused mainly by the reduction of transmitted solar radiation to the PV cells. In addition, operating cell temperatures of up to 16°C higher were anticipated, despite the fact that the cavity between outermost glass and STPV layer was naturally vented to outdoors to avoid high temperatures.

Park et al. (2010) showed, through experimental work, that highly absorptive STPV module backsheets (e.g., coloured or tinted glass, used for aesthetic purposes and reduction of solar heat gains) should be avoided, as they can result in PV cell overheating.

The thermal performance of STPV is an area that needs attention because it exerts a significant influence on the durability of the STPV and other window components, such as spacers, sealants and framing. High temperatures need to be predicted, either through testing and/or simulation. The allowable temperature rise depends on the STPV technology implemented (e.g., organic, Si-based, etc.). De Boer and van Helden (2001) predicted PV cell

operating temperatures of up to 65°C on an office STPV window while Wong et al. (2008) predicted temperatures up to 75°C on STPV skylights; Temperatures up to 60°C were measured, with no significant temperature gradient, on a commercial building STPV window (Yoon et al., 2011).

Finally, the daylighting and electric lighting controls implemented (Robinson, 2011; Wong et al., 2008) strongly affected the selection of ideal STPV optical properties, whereas the selection of the HVAC system (Chow et al., 2007; Miyazaki et al., 2005) had no impact.

5.2 Methodology

For this study, an integrated simulation approach (thermal, electrical and daylighting) is followed, proposed by Garde et al. (2011) and Reinhart and Wienold (2011), and adapted to the needs of the study (Figure 5.2). Major procedure steps are described below, with "Step 2" to "Step 5" automated through MATLAB (MathWorks, 2014).

Step 1: An office model is built using SketchUp 3D software (Trimble, 2014). The geometric model is used to generate (i) a Radiance-based model through the su2ds plugin (Kjenner, 2014) that is imported to Daysim software (Reinhart, 2014) for the office annual daylighting/lighting performance and (ii) an energy model through the Legacy OpenStudio plugin (National Renewable Energy Laboratory, 2014) that is imported to EnergyPlus software (Lawrence Berkeley National Laboratory, 2015b) for the office annual thermal and electrical performance.

Step 2: An EnergyPlus Weather (EPW) file is imported to DAYSIM and converted from 1-hr time-step to 5-min time-step (Reinhart and Walkenhorst, 2001). The new weather file is used as input weather file for Perez "all-weather" sky model (Perez et al., 1990). The simulation time step was selected based on daylight availability. Walkenhorst et al. (2002) suggested a 1-min time step instead of a 60-min time-step in order to reduce the errors in calculating daylight availability due to the short-term variability of daylight. However, the systematic underestimation was found to be in the range of 6-18%, while Janak (1999) found a difference of less than 3% between the two simulation time-steps. Considering the fact that occupants tend to be infrequent shade users (O'Brien et al., 2013; Van Den Wymelenberg, 2012) and that daylight and occupancy sensors tend to respond in the range of 5-min to 15-min time-steps in order to avoid occupant disturbance, a 5-min time step was considered satisfactory.

Step 3: A custom-made MATLAB routine is used to generate for manually-controlled roller shade use schedule, based on occupant behavioral statistical models developed by Reinhart and Voss (2003) (when assumed "active users") and Kapsis et al. (2013) (when assumed "inactive users"). The schedule is fed to DAYSIM that performs the annual daylight analysis (Reinhart and Walkenhorst, 2001).

Step 4: Lightswitch-2002 (Reinhart, 2004) routine embedded in DAYSIM is used to generate the electric lighting use schedule (either for "active" or "inactive" users,) based on the workplane illuminance levels due to daylight, calculated at "*Step 3*".

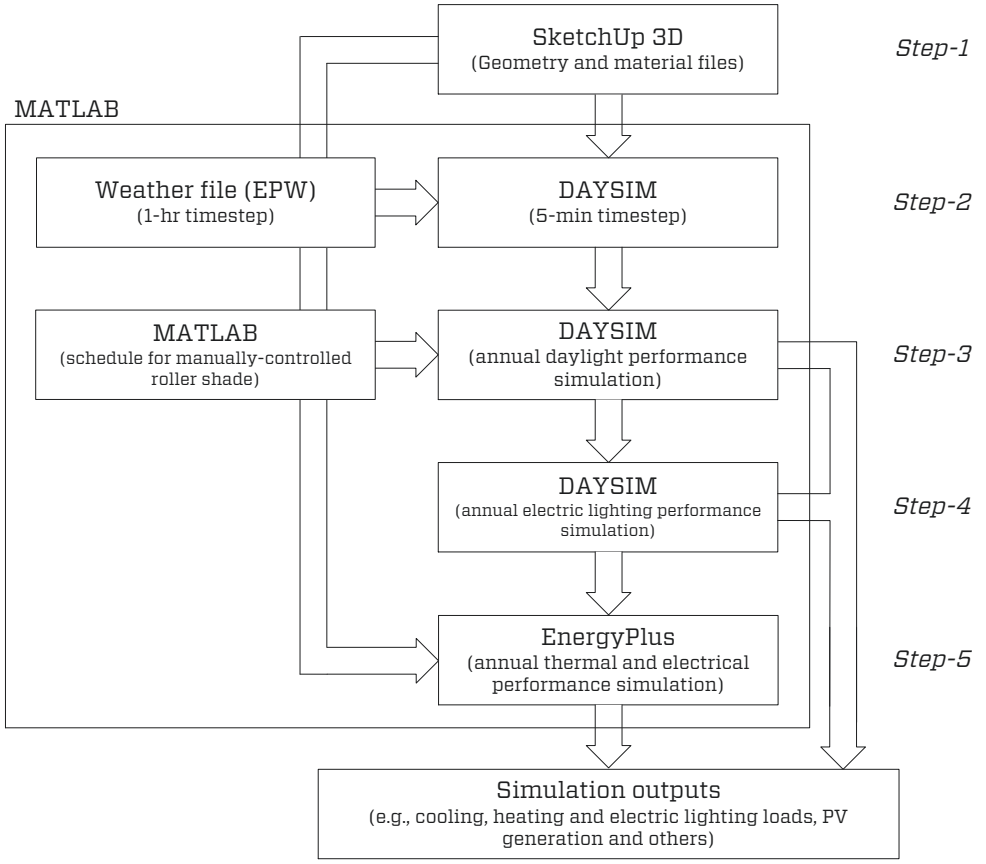

Figure 5.2. Integrated simulation methodology for the study of STPV windows on building applications.

Step 5: The various Schedules are then fed to EnergyPlus that performs the annual energy analysis. An output file is generated comprising the office energy consumption for cooling, heating, electric lighting and equipment, the PV electricity generation, the PV cell temperature profile, the solar heat gains and losses through the STPV window, and others.

The aforementioned methodology can be applied using alternative building performance simulation tools and extended to different advanced façade technologies (e.g. electrochromic windows, windows integrating advanced coatings and/or shading devices).

5.3 Simulation study of a cooling-dominated office utilizing STPV windows

A study was carried out for a cooling-dominated perimeter office zone utilizing STPV windows, adopting the above methodology. The office was located in Toronto, ON, Canada (latitude 43.7°N). Major office modelling assumptions are summarized in this section, while detailed subsections on STPV window daylighting, thermal and electrical modelling will follow.

The zone dimensions were 4 m (width) × 5 m (depth) × 3.2 m (height). Two WWR were studied: WWR=40% and WWR=60%, respectively (Figure 5.3). An exterior wall of U=0.301 W/(m^2·K) was considered. The spandrel and mullion thickness of 0.15 m was taken into account during daylighting and energy performance simulations. The interior walls were assumed to connect with similarly conditioned zones to the office of interest. A medium-weight

concrete floor was used, while furnishings were represented as internal zone surface area exposed to the zone air.

An occupancy density of 10 m^2/occupant was considered, assuming plug loads of 100W/occupant. Figure 5.4 presents the occupancy and plug load schedules (CEC, 2008), from Monday to Friday. An ideal heat recovery ventilation system with constant thermal efficiency of 80% was taken into account, with ventilation rates of 2.5 L/s/occupant and 0.3 L/s/m^2 of floor area (ASHRAE, 2004). The infiltration rate was kept constant at 0.15 L/s/m^2 of exterior surface area.

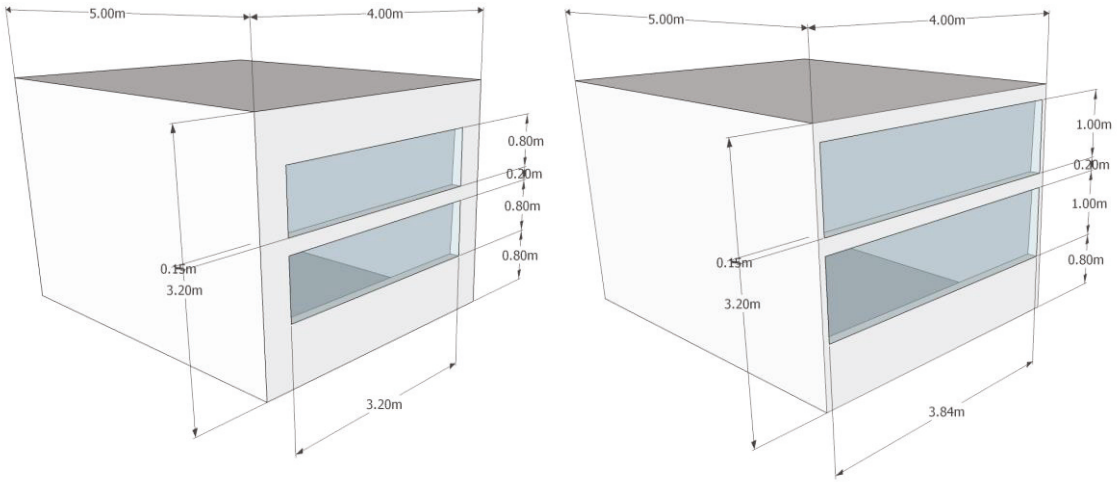

Figure 5.3. Office zone schematics with WWR=40% (left) and WWR=60% (right), utilizing STPV windows.

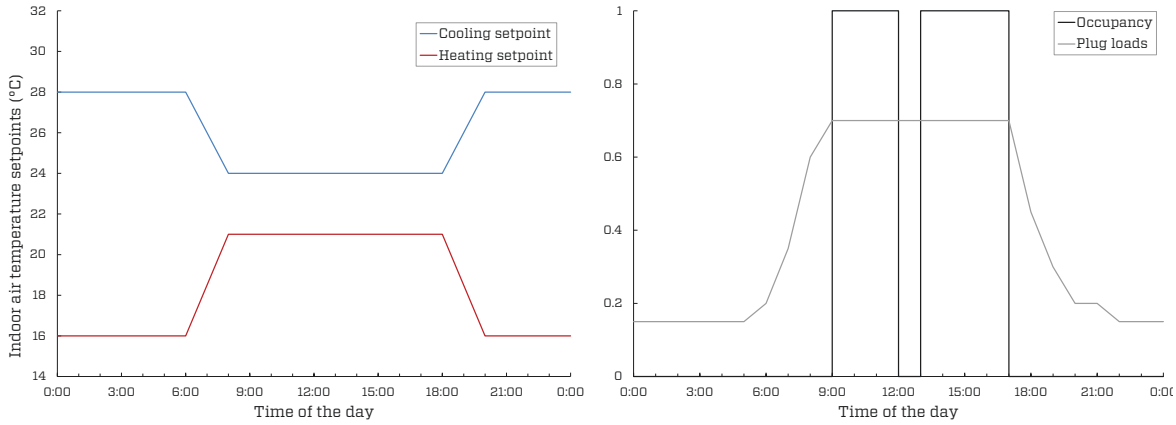

Figure. 5.4. Office air temperature setpoints (left) and weekday schedules for occupancy and plug loads (right).

An ideal air system, that meets cooling and heating loads at all times, was used. The annual office end-use electricity consumption was estimated by converting the thermal energy for heating and cooling to equivalent electric energy, assuming constant Coefficients Of Performance (COP) for cooling ($COP_{cooling}$=3) and heating ($COP_{heating}$=4), throughout the year as follows:

$$E_{yr} = \sum_{t} \left[\frac{E_{cooling}(t)}{COP_{cooling}} + \frac{E_{heating}(t)}{COP_{heating}} + E_{lighting}(t) + E_{plug}(t) - E_{STPV}(t) \right] \Big/ A_{floor} \quad (5.1)$$

where E_{yr} is the annual end-use electricity consumption (kWh/m^2/yr), A_{floor} is the office floor area (m^2) and, $E_{cooling}(t)$, $E_{heating}(t)$, $E_{lighting}(t)$, $E_{plug}(t)$ and $E_{STPV}(t)$ is the office cooling load, heating load, electric lighting, plug load and STPV electricity production (kWh) at a time step t, respectively.

5.3.1 STPV window daylight modelling

The annual daylight performance of various STPV window configurations was studied using DAYSIM, a Radiance-based software. The Radiance simulation parameters used for the analysis are summarized in Table 5.1.

The STPV windows were treated as if they had uniform optical properties. The effective transmittance (under visible and solar spectrum) is summarized in Table 5.2 for both the STPV module (outermost glass of the STPV window) and the STPV window (insulated double-glazing window unit). Five effective visible transmittance values of the STPV module were simulated: 10%, 20%, 30%, 40 and 50%. The minimum value of 10% was selected in order to ensure a certain minimum view to the outdoors. Floor, interior walls and ceiling were treated as perfectly diffuse (Lambertian) surfaces with visible reflectance of 20%, 60% and 80%, respectively. The corresponding thermal and electrical properties of the STPV window can be found at the related subsections below.

A roller shade was considered and treated as a translucent object with direct hemispherical transmittance of 5% and diffuse reflectance of 80%. It should be noted that both DAYSIM and EnergyPlus simulate a shade that is either fully open or fully closed, but not partly-closed. Observational studies have shown (Inoue et al., 1988; Rubin et al., 1987) that occupants will less likely move their roller shades from fully open to fully closed positions or vice versa. In most cases, the shade movements are incremental. Thus, the office model considered intermediate shade positions by "separating" the roller shade into four smaller shades. This way a single shade was replicated as if it was able to be controlled in 5-positions [0 (fully open), 0.25, 0.50, 0.75 and 1 (fully closed)].

Table 5.1. Radiance simulation model parameters

Ambient bounces	Ambient division	Ambient sampling	Ambient resolution	Ambient Accuracy	Direct threshold
7	1500	20	300	0.1	0

Table 5.2. Effective transmittance of the STPV module (outer glass layer) and corresponding STPV window (IGU).

Name of the STPV module	STPV10%	STPV20%	STPV30%	STPV40%	STPV50%
STPV module (outer glass layer only) Visible effective transmittance	10.0%	20.0%	30.0%	40.0%	50.0%
STPV module (outer glass layer only) Solar effective transmittance	8.9%	18.9%	28.9%	38.9%	48.9%
STPV window (IGU) Total visible transmittance	6.1%	12.2%	18.3%	24.4%	30.5%
STPV window (IGU) Total solar transmittance	4.2%	8.6%	13.1%	17.6%	22.1%

Note: The STPV modules are named based on their (front) visible transmittance.

In all cases, an absence sensor was used; the sensor switches the lights off, with a 5-min delay, when occupants exit the room and it keeps the lights off when occupants enter the room. The absence sensor was coupled with a continuous dimming control sensor, utilizing an ideally commissioned photocell, to maintain minimum workplane (0.8 m above floor) illuminance level at 500 lx during occupied hours; the sensor dims the lights to complement daylight and maintain minimum workplane illuminance levels, and switches the lights off when the minimum illuminance levels are met by daylight alone.

5.3.2 STPV window thermal modelling

Energy balance equations were employed to estimate the thermal performance of a STPV window, using EnergyPlus. A heat transfer model adopted for a double-glazed STPV window, with and without an interior roller shade, is presented below (Figure 5.5).

Analogous equations can be used for any additional glass, suspended film or shade layer. The detailed optical and thermal properties of window layers where extracted from LBNL WINDOW (Lawrence Berkeley National Laboratory, 2014a) and THERM (Lawrence Berkeley National Laboratory, 2014b). Each layer (e.g., PV module layer, inner glass layer) consists of two surfaces (e.g., for PV module layer, there is the outer surface and the inner surface). The heat balance equations presented are for each surface k (where k=1 for the outer surface of the outmost layer and k=2N for the inner surface of the innermost layer), for the centre-of-window, assuming: (i) all layers are thin enough to neglect any thermal capacity, (ii) one-dimensional heat transfer perpendicular to the window layers, (iii) each surface is isothermal with uniform thermal and optical properties, (iv) radiation absorbed in a layer is equally distributed on its two surfaces, (v) glass and STPV module are opaque to IR radiation and (vi) the STPV module is always the outermost layer of the STPV window assembly. Any layer transparent to IR radiation was treated similar to the roller shade on eq.(5.5a).

PV module (surface 1)

$$\left(E_o\varepsilon_1-\varepsilon_1\sigma T_1^4\right)+h_o(T_o-T_1)+\left[\frac{\alpha_1 S}{2}-\frac{P_{STPV}}{2A_{STPV}}\right]=U_{STPV}(T_1-T_2) \qquad (5.2)$$

PV module (surface 2)

$$U_{STPV}(T_1 - T_2) + \left[\frac{\alpha_1 S}{2} - \frac{P_{STPV}}{2A_{STPV}}\right] = \left[\sigma \frac{\varepsilon_2 \varepsilon_3}{1-(1-\varepsilon_2)(1-\varepsilon_3)}(T_2^4 - T_3^4)\right] + h_{cav}(T_2 - T_3) \quad (5.3)$$

Inner glass (surface 3)

$$\left[\sigma \frac{\varepsilon_2 \varepsilon_3}{1-(1-\varepsilon_2)(1-\varepsilon_3)}(T_2^4 - T_3^4)\right] + h_{cav}(T_2 - T_3) + \frac{\alpha_2 S}{2} = U_{glass}(T_3 - T_4) \quad (5.4)$$

Inner glass (surface 4) with roller shade

$$U_{Glass}(T_3 - T_4) + \frac{\alpha_2 S}{2} = \left[\frac{\varepsilon_4 \sigma\left[T_4^4(1-\rho_{sh}) - \varepsilon_{sh} T_5^4\right]}{1-\rho_4 \rho_{sh}} - \frac{E_{in}\varepsilon_4 \tau_{sh}}{1-\rho_4 \rho_{sh}}\right] + h_{gap}(T_4 - T_{gap}) \quad (5.5a)$$

Inner glass (surface 4) without roller shade

$$U_{glass}(T_3 - T_4) + \frac{\alpha_2 S}{2} = \left[\varepsilon_4 \sigma T_4^4 - E_i \varepsilon_4\right] + h_{in}(T_4 - T_{in}) \quad (5.5b)$$

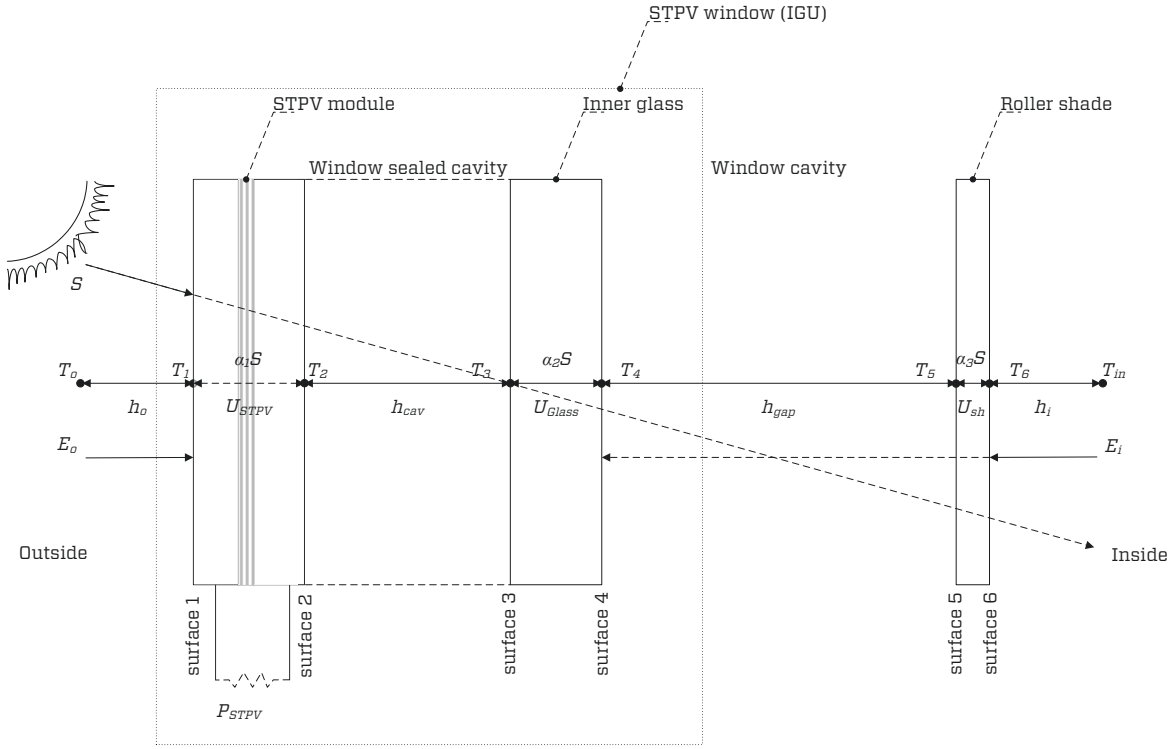

Figure 5.5. Energy balance schematic for a double glazed STPV window with interior roller shade.

where S is the solar radiation incident on the STPV window (W/m^2); E_o, E_i is the exterior and interior IR radiation incident on window surfaces, respectively (W/m^2); P_{STPV} is the power output of the STPV window (W); A_{STPV} is the STPV surface area (m^2); T_k is the average temperature of surface k (K); T_o, T_{in} are the outdoor air and indoor air temperature, respectively (K); ε_k is the emissivity of surface k; h_o, h_i are the outdoor and indoor air film convective heat transfer coefficient, respectively ([$W/(m^2 \cdot K)$]; h_{cav}, h_{gap} are the convective heat transfer coefficients in the STPV window sealed cavity, and the cavity between innermost glass surface and roller shade, respectively [$W/(m^2 \cdot K)$]; U_{STPV}, U_{glass} are the thermal conductance of the STPV module and inner glass, respectively [$W/(m^2 \cdot K)$]; α_j is the ratio of the solar radiation absorbed by the layer j; σ is the Stefan-Boltzmann constant [$5.6703 \cdot 10^{-8}$ $W/(m^2 \cdot K^4)$]; ρ_k is the IR reflectance of surface k; τ_{sh}, ρ_{sh} are the IR transmittance and reflectance of the roller shade, respectively. The thermal and optical properties of each window layer were calculated based on the ISO-15099 standard (ISO, 2003a) and ISO 9050 (ISO, 2003b), respectively.

It should be noted that the STPV cell operating temperature is equal to temperature of surface-1 (TSTPV=T1). Depending on the model accuracy required, the STPV module layer can be treated as three layers: "frontsheet" layer, "STPV cell and encapsulant" layer and "backsheet" layer (Delisle, 2008; Wong et al., 2008). On STPV modules utilizing Si-based opaque spaced cells, the "STPV cell and encapsulant" layer can be separated into two parts: "STPV cells" part and "encapsulant" part (Fung and Yang, 2008). The latter approach could provide a more accurate estimation of the PV cell operating temperature. Nonetheless, Robinson (2011) measured the temperature gradient across a double glazed, low-e (surface-3), poly-Si STPV window installed in a typical office. Through a year of monitoring data, temperature gradients of less than 1°C were observed. Similar experimental observations were made throughout the literature (Infield et al., 2006; Notton et al., 2005; Yoon et al., 2011) independent of the STPV packing factor, electrical efficiency, window assembly and size, reinforcing the notion of treating the "STPV cells and encapsulant" layer as an isothermal surface.

The STPV window assumed for the parametric study consists of (outer-to-inner-layers): (i) 10.9 mm STPV module, which optical and electrical properties varied, (ii) 12.7mm sealed cavity filled with Argon mix (10% Air/90% Argon) and (iii) 5.9 mm low-e ($\varepsilon 3=0.166$) coated glass. Table 5.3 summarizes the thermal properties of the STPV window for the three STPV module technologies simulated in this study: (i) poly-Si opaque spaced cells; (ii) a-Si/μc-Si (micromorphous) transparent thin film; (iii) organic (OPV) transparent thin film. It should be noted that the solar heat gain coefficient (SHGC) of the STPV window varies based on the power output of the STPV module (F. Chen et al., 2012); as the power output rises, the SHGC drops.

Table 5.3. Thermal properties of corresponding STPV window (IGU) for the three STPV module technologies simulated.

Name of the STPV module	STPV10%	STPV20%	STPV30%	STPV40%	STPV50%
SHGC w/o load	0.146	0.219	0.292	0.364	0.437
SHGC w load	0.135 (Poly-Si) 0.139 (a-Si/μc-Si) 0.138 (OPV)	0.208 (Poly-Si) 0.212 (a-Si/μc-Si) 0.211 (OPV)	0.282 (Poly-Si) 0.285 (a-Si/μc-Si) 0.285 (OPV)	0.356 (Poly-Si) 0.358 (a-Si/μc-Si) 0.358 (OPV)	0.429 (Poly-Si) 0.431 (a-Si/μc-Si) 0.431 (OPV)
U-value [W/(m²·K)]	1.634	1.634	1.634	1.634	1.634

Note: The STPV modules are named based on their (front) visible transmittance.

Hence, two SHGC values are reported: (i) SHGC without load; assuming no electric load is connected to the PV system, thus, all absorbed solar energy is transformed to heat and (ii) SHGC with load; assuming electric load is connected at maximum power point thus, part of absorbed solar energy is transformed to electricity.

Finally, thermal bridging occurs due to spacer separating the various window layers as well as due to window frame (Ge and Fazio, 2004; Gustavsen et al., 2007; ISO, 2003a). The edge-of-window might have significantly higher thermal conductance than the centre-of-window hence, frame effects were accounted on the heat balance equations.

5.3.3 STPV window electrical modelling

One of the simplest and most widely adopted model throughout literature (Miyazaki et al., 2005; Robinson and Athienitis, 2009; Wong et al., 2008) is the Evan's model. The model assumes that the electricity generation of a STPV module, operating at the maximum power point, is linearly dependent on the PV cell operating temperature (Evans, 1981). However, such PV electrical performance models tend to overestimate the electricity output of the module (E Skoplaki and Palyvos, 2009). For this study the equivalent one-diode model (Duffie and Beckman, 2006) was used (Figure 5.6), available on EnergyPlus. The module current (I) equals to the difference between light current I_L and, the diode current I_D and shunt current I_{sh}. It can be expressed as a function of five parameters (the model is also known as 5-parameter model):

$$I = I_L - I_D - I_{sh} = I_L - I_o\left(e^{(V+IR_S)/\alpha_I} - 1\right) - (V + IR_S)/R_{sh} \quad (5.6)$$

where I_o is the diode saturation current (A), R_s is the series resistance (Ω), R_{sh} is the shunt resistance (Ω) and α_I is the ideality factor (V). The shunt resistance expresses the leakage of current caused by defects, the series resistance expresses the voltage drop due to migration of charge carriers from the semiconductor to the contacts, and the ideality factor accounts for the thermal voltage and the various mechanisms accountable for moving carriers across the junction (Tian et al., 2012).

For given incident solar radiation (S) and operating cell temperature T_{STPV}, the five parameters need to be determined (I_L, I_o, R_s, R_{sh}, α) in order to calculate the module operating current and voltage. The power is calculated as the product of current I and voltage V:

$$P_{STPV} = IV \tag{5.7}$$

Employing various approaches (De Soto et al., 2006; Pvsyst.SA, 2014) an implicit solution of eq.(5.6) is possible based on the information available by the module manufacturer's datasheet as follows: (i) the short circuit current $I_{sc}(V=0)$, (ii) the open circuit voltage $V_{OC}(I=0)$, (iii) the maximum power point under reference conditions $P_{mp}(I_{mp},V_{mp})$, (iv) the temperature coefficient of the short circuit current $\mu_{I,SC}=\Delta I_{SC}/\Delta T_{STPV}$ and (v) the temperature coefficient of the open circuit voltage $\mu_{V,OC}=\Delta V_{OC}/\Delta T_{STPV}$. Eq.(5.6) is solved simultaneously with energy balance equations eq.(5.2) to eq.(5.5) for each simulation time-step in order to estimate the electrical performance of the STPV module. Table 5.4 provides the electrical data for the three STPV module technologies studied (Appendix C). The presented data is for STPV modules of visible effective transmittance of 10% (STPV10%) and WWR=60%.

Table 5.4. Electrical data for the three STPV module technologies simulated under STC.

STPV module technology	Poly-Si	a-Si/μc-Si	OPV
Name of the STPV module	STPV 10%		
Surface area (m^2)	1.88	1.88	1.88
Efficiency (%)	15%	10%	10%
Short Circuit Current (A)	10.01	1.65	29.59
Open Circuit Voltage (V)	37.22	167	11.3
Current at Maximum Power (A)	9.36	1.52	23.8
Voltage at Maximum Power (V)	30.12	123.9	7.9
Temperature Coefficient of Maximum Power (%/K)	-0.445	-0.270	+0.050
Temperature Coefficient of Short Circuit Current (%/K)	+0.054	+0.071	-0.210
Temperature Coefficient of Open Circuit Voltage (%/K)	-0.333	-0.270	-0.270

As the transmittance of the STPV module increases, the module efficiency decreases (Figure 5.7); as more solar energy is transmitted through, less solar energy is captured and transformed to electric current. Moreover, the efficiency of inorganic PV technologies (such as poly-Si and a-Si/μc-Si) drops with the increase of cell temperature. Conversely, OPV module efficiency slightly rises as the cell temperature increases. However, due to the relatively low OPV manufacturing process temperatures (Krebs, 2009), cell operating temperatures above 75°C should be avoided as it might cause accelerated cell degradation and possibly permanent failure. It should be noted that the maximum efficiencies were selected based on present and anticipated PV module efficiencies and they do not correspond to specific market products. Finally, an ideal PV inverter of 90% efficiency was utilized, always performing at the maximum power point.

5.4 Results and discussion

A comparative study was carried out to select the appropriate optical properties of the STPV windows under various office design parameters. The analysis focused on a cooling-dominated perimeter office building located in Toronto. Table 5.5 summarizes the office design parameters that constitute the "base line" scenario. More than two hundred different office and façade variations were simulated. The present parametric analysis focuses on the cases that demonstrated the highest impact on the energy, daylighting and thermal performance of the building.

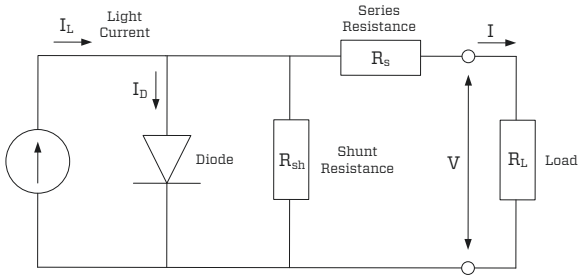

Figure 5.6. Equivalent circuit for the one-diode model.

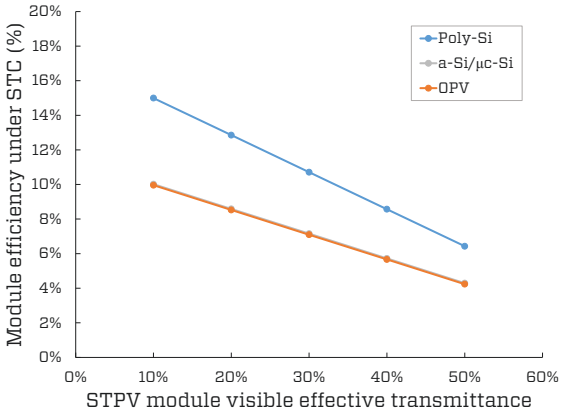

Figure 5.7. STPV module efficiencies as a function of the visible effective transmittance of the STPV module.

Table 5.5. Major assumptions for the base line office design used for the parametric analysis.

STPV window orientation	South
Window-to-wall ratio	60%
STPV module (outer glass layer only) Visible effective transmittance	10%, 20%, 30%, 40% & 50%
STPV module technology	Poly-Si
Lighting power density	7 W/m^2
Occupancy behaviour (for daylight/lighting controls)	"Inactive" users

For ease of understanding, all of the simulation results are presented as a function of the visible effective transmittance of the STPV module, which is to say the outermost layer of the window (Figure 5.5). The corresponding optical, thermal and electrical properties of the STPV window (IGU) can be found on Table 5.2, Table 5.3 and Table 5.4, respectively.

5.4.1 Window-to-wall ratio

The window-to-wall ratio is an important parameter in the selection of optical and thermal properties of a STPV module (De Boer and van Helden, 2001; Miyazaki et al., 2005; Vartiainen, 2001). For this study, two south-facing office configurations were examined: WWR=40% and WWR=60% (base line). It should be noted that electricity consumption is presented as a positive value while electricity production as a negative one. For this section, the electricity breakdown (electricity consumption for cooling, heating, electric lighting, plug loads and STPV electricity production) is also provided (Figure 5.8). Further results are presented as aggregated annual end-use electricity consumption calculated based on eq.(5.1), unless otherwise deemed necessary.

The electricity consumption of the office - excluding STPV electricity production - for WWR=40% was up to 11% reduced when compared to WWR=60%, resulting in the WWR=40% office being a more energy-conserving design. The lower WWR resulted in: (i) lower annual heating loads (up to 25%) due to lower overall exterior wall U-value and, (ii) lower annual cooling loads (up to 39%) due to lower solar heat gains (Carmody et al., 2004). However, there was an increase on electric lighting loads (up to 9%) due to reduced daylight availability (Dubois and Flodberg, 2012).

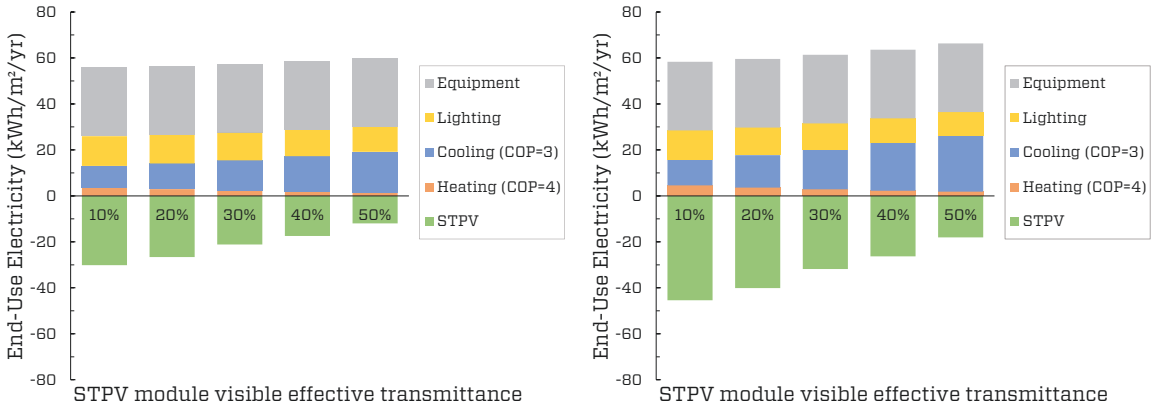

Figure 5.8. Energy breakdown for annual electricity consumption and production of a cooling-dominated, south-facing office with WWR=40% (left) and WWR=60% (right) as a function of the visible effective transmittance of the STPV module (outermost glass layer of the STPV window).

On the contrary, when the STPV annual electricity production was taken into consideration (Figure 5.9), the WWR=60% office had lower end-use energy consumption due to a larger STPV system [e.g. 1.13kWp (WWR=60%) over 0.75kWp (WWR=40%) for STPV10%] that accounted for up to 51% more annual electricity yield. For both façade design cases, the use of STPV10% resulted in the lowest end-use energy consumption (estimated as low as 13kWh/m^2/yr). The question that arises is: do we still arrive at the same result (in this case, use of STPV10%) if we modify other major building design parameters? Thus, an effort to provide an answer is made through the following analysis.

5.4.2 Façade orientation

Façade orientation plays a major role on the potential annual PV power production, solar heat gains and daylight availability. Literature (Chow et al., 2007; Miyazaki et al., 2005; Robinson and Athienitis, 2009) has demonstrated that South-West and South-East facing STPV windows have similar performance on an annual basis. For near-East or near-West oriented façades, merely use of technologies such as reflective glass, electrochromic glass and STPV windows should be avoided as they most likely result in excessive solar heat gains and potential glare due to low solar altitudes. Exterior vertical shading louvers (fixed or movable) should be preferred as they could provide a more effective shading façade solution, when properly designed.

For this study, two window orientations were simulated: (i) South-facing (base line) and (ii) SW-facing. An increase (up to 35%) on the end-use electricity consumption of the SW-facing office was predicted, when compared to the S-facing one (Figure 5.9). The higher end-use consumption was due to an increase on heating demand (up to 58%) and reduction on STPV electricity generation (up to 7%) due to reduced irradiance incident on the SW-window. Nevertheless, the use of STPV10% remained to be the preferred STPV design.

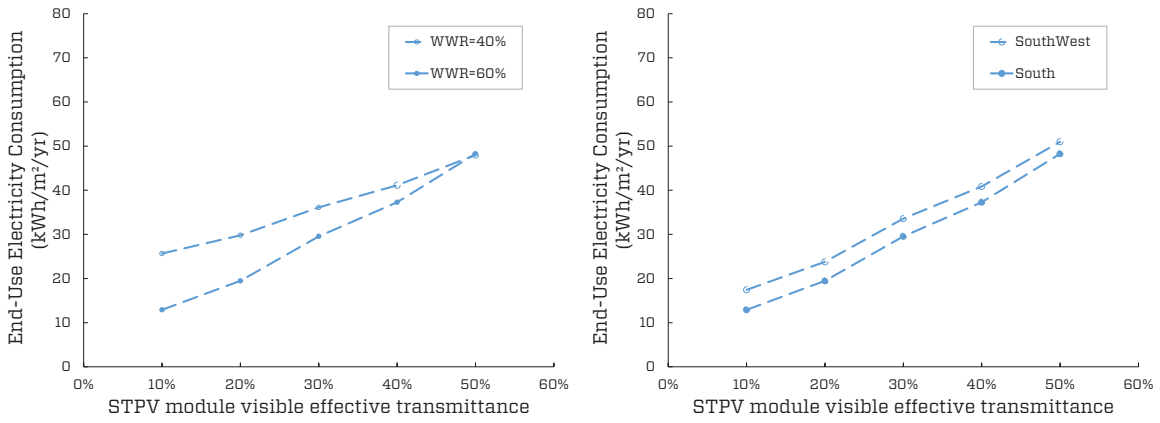

Figure 5.9. Annual end-use electricity consumption for an office with WWR=40% and WWR=60% (left) and for a S-facing and SW- facing office (right).

5.4.3 STPV cell technologies

The potential performance of market-available and emerging thin film STPV technologies in building applications was evaluated in comparison to market-existing poly-Si modules. The simulation was performed for three STPV module technologies: (i) poly-Si (base line), (ii) a-Si/μc-Si and (iii) OPV. The comparative analysis revealed that the selection of STPV technology had some impact on the annual energy performance of the office (less than 8% on heating and less than 4% on cooling loads caused mainly due to variation on SHGC). However, depending on the PV cell technology used, the annual electricity generation varied significantly (up to 170%), resulting in major differences on end-use electricity consumption (Figure 5.10). Poly-Si had the highest annual electricity yield due to relatively higher module efficiencies (up to 15%), despite its relatively high temperature coefficient (μ_{Pmp}=-0.445%/K). OPV had an annual electricity yield up to 49% higher than a-Si/μc-Si (but up to 29% less than poly-Si) due to its slightly positive temperature coefficient (μ_{Pmp}=+0.050%/K), resulting in "temperature-independent" module performance. Nevertheless, long-term exposure to relatively high operating temperatures (75°C and above) has the potential of causing accelerated OPV degradation. For this study, STPV cell operating temperatures up to 64°C were predicted (under T_o=17°C and S=765 W/m^2). As previously stated, the use of STPV10% resulted in the lowest office end-use energy consumption for all three STPV cell technologies.

5.4.4 Electric lighting power density

The electric lighting power density (LPD) installed is a key parameter in achieving net-zero energy targets (Garde et al., 2011; Guglielmetti et al., 2011) as it directly affects space heating and cooling loads. Combined with advanced lighting controls, energy efficient electric lighting is the "low hanging fruit" to achieve significant energy savings. Three electric LPD were examined under this study: (i) 3 W/m^2 (LED lighting), (ii) 7 W/m^2 (highly efficient fluorescent lighting, base line) and (iii) 14 W/m^2 (typical fluorescent lighting).

As the LPD changed, the parametric curve shifted up (when the LPD increased) or down (when LPD decreased) almost in a linear manner concluding that LPD is a less important design parameter in the selection of appropriate optical properties of the STPV module (Figure 5.10). When LED lighting was utilized (LPD=3 W/m^2) in conjunction with a STPV10% module, an annual end-use electricity consumption of as low as 5 kWh/m^2/yr was predicted.

5.4.5 Daylight and lighting controls

It has been shown that applied daylight/lighting control strategies can affect the selection of the ideal optical properties of the STPV window (Miyazaki et al., 2005; Robinson, 2011; Wong et al., 2008). For this study, two control strategies were assumed: (i) "inactive" occupants (base line) and (ii) "active occupants. For electric lighting use, probability functions developed by Reinhart (Reinhart, 2004) were adopted mimicking "active" or "inactive" users switching lights on and off based on workplane illuminance levels. Similarly, probability functions were adopted for manually controlled roller shades assuming that "active" users will frequently

control the shades based on solar penetration depth into the office space (Reinhart and Voss, 2003), while "inactive" users will have an average shade use rate of 0.5/day with average mean shade occlusion of 84% (Kapsis et al., 2013).

When "active" control behaviour was adopted, significant energy savings were achieved on the electric lighting loads (up to 54%) compared to "inactive" behavior (Figure 5.11). A minimal increase of annual cooling loads (less than 5%) was predicted due to the increase of solar gains. Interestingly, when considering the end-use electricity consumption for "active" behaviour — excluding STPV electricity production — it was found that the selection of STPV20% resulted in the most energy-conserving design (the use of STPV20% performed marginally (2%) better than STPV10%). The applied daylight/lighting control strategies affect the ideal selection of the STPV optical properties thus, emphasizing the need for further understanding and development of occupancy behavioural models for shading controls that can be universally applied to building performance models. Nevertheless, when the STPV annual electricity production was taken into consideration (Figure 5.11), the STPV10% resulted in the lowest annual end-use electricity office consumption due to higher STPV system electricity yield.

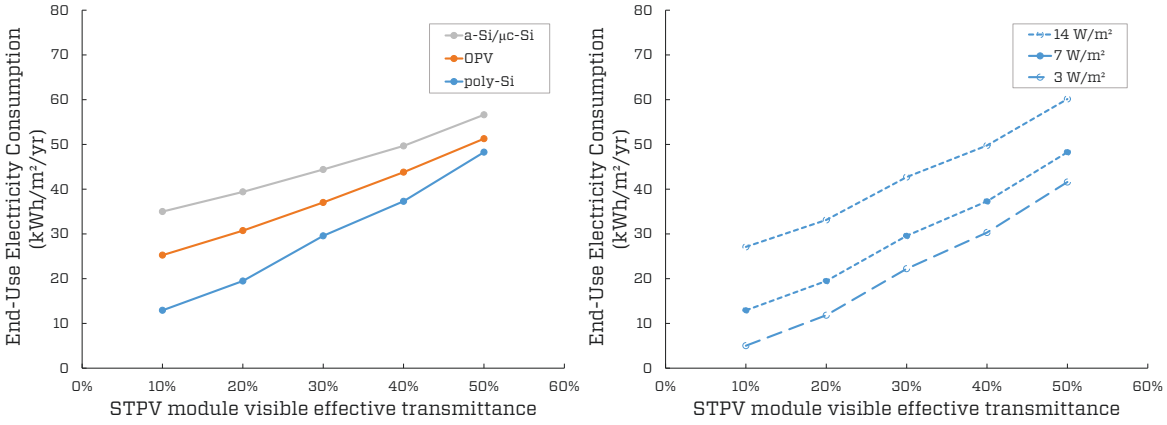

Figure 5.10. Annual end-use electricity consumption for three STPV module technologies (left) and for three electric lighting power densities (right).

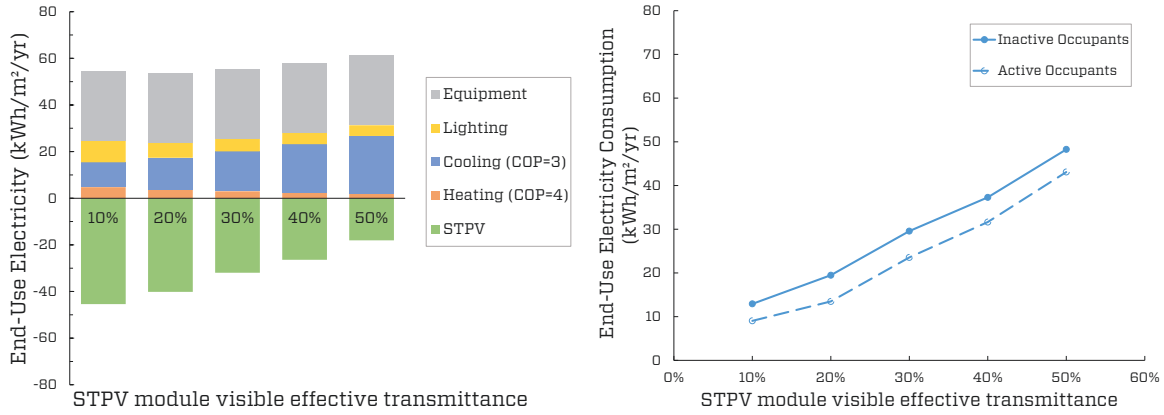

Figure 5.11. Annual end-use electricity consumption for an office with "active" and "inactive" users (left) and energy breakdown for annual electricity consumption and production of an office with "active" users (right).

5.5 Conclusions

This paper examined how STPV windows could affect the energy, daylighting and thermal performance of cooling dominated commercial building perimeter zones under continental climate. A general simulation methodology was proposed and utilized, integrating thermal, electrical and daylighting analysis. The impact of various building design parameters and PV cell technologies on the selection of ideal optical properties was examined.

The simulations revealed that the selection of the module optical properties is sensitive on the daylight and lighting controls applied on the building and photovoltaic cell technology utilized on the STPV window while parameters such as façade orientation, window-to-wall ratio and electric lighting power density had an impact on the building end-use energy consumption but not on the selection of ideal STPV optical properties, within the parameters value range simulated on this study. The use of a STPV module with 10% visible effective transmittance integrated as the outermost layer of a double-glazed, argon filled, low-e, window (STPV10%) resulted in the lowest annual end-use electricity consumption (as low as 5 kWh/m^2/yr). It should be noted that the ideal visible effective transmittance of the STPV module is expected to be higher than 10% for mixed-mode and heating-dominated buildings due to the need of increased passive solar heat gains required during the heating season. Finally, the simulation study predicted cell operating temperatures as high as 64°C. Such temperatures might cause accelerated degradation when organic thin film technologies are used.

Chapter 6
Semi-transparent photovoltaic windows: daylighting and visual comfort analysis for perimeter offices[4]

6.1 Introduction

This chapter provides an in-depth investigation of the potential impact of STPV windows on the daylighting and visual comfort performance of perimeter offices in a continental climate region (North-eastern United States and South-eastern Canada). This is a complementary study on the integral energy performance of STPV windows presented on Chapter 5. Quantitative daylight and glare performance indicators are used to assess the daylit environment through the parametric simulation of the three-section façade design concept (Figure 6.1).

6.2 Description of the perimeter office model utilizing STPV windows

The room modelled in Daysim (Reinhart, 2014) is a south-oriented perimeter office located in Toronto, ON, Canada (latitude 43.7°N). Daysim is an experimentally-validated Radiance-based simulation tool for dynamic daylight and lighting analysis (Gibson and Krarti, 2014; Reinhart and Walkenhorst, 2001). The Radiance simulation parameters used for the analysis are summarized in Table 5.1. A 5-min simulation time-step was selected as a means to capture the short-term dynamics of daylight (Janak, 1999).

Office space description: The office dimensions are 4 m (width) x 5 m (depth) x 3.2 m (height) with a spandrel and mullion thickness of 0.15 m, representing a typical perimeter office zone. The office surfaces are treated as perfectly diffuse with visible reflectance of 20% (floor), 60% (walls) and 80% (ceiling).

Daylighting controls: A translucent roller shade is used with direct hemispherical transmittance of 5% and diffuse reflectance of 80%. The shade can be set in five discrete positions (Kapsis et al., 2013): 0 (fully open), 0.25, 0.50, 0.75 and 1 (fully closed). Probability functions are adopted to emulate occupants manually adjusting the height of the roller shade based on the direct solar irradiance on the workplane (Reinhart and Voss, 2003).

[4] Part of the chapter has been published under: Kapsis, K., Dermardiros, V., & Athienitis, A. K. (2015). Daylight performance of perimeter office façades utilizing semi-transparent photovoltaic windows : a simulation study. In Energy Procedia (Vol. 78, pp. 334–339).

Electric lighting controls: An absence sensor is utilized to automatically switch electric lighting off when the occupants leave the office (with a 5-min delay) while a continuous dimming sensor (using an ideally commissioned photocell) maintained minimum workplane illuminance levels. Probability functions are implemented for occupants manually toggling lights on and off based on the workplane illuminance (Reinhart, 2004).

Daylight distribution and view-field: A mesh of 63 (7×9) equally spaced illuminance sensors is used to capture the workplane illuminance distribution (Figure 6.1). The continuous daylight autonomy (cDA), the spatial daylight autonomy (sDA) and the daylight glare probability (DGP) metrics are used to evaluate the annual daylighting/lighting performance during the 3650 occupied hours (8:00 to 18:00) of the year. Annual and seasonal cDA are presented as the percentage of occupied hours where the minimum workplane illuminance levels of 300 lx (cDA_{300lx}) and 500 lx (cDA_{500lx}) are partially or fully met. Knowing the electric lighting power density (LPD) installed, the electric lighting consumption ($E_{lighting}$) for a period of time (Δt) can be estimated as follows (Reinhart et al., 2006):

$$E_{lighting} = LPD \cdot (1 - cDA) \cdot \Delta t \quad (6\text{-}1)$$

LPD values depend on the lighting technology installed at the office space to provide the minimum illuminance levels. LPD values could vary from 10-14 W/m² for typical fluorescent lighting systems, 6-10 W/m² for high efficiency fluorescent to 3-6 W/m² for LED task/ambient lighting technologies (Dubois and Blomsterberg, 2011). These values are given for usable floor area.

While cDA signifies the percentage of occupied hours that the office is daylit alone, it is deduced by simple averaging on the points of interest and it does not provide indication on the spatial daylight distribution. Thus, the sDA is used as a complimentary metric (I.E.S.N.A, 2012). Annual sDA are presented as a percentage of the entire office workplane where the minimum workplane illuminance of 300 lx ($sDA_{300lx/50\%}$) and 500 lx ($sDA_{500lx/50\%}$) are met for 50% of the occupied period. The preferred daylight sufficiency is reached when $sDA_{300lx/50\%} \geq 75\%$.

Despite the various limitations that glare indices might present (Van Den Wymelenberg, 2014), it has been shown that DGP is currently the least likely to result to inaccurate glare predictions when compared to occupants' preference and acceptance of luminance patterns (Jakubiec and Reinhart, 2012; Van Den Wymelenberg and Inanici, 2014). As DGP is a directional view-dependent index (Wienold and Christoffersen, 2006), for this study it is assumed that the occupant is seated at the centre-of-the-room with the viewing-direction shown on Figure 6.1 (45° relative to the window).

6.3 Results and discussion

6.3.1 Effect of the visible transmittance of the STPV window

A parametric study for a STPV façade with WWR=60%, utilizing thin film technologies (uniform optical properties throughout the window surface), was performed. Five visible effective transmittance values of the STPV module were simulated: 10%, 20%, 30%, 40% and 50%. The optical properties of the double-glazed STPV windows are calculated based on ISO 9050 standard (ISO, 2003b). The minimum value of 10% is selected in order to ensure a minimum view to the outdoors. Moreover, effective visible transmittance higher than 50% will result to STPV window electrical conversion efficiencies lower than 5% resulting to a not cost effective technology. The daylight analysis reveals that the use of a thin film STPV module with effective visible transmittance of 30% (STPV30%) provides sufficient daylight within the perimeter office throughout the year, with $sDA_{300lx/50\%}$=100% and $sDA_{500lx/50\%}$=60% (Figure 6.2). The corresponding annual cDA_{300lx} varies from 51% (4.5 m from the window) to 85% (0.5 m from the window) while the annual cDA_{500lx} varies from 36% to 79% (Figure 6.3), respectively.

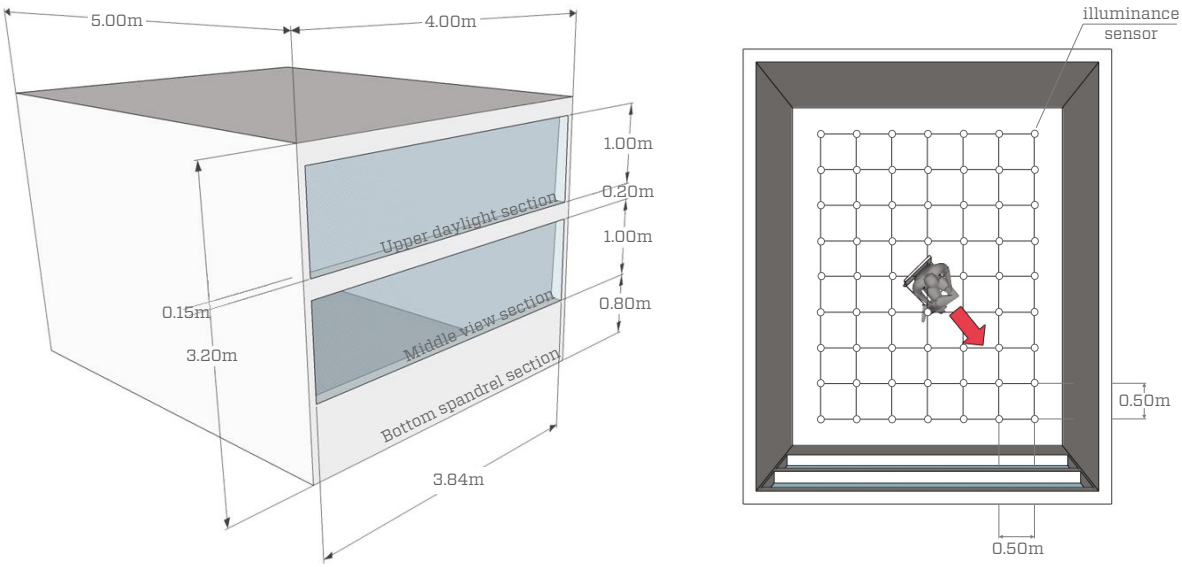

Figure 6.1. Schematic of the perimeter office adopting the three-section façade design with WWR=60% (left) and the location of the occupant and the workplane illuminance sensors (right).

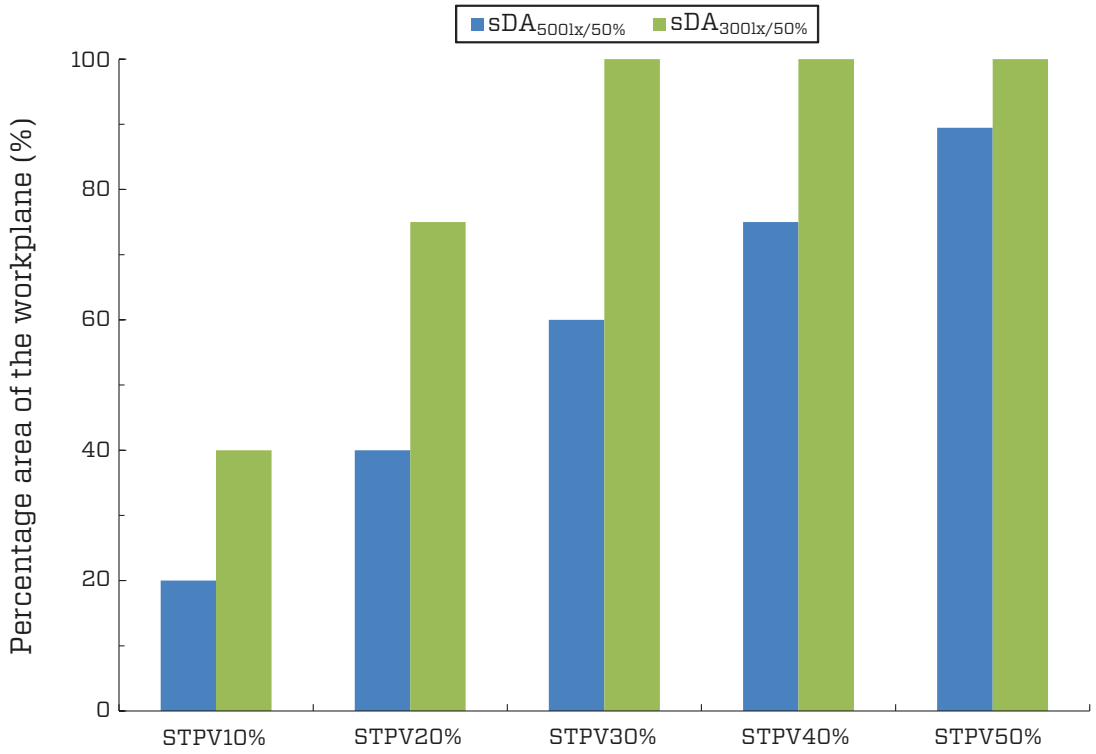

Figure 6.2. Annual sDA as a function of the total visible transmittance of the STPV window integrating thin film technologies, for an office with WWR=60%.

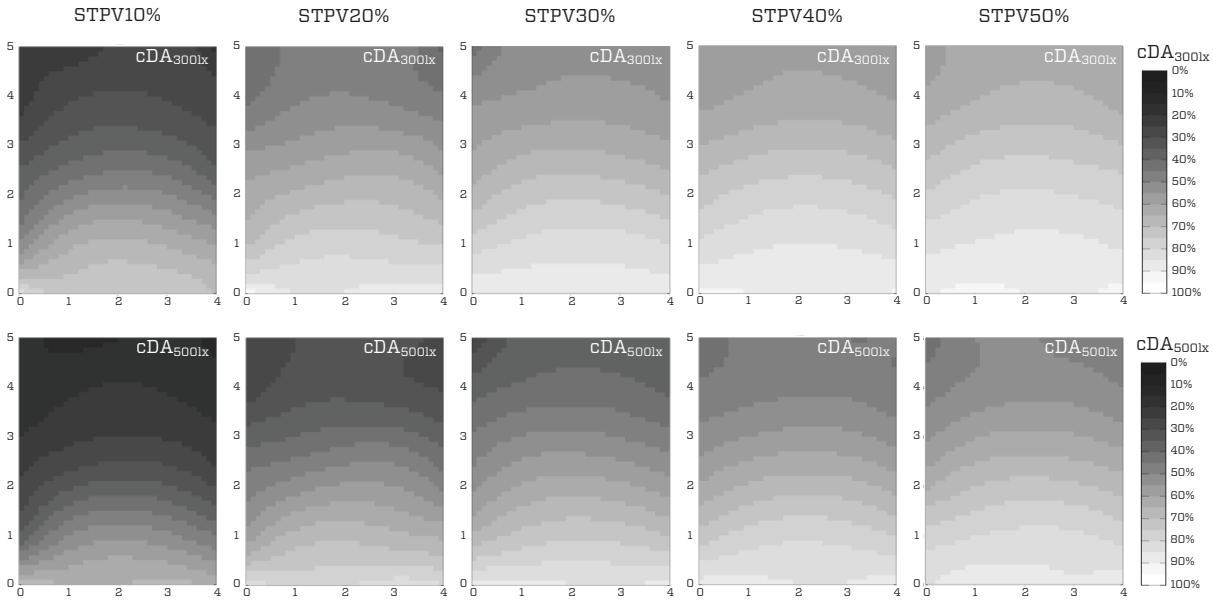

Figure 6.3. Annual cDA as a function of the total visible transmittance of the STPV window integrating thin film technologies, for an office with WWR=60%.

6.3.2 Effect of the window-to-wall ratio of the STPV façade

The WWR has shown to be a prominent parameter on the selection of the optical properties of the STPV window. Thus, further parametric analysis is performed for WWR=40%. The simulations indicate that the integration of a STPV thin film window with

effective visible transmittance of 40% (STPV40%) offers adequate daylight conditions throughout the year, with $sDA_{300lx/50\%}$=80% and $sDA_{500lx/50\%}$=45% (Figure 6.4). The corresponding cDA_{300lx} varies from 45% (4.5 m from the window) to 86% (0.5 m from the window) while the cDA_{500lx} varies from 30% to 80% (Figure 6.5), respectively.

It should be noted that the integral simulation results indicate that the use of a STPV module with the lowest visible effective transmittance (STPV10%) results in the lowest annual end-use electricity consumption, for both WWR=40% and WWR=60% (Figure 5.9). Such a low STPV module transmittance leads to high annual PV electricity yield and reduced cooling loads (STPV module efficiency is inversely proportional to the visible transmittance of the module and thus, to the solar gains) but obstructs daylight. If someone takes into consideration the fact that daylight and view to the outdoors has a positive impact on occupants' health and productivity (Boyce et al., 2003; Farley and Veitch, 2001) as well as the building retailing (Heschong et al., 2002), there is a trade-off to be made by the building design team: The use of a higher than 10% STPV visible transmittance (STPV30% for WWR=60% and STPV40% for WWR=40%) engenders an increase in energy expenditure that could be offset by the benefits of a more pleasant daylit environment.

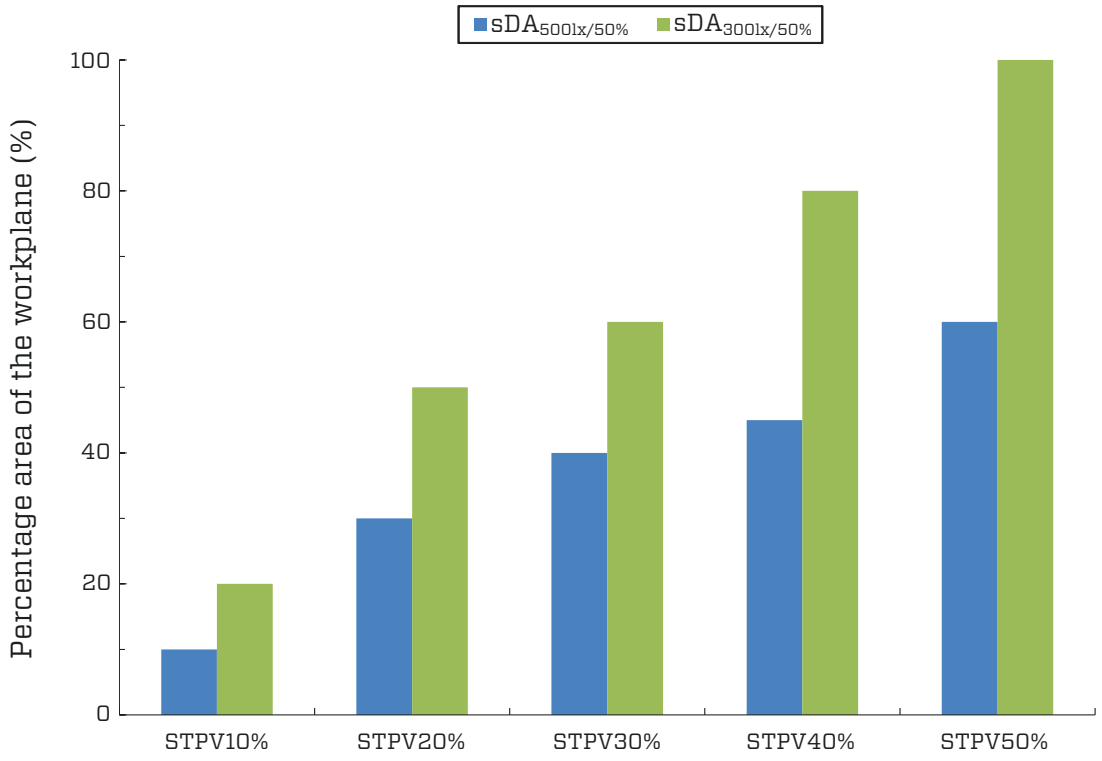

Figure 6.4. Annual sDA as a function of the total visible transmittance of the STPV window integrating thin film technologies, for an office with WWR=40%.

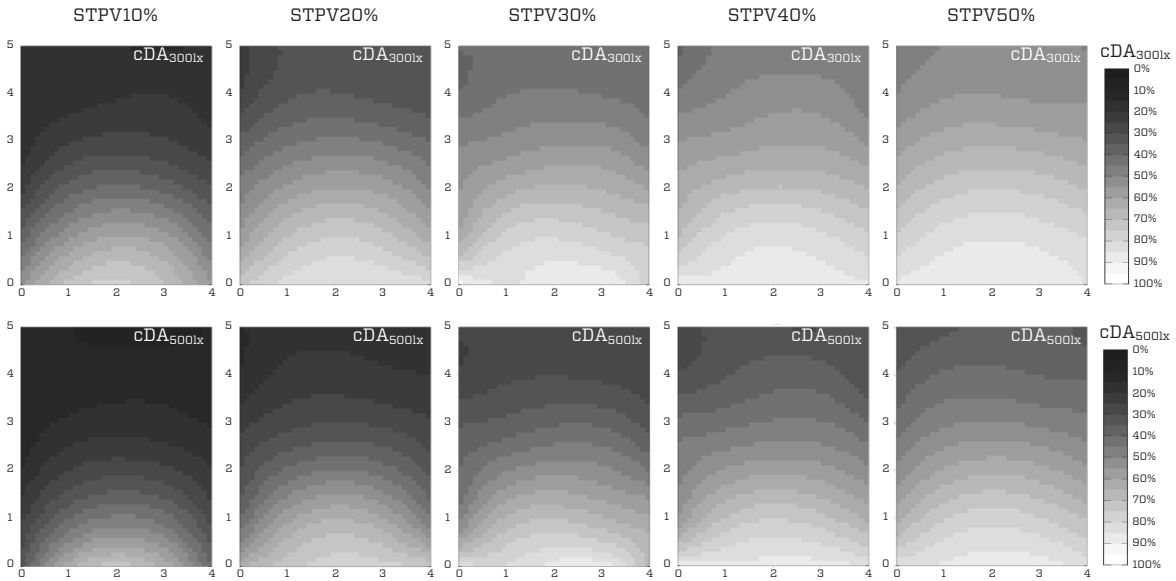

Figure 6.5. Annual sDA as a function of the total visible transmittance of the STPV window integrating thin film technologies, for an office with WWR=40%.

6.3.3 Effect of the STPV façade configuration

The performance of three STPV façade configurations are also studied (Figure 6.6): a) a three-section façade that utilizes transparent thin film PV, b) a three-section façade with Si-based spaced PV cells on the "view section" and thin film PV on the "daylight section" and c) a three-section façade with Si-based spaced PV cells.

One would think that the use of different STPV technologies might not affect annual and seasonal cDA as in all cases, the STPV modules used have the same visible effective transmittance of 30% (STPV30%). However, the analysis for a WWR=60% shows that when the thin film STPV window on the "daylight section" of a three-section façade is replaced with a STPV window integrating Si-based spaced cells then the annual cDA could increase by up to 7 to 16 percentage points (0.5 m and 4.5 m away from the façade, respectively) while seasonal cDA could increase by up to 11 to 22 percentage points (Figure 6.7). The increase is caused by the alternating shadow and bright spots on the workplane resulted by the opaque Si-based spaced cells integrated on the STPV window. If the thin film STPV window on the "view section" is replaced with a STPV window integrating Si-based spaced cells as well, then the increase on the annual and seasonal cDA is marginal, up to 3 percentage points. In addition, the use of STPV window integrating Si-based spaced cells on the "view section" will partly obstruct the view to the outdoors. Thus, the STPV façade configuration with Si-based spaced PV cells on the "daylight section" and thin film on the "view section" is preferred as it has the potential to maximize daylight utilization and the view to the outdoors.

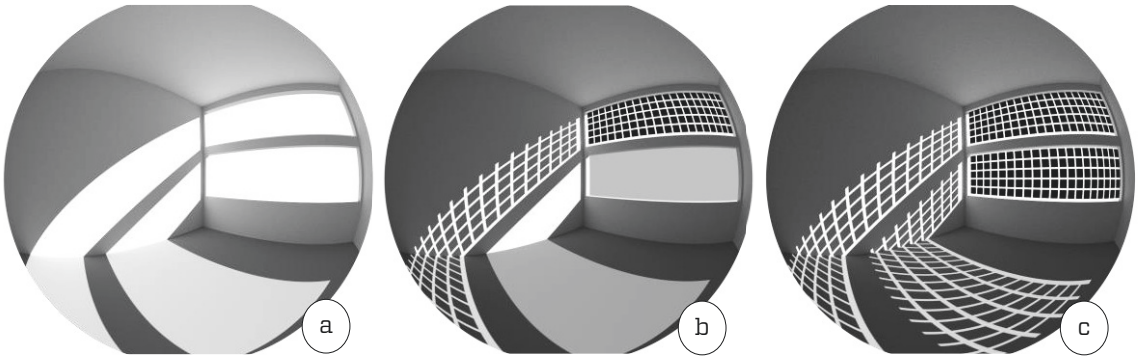

Figure 6.6. Photorealistic renderings of the view-field of the occupant for the three STPV façade configurations with WWR=60%, utilizing thin film STPV (left), Si-based spaced PV cells on the "view section" and thin film on the "daylight section" (centre), and Si-based spaced PV cells (right).

For all the three façade configurations, the DGP metric indicates that the glare is intolerable (DGP≥0.45) for less than 5% of the year (Figure 6.8). Despite the use of a roller shade, glare occurs during the fall/winter seasons (October to March) when the solar altitude is low and solar penetration depth is relatively high. Moreover, for both the façade configurations that integrate Si-based spaced cells on the "daylight section", the glare is perceptible (0.35≤DGP<0.40) less than 6.5% and disturbing (0.40≤DGP<0.45) less than 3.5% of the year, caused by the non-uniform luminance distribution between opaque PV cells and the light passing through the resulting space between the cells (Kim et al., 2008).

6.4 Conclusion

The potential impact of semi-transparent PV windows on the daylighting performance of commercial building perimeter zones was investigated through Radiance-based parametric simulations. The analysis was performed under continental climate (North-eastern United States and South-eastern Canada). The daylighting performance of various semi-transparent PV technologies and façade configurations was examined. The daylight simulation outcomes can be summarized as follows:

- The window-to-wall ratio and STPV technology integrated on the window impact the daylight performance of the STPV façade;
- The selection of a semi-transparent PV modules (the outer glass layer on a double-glazed window) with visible effective transmittance of 30% to 40% (STPV30% for WWR=60% and STPV40% for WWR=40%) could provide sufficient daylight within the perimeter zone throughout the year;
- While the use of STPV30% and STPV40% optimizes daylight utilization, it also increases the cooling costs when compared to modules with lower transmittance, due to increased solar gains. Thus, there is a trade-off to be made: Although the use of STPV30% and STPV40% results in an increase in energy expenditure, a daylit and visually comfortable indoor environment can be beneficial for the occupants;
- The three-section façade configuration integrating Si-based spaced PV cells on the upper section of the façade (daylight section) and "see-through" thin PV film on the

middle section (view section) has the potential to maximize daylight utilization and view to the outdoors while minimizing glare.

The last conclusion is drawn based on quantitative daylight performance indicators. However, daylight quality extends beyond measurable quantities. It is an "emergent state created by the interplay" of the daylit environment and the occupant and it is variable to e.g. mood state, task and aesthetic judgements (Veitch and Newsham, 1997). Such as it is, it can only be fully assessed through behavioural studies where actual people are involved.

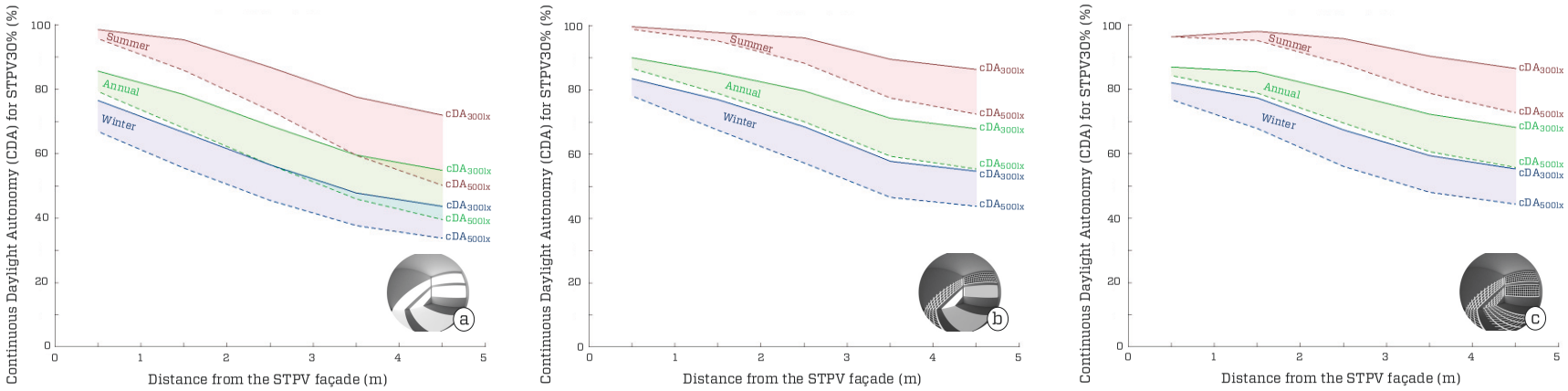

Figure 6.7. Annual and seasonal cDA for the three STPV façade configurations studied, for an office with WWR=60%.

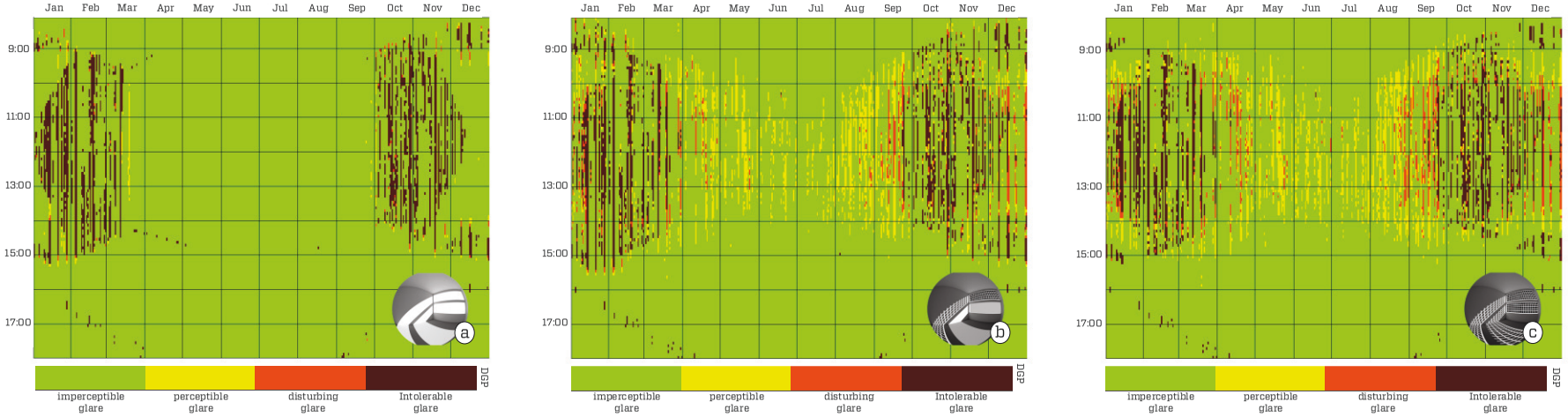

Figure 6.8. Annual DGP for the three STPV façade configurations studied, for an office with WWR=60%.

Chapter 7
Conclusions

The main conclusions of the modelling, design and experimental studies of Semi-Transparent Photovoltaic (STPV) windows conducted under this thesis can be summarized by the following points:

- The solar electricity generation of the STPV window must be considered during the experimental determination of the solar heat gain coefficient (SHGC). Failure to do so may lead to up of 23% higher SHGC measured values compared to a STPV window operating under maximum power point tracking conditions. Moreover, the need to update the existing standards to provide guidelines on how to test and certify STPV window technologies was made apparent;
- Window design parameters such as the packing factor (the percentage of the window surface that is covered with PV cells) and the thermal conductance (U-value) of the STPV window play a significant role on its operating cell temperatures and consequently, solar electricity yield. Nonetheless, the use of low-emissivity coatings have little to no impact on the temperature profile of the window;
- The design and performance of STPV windows is sensitive to the daylight and lighting controls applied on the building and photovoltaic cell technology integrated within the window. Parameters such as façade orientation, window-to-wall ratio and electric lighting power density have an impact on the building end-use energy consumption but not on the selection of ideal optical properties. For a typical office located in Toronto, Canada, the use of a STPV module as the outermost layer of a double-glazed, argon filled, low-e window with 10% visible effective transmittance resulted in the lowest annual end-use electricity consumption (as low as 5 $kWh/m^2/yr$) but lacked sufficient daylight. Alternatively, the selection of a STPV module with visible effective transmittance of 30% to 40% (for WWR=60% and WWR=40%, respectively) could provide sufficient daylight within the perimeter zone throughout the year but increase the cooling costs due to increased solar gains. Thus, there is a trade-off to be made: although the use of visible effective transmittance of 30% to 40% results in an increase in energy expenditure, it also creates a fully daylit and visually comfortable indoor environment;
- The three-section façade configuration integrating Si-based spaced PV cells on the upper section of the façade (daylight section) and "see-through" thin PV film on the middle section (view section) has the potential to maximize daylight utilization and view to the outdoors while minimizing glare.

7.1 Contributions

This thesis provides a systematic study of STPV windows suited for building applications through experimental work and simulations. The major contributions are:

- **Development of a general design methodology** for building designers on the selection of ideal STPV window properties specific to climate, façade configuration and building typology. The proposed methodology utilizes Building Performance Simulation (BPS) tools to study the integral (daylight, thermal and electrical) performance of STPV windows and their impact on building energy performance and occupancy comfort;
- **Development of an experimental standard test procedure** suited to determine the SHGC and thermal conductance (U-value) of STPV windows based on existing PV and window test standards. The proposed procedure utilizes an indoor solar simulator coupled with a solar calorimeter apparatus. For this study, the Concordia Solar Simulator and Environmental laboratory was used – a research facility that allows fully controllable conditions, repeatability and the ability to reach and maintain steady-state conditions necessary to determine performance parameters such as SHGC and U-value. The proposed test procedure can be extended to other advanced fenestration technologies such as electrochromic windows;
- **The in-depth study and understanding** of the impact that various window design parameters have on the temperature profile and solar energy yield of STPV windows. The impact of these parameters (namely SHGC, U-value, low-emissivity coatings and suspended films, cell technologies, as well as optical and thermal properties) was evaluated through experimental work and experimentally-verified numerical simulations;
- The development of low-order, reliable (with an accuracy of ±5°C) thermal models for the prediction of cell operating temperatures. The models can be used to easily assess the solar energy yield of STPV window systems during preliminary design stage;
- **The integral parameter (daylight, thermal and electrical) performance study of the three-section façade design concept** incorporating STPV technologies (namely Si-based opaque PV cells, a-Si/μc-Si and organic-based "see-through" thin films).

7.2 Outlook and future research needs

While a number of advances have been realized over the course of this thesis, further steps are necessary to foster a wider adoption of STPV window technologies on the built environment.

- **STPV building integration**. The importance of highly insulating spacers and frames is recognized and special attention is needed during design and assembly, allowing pressure equalization and thermal movement of the STPV module while minimizing thermal bridging. Extensive research is required for the appropriate selection of such components that will result in high performance, long lasting (25-30 years) STPV windows. In addition, guidelines and considerations for effective building integration of such technologies are necessary to allow the building industry to more easily adopt BIPV technologies based on existing practices and eventually allow them to become ubiquitous building envelope components;

- **Study of the performance of STPV windows on double-skin façade applications.** While the present study focuses on insulated glazing STPV windows, the integration of STPV cell technologies on the outer layer of a double-skin façade is possible, allowing the cogeneration of electricity and heat. Further research is required to develop models and guidelines that will assist building designers on the successful integration of STPV technologies on double skin façades;
- **Integrated STPV module electronics**. Current advancements within the power electronics industry allow the full integration of junction boxes, micro inverters and optimizers into the STPV window assembly. Research is needed to study the performance and longevity of such components and optimize their integration within the STPV window assembly;
- **Use of bifacial STPV solar cell technologies**. Typical STPV cell technologies tend to photogenerate electricity through absorption of photons incident on the front surface of the window (monofacial cells). Bifacial-based STPV windows can also utilize the photons reflected (e.g. from a highly reflective interior shading device) toward the rear side of the window and thus generate solar electricity from both front and rear sides. Parameters such as cell spacing and reflectance of interior shading devices have a major impact on the power output of bifacial windows and as such, need to be studied through experimental work and simulations;
- **Occupant-controlled shade patterns**. It has been shown that the patterns of occupants manually controlling shades have a large impact on the appropriate selection of façade optical and thermal properties – including STPV – due to "effective" available daylight and heat gains in the space. The current approach for designing a STPV façade is either assuming that there are no shades (design based on worst case scenario) or assuming a simplified control strategy (e.g. fully closed shades, when glare occurs). Occupant observational studies demonstrate that both scenaria are unrealistic, resulting in suboptimal façade design and performance. The necessity to develop reliable occupant behaviour models for shading controls that can be applied to building performance models is evident through literature. Such models will allow designers to better conceptualize designs which reduce energy usage and peak loads, while maintaining occupant comfort.

Bibliography

Abdulrazzaq, O., Saini, V., Bourdo, S., Dervishi, E., Biris, A.S., 2013. Organic Solar Cells: A Review of Materials, Limitations, and Possibilities for Improvement. Part. Sci. Technol. 31, 427–442.

Ando, E., Miyazaki, M., 2008. Durability of doped zinc oxide/silver/doped zinc oxide low emissivity coatings in humid environment. Thin Solid Films 516, 4574–4577.

ASHRAE, 2013. ASHRAE Handbook—Fundamentals. Atlanta, GA.

ASHRAE, 2004. ANSI/ASHRAE standard 62.1–2004. Atlanta, GA.

Athienitis, A.K., O'Brien, W. (Eds.), 2015. Modelling, Design, and Optimization of Net-Zero Energy Buildings, 1st ed. Wiley & sons, New York, NY.

Baetens, R., Jelle, B.P., Gustavsen, A., 2010. Properties, requirements and possibilities of smart windows for dynamic daylight and solar energy control in buildings: A state-of-the-art review. Sol. Energy Mater. Sol. Cells 94, 87–105.

Bahaj, A.S., James, P., Jentsch, M.F., 2008. Potential of emerging glazing technologies for highly glazed buildings in hot arid climates. Energy Build. 40, 720–731.

Bailie, C.D., Christoforo, M.G., Mailoa, J.P., Bowring, A.R., Unger, E.L., Nguyen, W.H., Burschka, J., Pellet, N., Lee, J.Z., Grätzel, M., Noufi, R., Buonassisi, T., Salleo, A., McGehee, M.D., 2014. Semi-transparent perovskite solar cells for tandems with silicon and CIGS. Energy Environ. Sci. 8, 956–963.

Baum, R., 2011. Architectural integration of light-transmissive photovoltaic systems An analysis at the cell and laminate level, in: UIA2011: The 24th World Congress of Architecture. Tokyo, JP.

Betancur, R., Romero-Gomez, P., Martinez-Otero, A., Elias, X., Maymó, M., Martorell, J., 2013. Transparent polymer solar cells employing a layered light-trapping architecture. Nat. Photonics 7, 995–1000.

Biancardo, M., Taira, K., Kogo, N., Kikuchi, H., Kumagai, N., Kuratani, N., Inagawa, I., Imoto, S., Nakata, J., 2007. Characterization of microspherical semi-transparent solar cells and modules. Sol. Energy 81, 711–716.

Bizzarri, G., Gillott, M., Belpoliti, V., 2011. The potential of semitransparent photovoltaic devices for architectural integration. Sustain. Cities Soc. 1, 178–185.

Bloem, J.J., Lodi, C., Cipriano, J., Chemisana, D., 2012. An outdoor Test Reference Environment for double skin applications of Building Integrated Photovoltaic Systems. Energy Build. 50, 63–73.

Bordass, B., Cohen, R., Standeven, M., Leaman, A., 2001. Assessing building performance in use 2: technical performance of the Probe buildings. Build. Res. Inf. 29, 103–113.

Boyce, P.R., Hunter, C., Howlett, O., 2003. The Benefits of Daylight through Windows. Troy, NY.

Bullock, J., Bechinger, C., Benson, D.K., Branz, H., 1996. Semi-transparent a-SiC:H solar cells for self-powered photovoltaic-electrochromic devices. J. Non. Cryst. Solids 198-200, 1163–1167.

Carmody, J., Selkowitz, S.E., Lee, E.. S., Arasteh, D., Willmert, T., 2004. Window systems for high-performance buildings, 1st ed, New York. W.W. Norton & Co, New York, NY.

CEC, 2008. Building energy efficiency standards for non residential buildings. Sacramento, CA.

Chen, C.C., Dou, L., Zhu, R., Chung, C.H., Song, T.B., Zheng, Y.B., Hawks, S., Li, G., Weiss, P.S., Yang, Y., 2012. Visibly transparent polymer solar cells produced by solution processing. ACS Nano 6, 7185–7190.

Chen, F., Wittkopf, S.K., Khai Ng, P., Du, H., 2012. Solar heat gain coefficient measurement

of semi-transparent photovoltaic modules with indoor calorimetric hot box and solar simulator. Energy Build. 53, 74–84.
Chow, T.T., Fong, K.F., He, W., Lin, Z., Chan, A.L.S., 2007. Performance evaluation of a PV ventilated window applying to office building of Hong Kong. Energy Build. 39, 643–650.
Chow, T.T., Li, C., Lin, Z., 2010. Innovative solar windows for cooling-demand climate. Sol. Energy Mater. Sol. Cells 94, 212–220.
Cossu, M., Murgia, L., Caria, M., Pazzona, A., 2010. Economic feasibility study of semitransparent photovoltaic technology integrated on greenhouse covering structures, in: International Conference Ragusa SHWA2010. Ragusa Ibla Campus, pp. 648–655.
De Boer, B.J., van Helden, W.G.J., 2001. PV MOBI- PV modules optimized for building integration, in: NorthSun. Leiden, NL, pp. 6–8.
De Soto, W., Klein, S.A., Beckman, W.A., 2006. Improvement and validation of a model for photovoltaic array performance. Sol. Energy 80, 78–88.
De Vries, D.W., 1998. Design of a photovoltaic/thermal combi-panel. Eindhoven University.
Deb, S., Lee, S.H., Tracy, C.E., Pitts, J.R., Gregg, B.A., Branz, H., 2001. Stand-alone photovoltaic-powered electrochromic smart window. Electrochim. Acta 46, 2125–2130.
Delisle, V., 2008. Modelling and performance study of a building integrated photovoltaic facade in northern canadian climate, in: EuroSun. Lisbon, PT.
Deubener, J., Helsch, G., Moiseev, A., Bornhöft, H., 2009. Glasses for solar energy conversion systems. J. Eur. Ceram. Soc. 29, 1203–1210.
Deutsche Gesellshaft fur Sonnenenergie, 2005a. Planning and installing photovoltaic systems A guide for installers, architects and engineers, 2nd ed, Solar Energy. Earthscan, London, UK.
Deutsche Gesellshaft fur Sonnenenergie, 2005b. Planning and installing photovoltaic systems A guide for installers, architects and engineers, Second. ed, Solar Energy. Earthscan, London.
Drachman, P., Adamson, K.A., 2012. Building Integrated Photovoltaics: BIPV and BAPV: Market Drivers and Challenges, Technology Issues, Competitive Landscape, and Global Market Forecasts. Chicago, IL.
Dubois, M.C., Blomsterberg, Å., 2011. Energy saving potential and strategies for electric lighting in future north european, low energy office buildings: A literature review. Energy Build. 43, 2572–2582.
Dubois, M.-C., Flodberg, K., 2012. Daylight utilisation in perimeter office rooms at high latitudes: Investigation by computer simulation. Light. Res. Technol. 45, 52–75.
Duffie, J.A., Beckman, W.A., 2006. Solar engineering of thermal processes, 3rd ed. Wiley & sons, Hoboken , NJ.
Dunn, L., Gostein, M., Emery, K., 2012. Comparison of pyranometers vs. PV reference cells for evaluation of PV array performance, in: Conference Record of the IEEE Photovoltaic Specialists Conference. pp. 2899–2904.
Dyer, A.L., Bulloch, R.H., Zhou, Y., Kippelen, B., Reynolds, J.R., Zhang, F., 2014. A Vertically Integrated Solar-Powered Electrochromic Window for Energy Efficient Buildings. Adv. Mater. 26, 4895–4900.
Eperon, G.E., Bryant, D., Troughton, J., Stranks, S.., Johnston, M.B., Watson, T., Worsley, D.A., Snaith, H.J., 2014. Efficient, Semitransparent Neutral-Colored Solar Cells Based on Microstructured Formamidinium Lead Trihalide Perovskite. J. Phys. Chem. Lett. 8, 591–598.
Evans, D.L., 1981. Simplified method for predicting photovoltaic array output. Sol. Energy 27, 555–560.
Farley, K.M.J., Veitch, J.A., 2001. A room with a view: a review of the effects of windows on work and well-being. Ottawa, ON.

Fernandes, L.L., Lee, E.S., McNeil, A., Jonsson, J.C., Nouidui, T., Pang, X., Hoffmann, S., 2015. Angular selective window systems: Assessment of technical potential for energy savings. Energy Build. 90, 188–206.
Fung, T.Y.Y., Yang, H., 2008. Study on thermal performance of semi-transparent building-integrated photovoltaic glazings. Energy Build. 40, 341–350.
Gaiddon, B., Kaan, H., Munro, D., 2009. Photovoltaics in the urban environment: lessons learnt from large-scale projects, 1st ed. Earthscan, London, UK.
Gaillard, L., Giroux-Julien, S., Ménézo, C., Pabiou, H., 2014a. Experimental evaluation of a naturally ventilated PV double-skin building envelope in real operating conditions. Sol. Energy 103, 223–241.
Gaillard, L., Ménézo, C., Giroux, S., Pabiou, H., Le-Berre, R., 2014b. Experimental Study of Thermal Response of PV Modules Integrated into Naturally-ventilated Double Skin Facades. Energy Procedia 48, 1254–1261.
Galasiu, A.D., Atif, M.R., MacDonald, R.A., 2004. Impact of window blinds on daylight-linked dimming and automatic on/off lighting controls. Sol. Energy 76, 523–544.
Gan, G., 2009. Effect of air gap on the performance of building-integrated photovoltaics. Energy 34, 913–921.
Garde, F., Lenoir, A., David, M., Ottenwelter, E., 2011. Towards Net Zero Energy Buildings in Hot Climates : Part 1 , New Tools and Methods, in: ASHRAE Winter Conference Las Vegas. Las Vegas. NV.
Ge, H., Fazio, P., 2004. Experimental investigation of cold draft induced by two different types of glazing panels in metal curtain walls. Build. Environ. 39, 115–125.
Gibson, T., Krarti, M., 2014. Comparative Analysis of Prediction Accuracy from Daylighting Simulation Tools. Leukos 11, 49–60.
Green, M.A., 2007. Thin-film solar cells: review of materials, technologies and commercial status. J. Mater. Sci. Mater. Electron. 18, 15–19.
Green, M.A., Ho-Baillie, A., Snaith, H.J., 2014. The emergence of perovskite solar cells. Nat. Photonics 8, 506–514.
Gu, M., Ouyang, Z., Jia, B., Stokes, N., Chen, X., Fahim, N., Li, X., Ventura, M.J., Shi, Z., 2012. Nanoplasmonics: a frontier of photovoltaic solar cells. Nanophotonics 1, 235–248.
Guardo, A., Coussirat, M., Egusquiza, E., Alavedra, P., Castilla, R., 2009. A CFD approach to evaluate the influence of construction and operation parameters on the performance of Active Transparent Façades in Mediterranean climates. Energy Build. 41, 534–542.
Gueymard, C.A., DuPont, W.C., 2009. Spectral effects on the transmittance, solar heat gain, and performance rating of glazing systems. Sol. Energy 83, 940–953.
Gueymard, C.A., Wilcox, S.M., 2011. Assessment of spatial and temporal variability in the US solar resource from radiometric measurements and predictions from models using ground-based or satellite data. Sol. Energy 85, 1068–1084.
Guglielmetti, R., Scheib, J., Pless, S.D., Torcellini, P., Petro, R., 2011. Energy use intensity and its Influence on the integrated daylighting design of a large net zero energy building, in: ASHRAE Proceedings. Las Vegas. NV.
Gunay, B., O'Brien, W. illia., 2016. Implementation and comparison of existing occupant behaviour models in EnergyPlus. J. Build. Perform. Simul. 1493.
Gustavsen, A., Jelle, B.P., Arasteh, D., Kohler, C., 2007. State-of-the-Art Highly Insulating Window Frames – Research and Market Review State-of-the-Art. Oslo, NO.
Haldi, F., Robinson, D., 2010. Adaptive actions on shading devices in response to local visual stimuli. J. Build. Perform. Simul. 3, 135–153.
Han, J., Lu, L., Peng, J., Yang, H., 2013. Performance of ventilated double-sided PV façade compared with conventional clear glass façade. Energy Build. 56, 204–209.
Han, J., Lu, L., Yang, H., 2010. Numerical evaluation of the mixed convective heat transfer in

a double-pane window integrated with see-through a-Si PV cells with low-e coatings. Appl. Energy 87, 3431–3437.
Han, J., Lu, L., Yang, H., 2009. Thermal behavior of a novel type see-through glazing system with integrated PV cells. Build. Environ. 44, 2129–2136.
Harrison, S.J., Collins, M.R., 1999. Queen's university solar calorimeter. Design, calibration and operating procedure, in: Solar Energy Society of Canada Conference. Edmonton, AB.
Harrison, S.J., Dubrous, F.M., 1993. Uncertainties in the evaluation of window SHGC and U-values measured using an indoor solar simulator facility. ASHRAE Trans. 98, 638–645.
Harrison, S.J.J., Wonderen, S.J., 1994. Determining window solar heat gain coefficient. ASHRAE J. 36, 26–32.
Heschong, L., Wright, R., Okura, S., 2002. Daylight impact on retail sales performance. J. Illum. Eng. Soc. 31.
I.E.S.N.A, 2012. LM-83-12 IES Spatial Daylight Autonomy (sDA) and Annual Sunlight Exposure (ASE). New York, NY.
IEA-PVPS, 2015. Trends 2015 in photovoltaic applications: Survey report of Selected IEA countries between 1992 and 2014. Paris, FR.
Infield, D., Eicker, U., Fux, V., Mei, L., Schumacher, J., 2006. A simplified approach to thermal performance calculation for building integrated mechanically ventilated PV facades. Build. Environ. 41, 893–901.
Inkarojrit, V., 2008. Monitoring and modelling of manually-controlled Venetian blinds in private offices: a pilot study. J. Build. Perform. Simul. 1, 75–89.
Inkarojrit, V., 2005. Balancing Comfort: Occupants' control of wondow blinds in private offices. University of California, Berkeley.
Inoue, T., Kawase, T., Ibamoto, T., Takakusa, S., Matsuo, Y., 1988. The developement of an optimal control system for window shading devices based on investigations in office buildings. ASHRAE Trans. 94, 1034–1049.
ISO, 2015. ISO/DIS 19467 Thermal performance of windows and doors- Determination of solar heat gain coefficient using solar simulator [WWW Document]. URL http://www.iso.org/iso/home/store/catalogue_tc/catalogue_detail.htm?csnumber=64989 (accessed 12.20.15).
ISO, 2013. ISO 9806:2013 Solar energy-Solar thermal collectors-Test methods. Geneva, CH.
ISO, 2003a. ISO-15099: Thermal performance of windows, doors and shading devices Detailed calculations.
ISO, 2003b. ISO 9050: Glass in building-Determination of light transmittance, solar direct transmittance, total solar energy transmittance, ultraviolet transmittance and related glazing factors.
Jakubiec, J., Reinhart, C., 2012. The "adaptive zone" - A concept for assessing discomfort glare throughout daylit spaces. Light. Res. Technol. 44, 149–170.
James, P., Jentsch, M., Bahaj, A., 2009. Quantifying the added value of BiPV as a shading solution in atria. Sol. Energy 83, 220–231.
Janak, M., 1999. Coupling building energy and lighting simulation, in: 5th International IBPSA. Madison, WI.
Jelle, B.P.B.P., Hynd, A., Gustavsen, A., Arasteh, D., Goudey, H., Hart, R., 2012. Fenestration of today and tomorrow: A state-of-the-art review and future research opportunities. Sol. Energy Mater. Sol. Cells 96, 1–28.
Jorgensen, G.J., Terwilliger, K.M., DelCueto, J.A., Glick, S.H., Kempe, M.D., Pankow, J.W., Pern, F.J., McMahon, T.J., 2006. Moisture transport, adhesion, and corrosion protection of PV module packaging materials. Sol. Energy Mater. Sol. Cells 90, 2739–2775.
Jørgensen, M., Norrman, K., Krebs, F.C., 2008. Stability/degradation of polymer solar cells.

Sol. Energy Mater. Sol. Cells 92, 686–714.
Kapsis, K., Athienitis, A.K., 2015. A study of the potential benefits of semi-transparent photovoltaics in commercial buildings. Sol. Energy 115, 120–132.
Kapsis, K., Athienitis, A.K., Harrison, S.J., 2016. Determination of solar heat gain coefficient for semi-transparent photovoltaic windows: an experimental study. ASHRAE Trans. 125.
Kapsis, K., O'Brien, W., Athienitis, A.K., 2013. Time-lapse photography and image recognition to monitor occupant-controlled shade patterns: analysis and results, in: 13th International Conference of the International Building Performance Simulation Association. Chambéry, FR.
Kempe, M.D., 2010. Ultraviolet light test and evaluation methods for encapsulants of photovoltaic modules. Sol. Energy Mater. Sol. Cells 94, 246–253.
Kempe, M.D., Jorgensen, G.J., Terwilliger, K.M., McMahon, T.J., Kennedy, C.E., Borek, T.T., 2007. Acetic acid production and glass transition concerns with ethylene-vinyl acetate used in photovoltaic devices. Sol. Energy Mater. Sol. Cells 91, 315–329.
Kim, W., Ahn, H.T., Kim, J.T., 2008. A first approach to discomfort glare in the presence of non-uniform luminance. Build. Environ. 43, 1953–1960.
King, D.L., Boyson, W.E., Kratochvill, J.A., 2004. Photovoltaic Array Performance Model. Albuquerque, NM.
Kjenner, J., 2014. su2ds: Daylight analysis plug-in for Sketchup [WWW Document]. Manasc Isaac Archit. URL https://code.google.com/p/su2ds/ (accessed 11.11.14).
Klein, S., Rohde, M., Buschbaum, S., Severin, D., 2012. Throughput optimized a-Si/μc-Si tandem solar cells on sputter-etched ZnO substrates. Sol. Energy Mater. Sol. Cells 98, 363–369.
Klems, J.H., 2000. Solar heat gain through fenestration systems containing shading: Procedures for estimating performace from minimal data, Lawrence Berkeley National Laboratory.
Koyunbaba, B.K., Yilmaz, Z., 2012. The comparison of Trombe wall systems with single glass, double glass and PV panels. Renew. Energy 45, 111–118.
Krebs, F.C., 2009. Fabrication and processing of polymer solar cells: A review of printing and coating techniques. Sol. Energy Mater. Sol. Cells 93, 394–412.
Kuhn, T.E., Buhler, C., Platzer, W.J., 2001. Evaluation of overheating protection with sun-shading systems. Sol. Energy 69, 59–74.
Lam, T.C., Ge, H., Fazio, P., 2016. Energy positive curtain wall configurations for a cold climate using the Analysis of Variance (ANOVA) approach. Build. Simul. 9, 297–310.
Lawrence Berkeley National Laboratory, 2015a. Optics 6 [WWW Document]. URL https://windows.lbl.gov/software/optics/optics.html (accessed 6.10.14).
Lawrence Berkeley National Laboratory, 2015b. EnergyPlus 8.2 [WWW Document]. URL http://apps1.eere.energy.gov/buildings/energyplus/ (accessed 1.20.15).
Lawrence Berkeley National Laboratory, 2014a. WINDOW 7.1 [WWW Document]. URL http://windows.lbl.gov/software/window/7/ (accessed 6.10.14).
Lawrence Berkeley National Laboratory, 2014b. THERM 7.1 [WWW Document]. URL http://windows.lbl.gov/software/therm/7/index.html (accessed 6.10.14).
Li, D.H.W., Lam, T.N.T., Chan, W.W.H., Mak, A.H.L., 2009a. Energy and cost analysis of semi-transparent photovoltaic in office buildings. Appl. Energy 86, 722–729.
Li, D.H.W., Lam, T.N.T., Cheung, K.L., 2009b. Energy and cost studies of semi-transparent photovoltaic skylight. Energy Convers. Manag. 50, 1981–1990.
Li, G., Zhu, R., Yang, Y., 2012. Polymer solar cells. Nat. Photonics 6, 153–161.
Lindsay, C., Littlefair, P.J., 1992. Occupant use of venetian blinds in offices. Build. Res. Establ.
Liu, D., Kelly, T.L., 2013. Perovskite solar cells with a planar heterojunction structure prepared using room-temperature solution processing techniques. Nat. Photonics 8, 133–138.

Lunt, R.R., Bulovic, V., 2011. Transparent, near-infrared organic photovoltaic solar cells for window and energy-scavenging applications. Appl. Phys. Lett. 98.
Lynn, N., Mohanty, L., Wittkopf, S., 2012. Color rendering properties of semi-transparent thin-film PV modules. Build. Environ. 54, 148–158.
Lyons, P.R., Arasteh, D., Huizenga, C., 2000. Window performance for human thermal comfort, in: ASHRAE Proceedings. ASHRAE; 1999, Dallas, TX, pp. 594–604.
Mahdavi, A., Mohammadi, A., Kabir, E., Lambeva, L., 2008. Occupants' operation of lighting and shading systems in office buildings. J. Build. Perform. Simul. 1, 57–65.
Mäki, A., Valkealahti, S., Member, S., 2012. Power losses in long string and parallel-connected short strings of series-connected silicon-based photovoltaic modules due to partial shading conditions. IEEE Trans. Energy Convers. 27, 173–183.
Marinoski, D.L., Güths, S., Lamberts, R., 2012. Development of a calorimeter for determination of the solar factor of architectural glass and fenestrations. Build. Environ. 47, 232–242.
Markvart, J., Iversen, A., Logadóttir, Á., Johnsen, K., 2012. Indoor light and visual comfort with solar cells in glass facades. Aalborg.
MathWorks, 2014. MATLAB [WWW Document]. URL http://www.mathworks.com/products/matlab/ (accessed 11.11.14).
Midtdal, K., Jelle, B.P.B.P., 2013. Self-cleaning glazing products: A state-of-the-art review and future research pathways. Sol. Energy Mater. Sol. Cells 109, 126–141.
Mitchell, R., Kohler, C., Curcija, D., Zhu, L., Vidanovic, S., Czarnecki, S., Arasteh, D., 2013. THERM 6.3 / WINDOW 6.3 NFRC Simulation Manual.
Miyazaki, T., Akisawa, A., Kashiwagi, T., 2005. Energy savings of office buildings by the use of semi-transparent solar cells for windows. Renew. Energy 30, 281–304.
Moeck, M., Lee, E.S., Rubin, M.D., Sullivan, R.T., Selkowitz, S.E., 1998. Visual quality assessment of electrochromic and conventional glazings. Sol. Energy Mater. Sol. Cells 54, 157–164.
National Renewable Energy Laboratory, 2016. Research cell efficiency records [WWW Document]. URL http://www.nrel.gov/ncpv/images/efficiency_chart.jpg (accessed 1.2.16).
National Renewable Energy Laboratory, 2014. Legacy OpenStudio Plug-in for SketchUp [WWW Document]. URL http://apps1.eere.energy.gov/buildings/energyplus/ (accessed 11.11.14).
NFRC, 2014a. NFRC 100: Procedure for Determining Fenestration Product U-factors.
NFRC, 2014b. NFRC 300: Test Method for Determining the Solar Optical Properties of Glazing Materials and Systems.
NFRC, 2014c. NFRC 102 Proceduce for Measuring the Steady-State Thermal Transmittance of Fenestration Systems. Greenbelt, MD.
NFRC, 2014d. NFRC 200: Procedure for Determining Fenestration Product Solar Heat Gain Coefficient and Visible Transmittance at Normal Incidence.
NFRC, 2010. NFRC 201 Procedure for Interim Standard Test Method for Measuring the Solar Heat Gain Coefficient of Fenestration Systems Using Calorimetry Hot Box Methods. Greenbelt, MD.
Ng, P.K., Mithraratne, N., Kua, H.W., 2013. Energy analysis of semi-transparent BIPV in Singapore buildings. Energy Build. 66, 274–281.
Nordmann, T., Clavadetscher, L., 2003. Understanding temperature effects on PV system performance, in: 3rd World Conference onPhotovoltaic Energy Conversion. pp. 2–5.
Notton, G., Cristofari, C., Mattei, M., Poggi, P., 2005. Modelling of a double-glass photovoltaic module using finite differences. Appl. Therm. Eng. 25, 2854–2877.
O'Brien, W., Kapsis, K., Athienitis, A.K., 2013. Manually-operated window shade patterns in office buildings: A critical review. Build. Environ. 60, 319–338.

Olivieri, L., Caamaño-Martín, E., Moralejo-Vázquez, F.J., Martín-Chivelet, N., Olivieri, F., Neila-Gonzalez, F.J., 2014. Energy saving potential of semi-transparent photovoltaic elements for building integration. Energy 76, 572–583.

Olivieri, L., Caamaño-Martin, E., Neila, J., Olivieri, F., Neila, J., 2013. Integral energy performance characterization of semi-transparent photovoltaic elements for building integration under real operation conditions. Energy Build. 68, 280–291.

Osterhaus, W.K.E., 2005. Discomfort glare assessment and prevention for daylight applications in office environments. Sol. Energy 79, 140–158.

Park, K.E., Kang, G.H., Kim, H.I., Yu, G.J., Kim, J.T., 2010. Analysis of thermal and electrical performance of semi-transparent photovoltaic (PV) module. Energy 35, 2681–2687.

Peng, J., Lu, L., Yang, H., 2013. An experimental study of the thermal performance of a novel photovoltaic double-skin facade in Hong Kong. Sol. Energy 97, 293–304.

Pereira, F.O.R., Sharples, S., 1991. The development of a device for measuring solar heat gain and shading coefficients of windows in scale models. Energy Build. 17, 271–281.

Perez, R., Ineichen, P., Seals, R., Michalsky, J., Stewart, R., 1990. Modelling daylight availability and irradiance components from direct and global irradiance. Sol. Energy 44, 271–289.

Pern, F.J., Glick, S.H., 2000. Photothermal stability of encapsulated Si solar cells and encapsulation materials upon accelerated exposures. Sol. Energy Mater. Sol. Cells 61, 153–188.

Pigg, S., Eilers, M., Reed, J., 1996. Behavioral aspects of lighting and occupancy sensors in private offices: a case study of a university office building, in: ACEEE 1996 Summer Study on Energy. pp. 161–170.

Pineault, N., Dubois, M.C., 2008. Effect of Window Glazing Type on Daylight Quality : Scale Model Study of a Living Room under Natural Sky. Leukos 5, 83–99.

Pvsyst.SA, 2014. User's Guide: PVsyst Contextual Help [WWW Document]. URL http://files.pvsyst.com/help/ (accessed 11.11.14).

Qiu, Z., Chow, T.T., Li, P., Li, C., Ren, J., Wang, W., 2009. Performance evaluation of the photovoltaic double skin facade, in: 11th International IBPSA. Glasgow, UK, pp. 2251–2257.

Reddy, T.A., 2011. Applied Data Analysis and Modeling for Energy Engineers and Scientists. Springer US, Boston, MA.

Reinhart, C.F., 2014. Daysim [WWW Document]. URL http://daysim.ning.com/ (accessed 11.11.14).

Reinhart, C.F., 2004. Lightswitch-2002: a model for manual and automated control of electric lighting and blinds. Sol. Energy 77, 15–28.

Reinhart, C.F., Mardaljevic, J., Rogers, Z., 2006. Dynamic daylight performance metrics for sustainable building design. Leukos 3, 1–25.

Reinhart, C.F., Voss, K., 2003. Monitoring manual control of electric lighting and blinds. Light. Res. Technol. 35, 243–260.

Reinhart, C.F., Walkenhorst, O., 2001. Validation of dynamic RADIANCE-based daylight simulations for a test office with external blinds. Energy Build. 33, 683–697.

Reinhart, C.F., Wienold, J., 2011. The daylighting dashboard–a simulation-based design analysis for daylit spaces. Build. Environ. 46, 386–396.

Rekinger, M., Thies, F., Masson, G., Orlandi, S., 2014. Global Market Outlook for Solar Power 2015-2019.

Roberts, S., Guariento, N., 2009. Building integrated photovoltaics: a handbook, 1st ed. Birkhauser, Basel, CH.

Robinson, L., 2011. Numerical and experimental study of semi-transparent photovoltaics

integrated into commercial building facades. CONCORDIA UNIVERSITY.
Robinson, L., Athienitis, A.K., 2009. Design methodology for optimization of electricity generation and daylight utilization for facade with semi-transparent photovoltaics, in: 11th International IBPSA. Glasgow, pp. 811–818.
Ross, R.., 1976. Interface design considerations for terrestrial solar cell modules, in: 12th Photovoltaic Specialists Conference. Baton Rouge, LA.
Rubin, A., Collins, B., Tibbott, R., 1987. Window blinds as a potential energy saver: A case study.
Sai, H., Matsui, T., Matsubara, K., Kondo, M., Yoshida, I., 2014. 11.0%-Efficient Thin-Film Microcrystalline Silicon Solar Cells With Honeycomb Textured Substrates. IEEE J. Photovoltaics 4, 1349–1353.
Sharma, V., Chandel, S.S., 2013. Performance and degradation analysis for long term reliability of solar photovoltaic systems: A review. Renew. Sustain. Energy Rev. 27, 753–767.
Skoplaki, E., Palyvos, J.A., 2009. On the temperature dependence of photovoltaic module electrical performance: A review of efficiency/power correlations. Sol. Energy 83, 614–624.
Skoplaki, E., Palyvos, J.A., 2009. Operating temperature of photovoltaic modules: A survey of pertinent correlations. Renew. Energy 34, 23–29.
Snaith, H.J., 2013. Perovskites : The emergence of a new era for low cost , high efficiency solar cells. J. Phys. Chem. Lett 4, 3623−3630.
Stamenic, L., Lubun, M., 2007. Simulated, tested and actual performance for the largest northern BIPV installation in the world, in: 22nd European Photovoltaic Solar Energy Conference. Milan, IT.
Sutter, Y., Dumortier, D., Fontoynont, M., 2006. The use of shading systems in VDU task offices: A pilot study. Energy Build. 38, 780–789.
Temby, O., Kapsis, K., Berton, H., Rosenbloom, D., Gibson, G., Athienitis, A.K., Meadowcroft, J., 2014. Building-Integrated Photovoltaics : Distributed Energy Development for Urban Sustainability. Environ. Sci. Policy Sustain. Dev.
Tian, H., Mancilla-David, F., Ellis, K., Muljadi, E., Jenkins, P., 2012. A cell-to-module-to-array detailed model for photovoltaic panels. Sol. Energy 86, 2695–2706.
Tina, G., Cosentino, F., Notton, G., 2010. Effect of thermal gradient of electrical efficiency of hybrid PV/T, in: 25th European Photovoltaic Solar Energy Conference and exhibition/5th World Conference on Photovoltaic Energy Conversion. Valencia, SP.
Trimble, 2014. SketchUp 3D [WWW Document]. URL http://www.sketchup.com/ (accessed 11.11.14).
Tseng, C.C., Goswami, D.Y., 2001. Effect of tilt angle and temperature difference on solar heat gain coefficient measurement of fenestration system. ASHRAE Trans. 107.
Tzempelikos, A., Athienitis, A.K., 2007. The impact of shading design and control on building cooling and lighting demand. Sol. Energy 81, 369–382.
U.S.DOE, 2012. EnergyPlus Engineering Reference: The reference to EnergyPlus Calculations. Berkeley, CA.
Van Den Wymelenberg, K., 2012. Patterns of occupant interaction with window blinds: A literature review. Energy Build. 51, 165–176.
Van Den Wymelenberg, K., Inanici, M., 2014. A Critical Investigation of Common Lighting Design Metrics for Predicting Human Visual Comfort in Offices with Daylight. Leukos 10, 145–164.
Van Den Wymelenberg, K.G., 2014. Visual Comfort, Discomfort Glare, and Occupant Fenestration Control: Developing a Research Agenda. Leukos 10, 207–221.
Van Wonderen, S.J., 1996. Solar heat gain performance evaluation of commercial solar-control glazings and shading devices. Queen's university.

Vartiainen, E., 2001. Electricity benefits of daylighting and photovoltaics for various solar facade layouts in office buildings. Energy Build. 33, 113–120.
Vartiainen, E., Peippo, K., Lund, P.D., 2000. Daylight measurements and calculations with an a-Si photovoltaic solar facade. Sol. Energy 68, 223–235.
Vats, K., Tiwari, G.N., 2012. Performance evaluation of a building integrated semitransparent photovoltaic thermal system for roof and façade. Energy Build. 45, 211–218.
Vats, K., Tomar, V., Tiwari, G.N., 2012. Effect of packing factor on the performance of a building integrated semitransparent photovoltaic thermal (BISPVT) system with air duct. Energy Build. 53, 159–165.
Veitch, J.A., Galasiu, A.D., 2012. The physiological and psychological effects of windows, daylight, and view at home: Review and research agenda. Ottawa, ON.
Veitch, J.A., Newsham, G.R., 1997. Determinants of lighting quality I: State of the science, in: IESNA Annual Conference.
Walkenhorst, O., Luther, J., Reinhart, C.F., Timmer, J., 2002. Dynamic annual daylight simulations based on one-hour and one-minute means of irradiance data. Sol. Energy 72, 385–395.
Wienold, J., Christoffersen, J., 2006. Evaluation methods and development of a new glare prediction model for daylight environments with the use of CCD cameras. Energy Build. 38, 743–757.
Willeke, G.P., Weber, E., Blieske, U., Stollwerck, G., 2013. Glass and Other Encapsulation Materials, in: Semiconductors and Semimetals. pp. 199–258.
Wong, P.W., Shimoda, Y., Nonaka, M., Inoue, M., 2005. Field study and modeling of semi-transparent PV in power, thermal and optical aspects. J. Asian Archit. Build. Eng. 549–556.
Wong, P.W., Shimoda, Y., Nonaka, M., Inoue, M., Mizuno, M., 2008. Semi-transparent PV: Thermal performance, power generation, daylight modelling and energy saving potential in a residential application. Renew. Energy 33, 1024–1036.
Wright, J.L., Collins, M.R., Kotey, N.A., Barnaby, C.S., 2009. ASHRAE 1311 Improving Cooling Load Calculations for Fenestration with Shading Devices. Atlanta, GA.
Yamada, N., Kanno, K., Hayashi, K., Tokimitsu, T., 2011. Performance of see-through prism CPV module for window integrated photovoltaics. Opt. Express 19, 649–656.
Yoon, S., Song, J.H., Lee, J.S., 2011. Practical application of building integrated photovoltaic (BIPV) system using transparent amorphous silicon thin-film PV module. Sol. Energy 85, 723–733.
Zhang, Y., Barrett, P., 2012. Factors influencing occupants' blind-control behaviour in a naturally ventilated office building. Build. Environ. 54, 137–147.
Zhao, Y., Lunt, R.R., 2013. Transparent luminescent solar concentrators for large-area solar windows enabled by massive stokes-shift nanocluster phosphors. Adv. Energy Mater. 3, 1143–1148.
Zhao, Y., Meek, G.A., Levine, B.G., Lunt, R.R., 2014. Near Infrared Harvesting Transparent Luminescent Solar Concentrators. Adv. Opt. Mater. 2, 606–611.
Zondag, H.A., De Vries, D.W., Van Helden, W.G.J., Van Zolingen, R.J.C., Van Steenhoven, A.A., 2002. The thermal and electrical yield of a PV-thermal collector. Sol. Energy 72, 113–128.

Appendix A
Irradiance and Wind Test Conditions

The STPV windows were tested and characterized under the Solar Simulator and Environmental Chamber (SSEC) laboratory at Concordia University, Montreal, Canada. The average emulated solar irradiance varied between 750 W/m^2 and 1031 W/m^2 with a uniformity of 97% and a temporal stability of ±1% during the testing period. Figure A-1 illustrates the measured irradiance uniformity on a scanning grid of 0.10 m on the surface of the STPV window. An interpolation was performed between measured point values using Gaussian process regression (Reddy, 2011). Each estimated point value is weighted by its distance away from the measured point value as follows:

$$S_A = \sum_{i=1}^{n} (w_i \cdot S_i) \tag{A.1}$$

where S_A is the estimated irradiance value of grid node A, n is the number of neighbouring data values used in the estimation, S_i is the irradiance measured value at location i with weight w_i. The value of weights will sum to 1 to ensure that there is no bias towards clustered data points.

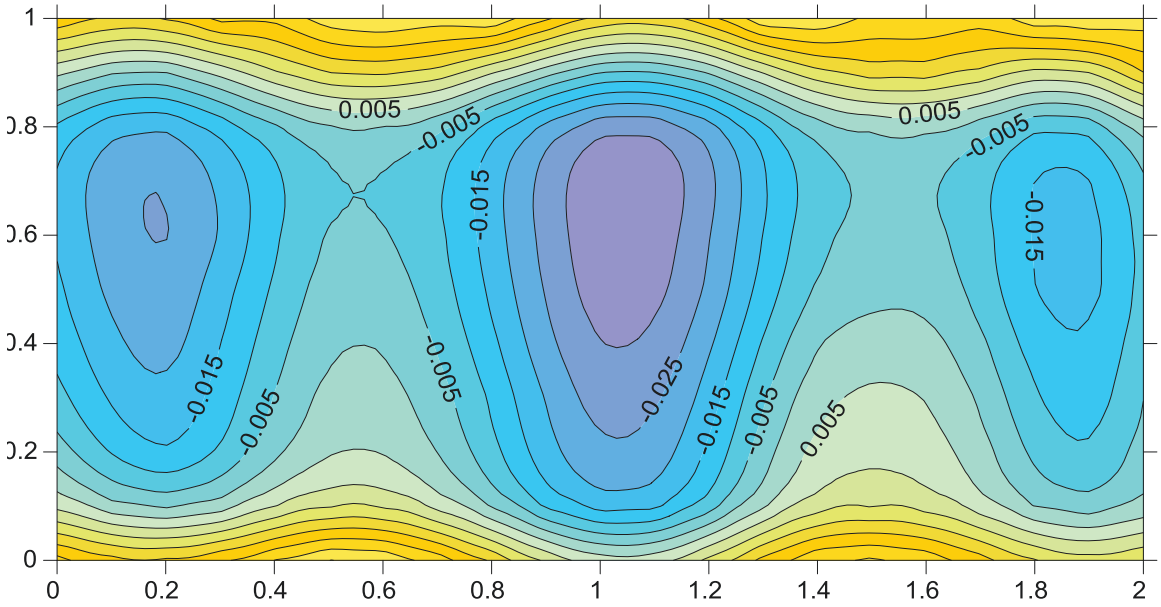

Figure A-1. Spatial relative change of irradiance uniformity on a scanning grid of 0.10 m.

The average wind speed varied between still air and 14 m/s with a spatial and temporal variation of ± 1 m/s during the testing period (ISO, 2013). In addition, the convective heat transfer coefficient was measured directly with a hot plate apparatus. A correlation between wind-induced heat transfer coefficient and wind speed was developed based on the experimental data, using regression analysis (Figure A-2). The correlation is specific to the Solar Simulator configuration.

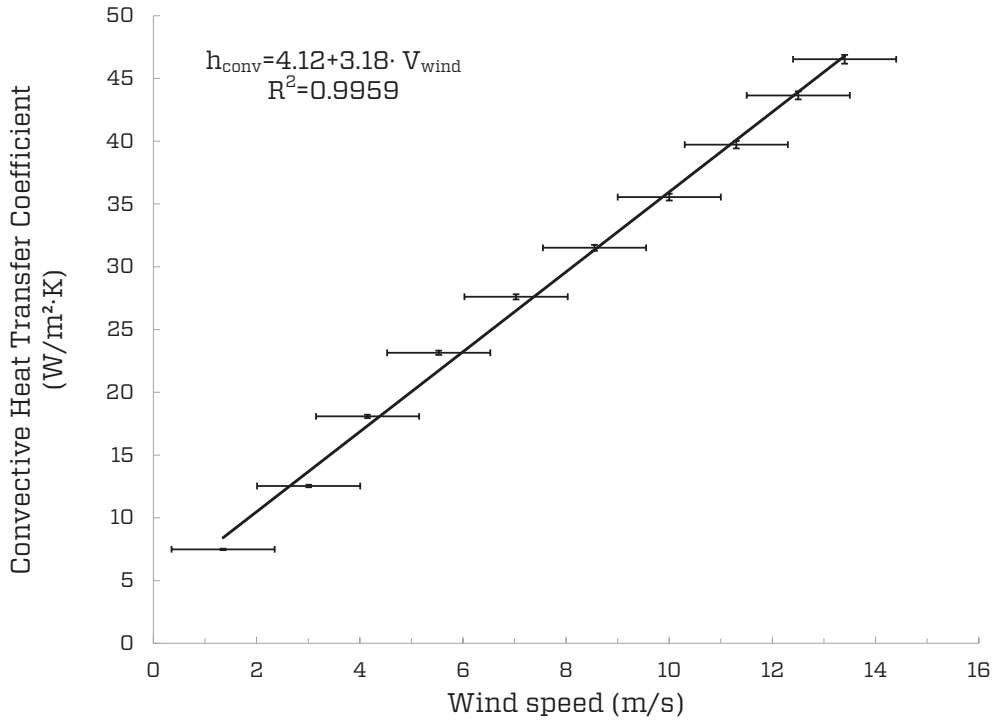

Figure A-2. Wind-induced convective heat transfer coefficient as a linear function of wind speed for the Solar Simulator.

Appendix B
Calculation of SHGC and U-Value, and Corresponding Measurement Uncertainties

Through linear regression of the performance points i=1...n, the U-value is determined as the slope of the regression line through an iterative process for each step n (Harrison and Dubrous, 1993; Reddy, 2011):

$$U_n = \frac{\sum_i a_{n,i}^2 \left(\frac{\Delta T_{STPVi}}{S_i}\right)\eta_i - \sum_j a_{n,i}^2 \eta_i \cdot \sum_j a_{n,j}^2 \left(\frac{\Delta T_{STPVj}}{S_j}\right)}{\sum_i a_{n,i}^2 \left(\frac{\Delta T_{STPVi}}{S_i}\right)^2 - \sum_i \left[a_{n,i}^2 \left(\frac{\Delta T_{STPVi}}{S_i}\right)\right]^2} \tag{B.1}$$

The SHGC is calculated as the intercept of the regression line with the axis of ordinates:

$$SHGC_n = \frac{\sum_i a_{n,i}^2 \left(\frac{\Delta T_{STPVi}}{S_i}\right)^2 \cdot \sum_j a_{n,j}^2 \eta_j^2 - \sum_i a_{n,i}^2 \left(\frac{\Delta T_{STPVi}}{S_i}\right) \cdot \sum_j a_{n,j}^2 \left(\frac{\Delta T_{STPVj}}{S_j}\right)\eta_j}{\sum_i a_{n,i}^2 \left(\frac{\Delta T_{STPVi}}{S_i}\right)^2 - \sum_i \left[a_{n,i}^2 \left(\frac{\Delta T_{STPVi}}{S_i}\right)\right]^2} \tag{B.2}$$

while $\delta_{n,i}$ and $a_{n,i}$ are obtained from the previous iteration (n-1):

$$\delta_{n,i}^2 = U_{n-1}^2 \cdot \delta\left(\frac{\Delta T_{STPVi}}{S_i}\right)^2 + \delta\eta_i^2 \tag{B.3}$$

and

$$a_{n,i}^2 = \frac{\frac{1}{\delta_{n,i}^2}}{\sum \frac{1}{\delta_{n,i}^2}} \tag{B.4}$$

with the corresponding variances given by:

$$\sigma_U^2 = \frac{1}{\sum_i \frac{1}{\delta_{n,i}^2}} \cdot \frac{1}{\sum_i a_{n,i}^2 \left(\frac{\Delta T_{STPVi}}{S_i}\right)^2 - \left[\sum_i a_{n,i}^2 \left(\frac{\Delta T_{STPVi}}{S_i}\right)\right]^2} \tag{B.5}$$

and

$$\sigma^2_{SHGC} = \frac{1}{\sum_i \frac{1}{\delta^2_{n,i}}} \cdot \frac{\sum_i a^2_{n,i} \left(\frac{\Delta T_{STPVi}}{S_i} \right)^2}{\sum_i a^2_{n,i} \left(\frac{\Delta T_{STPVi}}{S_i} \right)^2 - \left[\sum_i a^2_{n,i} \left(\frac{\Delta T_{STPVi}}{S_i} \right) \right]^2} \tag{B.6}$$

Appendix C
Equivalent One-Diode Model Inputs

Table C-1 Electrical model inputs for poly-Si based STPV windows simulated in this study.

Name of the STPV module	STPV10%	STPV20%	STPV30%	STPV40%	STPV50%
STPV cell technology	polycrystalline Silicon (poly-Si)				
Surface area (m^2)	1.88				
Efficiency (%)	0.150	0.129	0.107	0.086	0.064
Transmittance-Absorbance Product	0.95				
Semiconductor Bandgap (eV)	1.12				
Short Circuit Current (A)	10.01				
Open Circuit Voltage (V)	37.22	31.9	26.59	21.27	15.95
Current at Maximum Power (A)	9.36				
Voltage at Maximum Power (V)	30.12	25.82	21.51	17.21	12.91
Temperature Coefficient of Maximum Power (%/K)	-0.445				
Temperature Coefficient of Short Circuit Current (%/K)	+0.054				
Temperature Coefficient of Open Circuit Voltage (%/K)	-0.333				

Table C-2 Electrical model inputs for a-Si/μc-Si based STPV windows simulated in this study.

Name of the STPV module	STPV10%	STPV20%	STPV30%	STPV40%	STPV50%
Cell technology	a-Si/μc-Si (micromorph)				
Surface area (m^2)	1.88				
Efficiency (%)	0.100	0.086	0.072	0.057	0.043
Transmittance-Absorbance Product	0.95				
Semiconductor Bandgap (eV)	1.4				
Short Circuit Current (A)	1.65	1.41	1.18	0.94	0.71
Open Circuit Voltage (V)	167				
Current at Maximum Power (A)	1.52	1.3	1.09	0.87	0.65
Voltage at Maximum Power (V)	123.9				
Temperature Coefficient of Maximum Power (%/K)	-0.270				
Temperature Coefficient of Short Circuit Current (%/K)	+0.071				
Temperature Coefficient of Open Circuit Voltage (%/K)	-0.270				

Table C-3 Electrical model inputs for OPV based STPV windows simulated in this study.

Name of the STPV module	STPV10%	STPV20%	STPV30%	STPV40%	STPV50%
Cell technology	organic tandem (OPV)				
Surface area (m^2)	1.88				
Efficiency (%)	0.100	0.086	0.072	0.057	0.043
Transmittance-Absorbance Product	0.95				
Semiconductor Bandgap (eV)	1.7				
Short Circuit Current (A)	29.59	25.36	21.14	16.91	12.68
Open Circuit Voltage (V)	11.3				
Current at Maximum Power (A)	23.8	20.4	17	13.6	10.2
Voltage at Maximum Power (V)	7.9				
Temperature Coefficient of Maximum Power (%/K)	+0.050				
Temperature Coefficient of Short Circuit Current (%/K)	-0.210				
Temperature Coefficient of Open Circuit Voltage (%/K)	-0.270				